

Dissertation zur Erlangung des Doktorgrades
der Fakultät für Chemie und Pharmazie
der Ludwig-Maximilians-Universität München



The vascular barrier protecting *Crataegus* extract WS[®] 1442 triggers
endothelial calcium signaling:
Underlying mechanisms and bioactive principles

Elisabeth Armella Willer
aus München, Deutschland

2012

Erklärung

Diese Dissertation wurde im Sinne von § 7 der Promotionsordnung vom 28. November 2011 von Frau Prof. Dr. Angelika M. Vollmar betreut.

Eidesstattliche Versicherung

Diese Dissertation wurde eigenständig und ohne unerlaubte Hilfe erarbeitet.

München, den 8. März 2012

Elisabeth Armella Willer

Dissertation eingereicht am:	08.03.2012
1. Gutachter:	Prof. Dr. Angelika M. Vollmar
2. Gutachter:	PD Dr. Robert Fürst
Mündliche Prüfung am:	17.04.2012

With sincere thanks to my parents

CONTENTS

CONTENTS.....	4
1 INTRODUCTION	9
1.1 Background and aim of the study	10
1.2 <i>Crataegus</i> extract WS [®] 1442	11
1.2.1 Phytochemical composition of <i>Crataegus</i> leaves and flowers	11
1.2.1.1 Flavonoids	11
1.2.1.2 Oligomeric proanthocyanidins (OPCs)	12
1.2.2 Pharmacology, efficacy and safety of <i>Crataegus</i> preparations	13
1.3 The vascular endothelium.....	13
1.3.1 Regulation of endothelial permeability	14
1.3.2 Ca ²⁺ -signaling in endothelial cells	16
2 MATERIALS AND METHODS	18
2.1 Materials	19
2.1.1 <i>Crataegus</i> extract WS [®] 1442	19
2.1.2 Fractions of <i>Crataegus</i> extract WS [®] 1442.....	19
2.1.3 Biochemicals, inhibitors and cell culture reagents.....	21
2.2 Cell culture	22
2.2.1 Buffers, solutions and reagents.....	22
2.2.2 Endothelial cells	24
2.2.2.1 HMEC-1 – human dermal microvascular endothelial cells.....	24
2.2.2.2 HUVECs – human umbilical vein endothelial cells.....	24
2.2.2.3 EA.hy926 cells.....	25
2.2.3 Passaging.....	25
2.2.4 Freezing and thawing	25
2.3 Cell viability assays	26
2.3.1 CellTiter-Blue [®] Cell Viability Assay.....	26
2.3.2 Trypan Blue staining.....	26
2.3.3 ATP measurement	26

2.4	Western Blot analysis	27
2.4.1	Sample preparation	27
2.4.2	Protein quantification – Bradford assay.....	27
2.4.3	SDS-Page electrophoresis	28
2.4.4	Tank electroblotting	29
2.4.5	Protein detection	29
2.4.5.1	Enhanced chemiluminescence.....	30
2.4.5.2	Infrared imaging	30
2.4.5.3	Quantification	30
2.5	Macromolecular permeability assay	31
2.6	Immunocytochemistry and confocal laser scanning microscopy	31
2.7	Patch clamp recordings	32
2.8	Calcium imaging	33
2.8.1	Fura-2 measurements	34
2.8.1.1	Perfusion system.....	35
2.8.1.2	Static tempered system.....	36
2.8.2	FRET analysis using D1ER.....	36
2.8.2.1	Cell transfection.....	37
2.8.2.2	FRET measurements	37
2.9	Statistical analysis	38
3	RESULTS	39
3.1	Mechanisms of WS[®] 1442-induced Ca²⁺-signaling in endothelial cells	40
3.1.1	WS [®] 1442 elevates cytosolic Ca ²⁺ levels in human endothelial cells	40
3.1.2	WS [®] 1442 does neither influence endothelial barrier function nor endothelial cell contraction	42
3.1.3	Cell viability is not affected by WS [®] 1442.....	43
3.1.4	WS [®] 1442 does not interfere with the endothelial Na ⁺ /K ⁺ -ATPase	45
3.1.5	WS [®] 1442 increases [Ca ²⁺] _i by emptying the ER with two different mechanisms involved	47
3.1.6	WS [®] 1442 inhibits store-operated Ca ²⁺ entry and Ca ²⁺ extrusion capacity	49

3.1.7	WS [®] 1442 induced Ca ²⁺ -signaling in EA.hy926 cells	53
3.1.7.1	WS [®] 1442 increases cytosolic Ca ²⁺ levels and inhibits Ca ²⁺ extrusion capacity in EA.hy926 cells.....	53
3.1.7.2	WS [®] 1442 raises [Ca ²⁺] _i by depleting the ER	55
3.2	In search of the bioactive compounds of WS[®] 1442	56
3.2.1	Subfractions 32.x differently inhibit agonist-induced Ca ²⁺ -signaling.....	56
3.2.1.1	Subfractions 32.x.....	57
3.2.1.2	Subfractions 32.1_x.....	58
3.2.1.3	Subfractions 32.4_x.....	59
3.2.1.4	Ca ²⁺ -active subfractions of WS [®] 1442 neither impair endothelial barrier integrity nor contractile machinery.....	61
3.2.2	Subfractions 34.x differently affect cAMP pathway	63
4	DISCUSSION AND CONCLUSIONS	68
4.1	WS[®] 1442 protects endothelial barrier integrity despite increasing [Ca²⁺]_i.....	69
4.1.1	Key role of SOCE in endothelial hyperpermeability	69
4.1.2	Suggested modes of SOCE inhibition induced by WS [®] 1442	70
4.2	WS[®] 1442 and its influence on Ca²⁺ extrusion capacity	71
4.3	Na⁺/K⁺-ATPase and WS[®] 1442.....	72
4.4	Comparison between HUVECs and EA.hy926 cells concerning WS[®] 1442-induced Ca²⁺-signaling	72
4.5	Bioactive compounds of WS[®] 1442.....	73
4.5.1	Flavonoids and their role in Ca ²⁺ -signaling.....	73
4.5.2	Oligomeric proanthocyanidins and endothelial barrier function.....	75
5	SUMMARY	76
6	REFERENCES	79

7	APPENDIX	89
7.1	Abbreviations	90
7.2	Publications.....	92
7.2.1	Original publications	92
7.2.2	Poster presentations	92
7.3	Curriculum vitae.....	94
7.4	Acknowledgements	95

1 INTRODUCTION

1.1 Background and aim of the study

Vascular barrier dysfunction, *i.e.* endothelial hyperpermeability and the subsequent edema formation, is involved in the initiation or progression of many diseases, such as sepsis, atherosclerosis, diabetes or cancer.¹ Despite this knowledge, a pharmacological treatment that interferes with barrier-regulating systems in endothelial cells is still missing. We recently reported that the hawthorn (*Crataegus spp.*) extract WS[®] 1442 – a well established phytopharmaceutical to treat mild forms of heart failure – offers a promising novel approach for protecting against endothelial barrier impairment by *activating* cAMP/Epac1/Rap1- and *inhibiting* Ca²⁺/PKC/RhoA-signaling.²

In the present study, we focus on endothelial Ca²⁺-signaling phenomena. Based on previous experiments of WS[®] 1442-evoked inhibition of a thrombin-generated increase of cytosolic calcium (Ca²⁺) levels,² we hypothesized that WS[®] 1442 preincubation *per se* might elevate Ca²⁺ baseline levels. This is challenging, since an increase of intracellular Ca²⁺ concentration ([Ca²⁺]_i) followed by a so-called store-operated calcium entry (SOCE) usually leads to the induction of hyperpermeability.³

In addition, Ca²⁺/PKC/RhoA and cAMP/Epac1/Rap1 pathways were each found to be affected by only one distinct phytochemical group of the extract.⁴ However, individual bioactive compounds could not be identified yet.

Thus, the aims of the present study were to

- 1) examine the mechanisms of how WS[®] 1442 affects [Ca²⁺]_i in the human endothelium, and to
- 2) identify or at least narrow down the bioactive compounds of WS[®] 1442 that are responsible for the endothelial activity by bioguided fractionation.

1.2 *Crataegus* extract WS[®] 1442

WS[®] 1442 represents an aqueous alcoholic special extract from leaves and flowers of predominantly *Crataegus monogyna* and *laevigata*. The extract is standardized to a content of 17.3-20.1% oligomeric proanthocyanidins (OPCs). The original hawthorn plant (*Crataegus spp.*) belongs to the rose family and grows as shrubs or trees with thorny branches all over the Northern hemisphere. In general, hawthorn is one of the oldest known medicinal plants in the Western world.⁵ It is utilized as a herbal remedy to treat chronic heart failure worldwide.⁶ In various European countries, WS[®] 1442 has even become an approved or registered drug for the treatment of congestive heart failure according to the New York Heart Association (NYHA) functional class II.

1.2.1 Phytochemical composition of *Crataegus* leaves and flowers

Crataegus preparations of leaves and flowers mainly contain two phytochemical groups, flavonoids (1.5–2.0%) and OPCs (2.5%).⁷ Both groups have been identified to exert the cardiovascular protective activity of hawthorn.^{8,9} Apart from those, pentacyclic triterpenic acids (ursolic and oleanolic acid), phenol carboxylic acids (chlorogenic and caffeic acid), aliphatic alcohols, amines, purines as well as polymeric carbohydrates have been isolated from *Crataegus* extracts to a lesser extent.^{9,10}

1.2.1.1 Flavonoids

Flavonoids (lat. flavus = yellow), of which more than 4000 have been identified so far, represent a group of ubiquitous secondary plant metabolites belonging to the major class of polyphenols. Concerning biosynthesis, shikimic acid serves as a precursor of flavonoids. The flavonoid backbone (C₆-C₃-C₆) contains two aromatic rings that are linked to each other by a C₃ bridge of different oxidation states. According to their chemical structure, flavonoids can be categorized into flavans/catechins, flavanones/flavanonols, flavones/flavonols, anthocyanidins and chalcones. In each case, the flavonoid backbone can be derivatized for instance by O- or C-glycosylation, hydroxylation or methylation.¹⁰

Investigating *Crataegus* leaves and flowers, a series of flavones, flavanones and predominantly flavone glycosides (hyperoside, rutin, vitexin) has been detected.^{6,7} Interestingly, flavone glycosides are mainly based on apigenin and luteolin whereas

quercetin, kaempferol, and 8-methoxykaempferol provide the basic structures of the different flavonol glycosides.⁷ For glycosylation, β -D-glucose, α -L-rhamnose, α -L-4-acetyl-rhamnose, xylose, arabinose, rutinose, and neohesperidose have been identified. Furthermore, apigenin and luteolin based flavones found in *Crataegus* form C- and O-glycosides while flavonols only build O-glycosides.⁶ Obviously, the flavonoids themselves already represent a huge variety of phytochemical compounds in this drug.

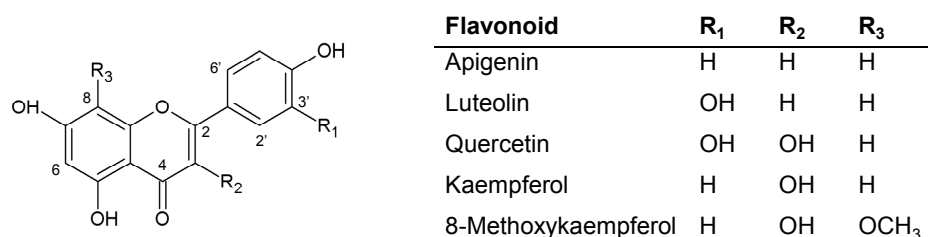


Figure 1 Common flavonoids of *Crataegus* leaves and flowers

1.2.1.2 Oligomeric proanthocyanidins (OPCs)

Besides monomeric flavonoids, plants also synthesize a group of condensed flavanols, called oligomeric proanthocyanidins. This name originates from the fact that OPCs can be hydrolyzed into colored anthocyanidins upon acidification. Depending on the hydroxylation pattern of the monomers, OPCs are subdivided into prodelphinidins, propelargonidins and procyanidins. At this, the procyanidins represent the most widely spread group of OPCs in plant kingdom.¹⁰

With regard to *Crataegus* leaves and flowers, procyanidins composed of predominantly two to six monomers of the diastereomeric couple epicatechin and catechin were found. In particular, the dimers B1, B2 (Figure 2A), B4, B5, trimer C1 (Figure 2B) and tetramer D1 have been isolated and identified. However, glycosylated OPCs have not been described in *Crataegus* leaves and flowers to date.^{7,10}

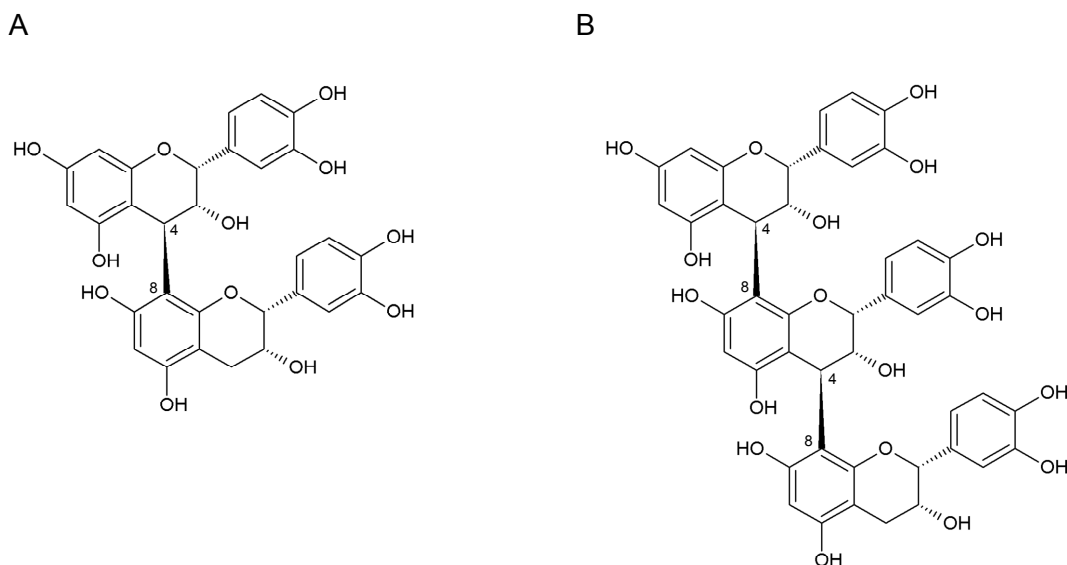


Figure 2 Chemical structure of procyanidin B2 (A) and C1 (B). B-group procyanidins contain a C-C bond between C₄ (upper monomer) and C₆ or C₈ (lower monomer). Trimeric procyanidins are named C-group procyanidins.

1.2.2 Pharmacology, efficacy and safety of *Crataegus* preparations

Several well-performed clinical trials¹¹⁻¹³ and meta-analyses¹⁴ have proven *Crataegus* extracts to be efficacious and safe¹⁵ in the treatment of mild heart failure. In a pooled study, only baseline severity, but not gender turned out to govern the physiological outcomes of WS[®] 1442 treatment.¹⁶ By the aid of animal models as well as *in vitro* experiments, *Crataegus* extracts were shown to exert positive inotropic,^{17,18} anti-arrhythmic¹⁹ and cardio-protective activities.²⁰⁻²⁴ Besides the direct action on the heart, *Crataegus* extracts have been found to influence the vascular endothelium by a NO-mediated vasorelaxation.²⁵⁻²⁸ Furthermore, *Crataegus* extracts were demonstrated to impair platelet function,²⁹ lipid metabolism³⁰ and inflammation.³¹

1.3 The vascular endothelium

The vascular endothelium represents a monolayer of closely juxtaposed endothelial cells (ECs), which line the inner surface of all blood vessels. These cells are covered with a polysaccharide rich layer (glycocalyx) and are attached to a basement membrane (basal lamina). The endothelium is no longer considered as an inert structure to separate blood and tissues, but displays a dynamic size-selective, semi-permeable barrier to regulate the flux of fluids and solutes as well as the entry of

leukocytes into surrounding tissue.³² Moreover, it is perceived as a multifunctional disseminated organ that plays a crucial role in various pathological as well as physiological processes, such as regulation of vascular tone, transport of nutrients, blood flow homeostasis, host defence, or angiogenesis.³³

1.3.1 Regulation of endothelial permeability

Vascular permeability in general describes the passage of proteins, fluids and solutes across the endothelial barrier.³⁴ Macromolecules cross the endothelial barrier transcellularly in a caveolae-mediated vesicular way, whereas molecules less than 3 nm in diameter diffuse between the adjacent cells in a paracellular manner.³⁵ Under physiological conditions, paracellular permeability is limited by interendothelial junctions (IEJs) that are comprised of tight junctions and predominantly adherens junctions (AJs).³⁴ Vascular endothelial (VE)-cadherin represents the most important transmembrane protein forming AJs in ECs. By the aid of catenins, VE-cadherin is associated to the cytoskeleton. Hence, a dynamic homeostasis between acto-myosin mediated cell contraction and intercellular adhesive forces is crucial to retain endothelial barrier function.

However, this barrier function is altered upon pathological conditions such as atherosclerosis, diabetes, inflammation, tumor metastasis or hypertension.³⁶ In most cases, endothelial barrier breakdown, *i.e.* the formation of intercellular gaps,³⁷ is caused by the activation of the contractile machinery leading to the formation of stress fibers and the subsequent disruption of IEJs followed by degradation or internalization.³⁴ Basically, two main signaling pathways regulate paracellular endothelial permeability. Figure 3 illustrates these pathways in agreement with the models described in literature.

On the one hand, there is the barrier protecting cyclic adenosine monophosphate (cAMP) pathway leading to stabilization of IEJs as well as the cortical actin rearrangement. cAMP is able to activate protein kinase A (PKA) which phosphorylates vasodilator-stimulated phosphoprotein (VASP) and subsequently leads to the activation of the Rho GTPase Rac1.³⁸ Rac1 induces translocation of cortactin to the cell borders that promotes the rearrangement of the actin cytoskeleton towards a cortical actin ring.³⁷ Furthermore, cAMP activates the exchange protein directly activated by cAMP (EPAC1) in a PKA independent manner. EPAC1 functioning as guanine nucleotide exchange factor (GEF) activates the Ras-like GTPase Rap1 which results in the

augmentation of VE-cadherin-based cell-cell contacts.^{39,40} Additionally, Rap1 is able to activate Rac1 by the aid of the two GEFs Tiam1 and Vav2.⁴¹

On the other hand, there is the Ca^{2+} -triggered barrier-disrupting pathway causing stress fiber formation and endothelial cell contraction. The Ca^{2+} /calmodulin dependent myosin light chain kinase (MLCK) phosphorylates myosin light chain (MLC) thereby enabling acto-myosin driven endothelial cell contraction. This contraction can be antagonized by myosin light chain phosphatase (MLCP)-evoked dephosphorylation. In addition, Ca^{2+} dependent protein kinase C α (PKC α) activation leads to the formation of actin stress fibers in a RhoA dependent manner. Furthermore, the small GTPase RhoA is able to inhibit MLCP through its downstream effector Rho kinase (ROCK) which enhances MLC phosphorylation.

Besides this explicit separation of both pathways – cAMP and Ca^{2+} – certain interactions exist. These are indicated in Figure 3 as dotted lines. cAMP-dependent PKA is able to prevent MLCK⁴² as well as RhoA⁴³ activity, thereby protecting endothelial barrier function. Then, Rac1 controls RhoA activity.³⁷ Apart from that, PKC α can phosphorylate VE-cadherin³⁵ which disrupts junctional integrity.

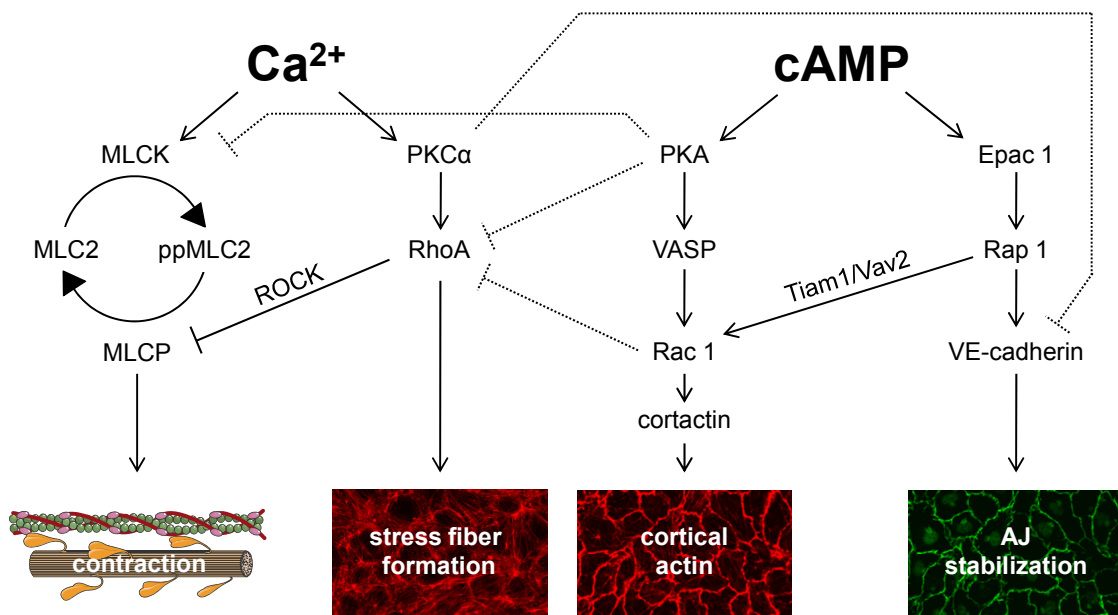


Figure 3 Signaling scheme of endothelial barrier function. Solid lines demonstrate signaling within one pathway. Dotted lines indicate interactions between the two different signaling pathways. Arrows describe activation, dead ends illustrate inhibition.

For our experiments, we used the biogenic amine histamine and the serine protease thrombin to provoke transient endothelial hyperpermeability. Both agents operate *via* Ca^{2+} /PKC/RhoA signaling.³²

1.3.2 Ca²⁺-signaling in endothelial cells

Besides endothelial permeability various endothelial functions depend on changes in intracellular Ca²⁺ concentration ([Ca²⁺]_i). Therefore, calcium ions act as a highly versatile second messenger system in the endothelium. One of the most prominent examples is the Ca²⁺/calmodulin dependent activation of endothelial NO synthase (eNOS) leading to the production of NO⁴⁴ and subsequent vasodilation. Apart from that, cellular processes such as cell proliferation, angiogenesis or, as previously mentioned, endothelial permeability are also regulated by increasing [Ca²⁺]_i.⁴⁵ Usually, intracellular concentrations of free Ca²⁺ amount to approximately 100 nM, *i.e.* 20,000 fold lower than extracellular concentrations.⁴⁶ To ensure this Ca²⁺ gradient across the plasma membrane, intracellular Ca²⁺ is trapped in special Ca²⁺ stores mainly by means of endogenous Ca²⁺ chelators. In endothelial cells, the endoplasmic reticulum (ER) represents the major intracellular Ca²⁺ store and accounts for 75% of the total intracellular Ca²⁺ reserve. Here, Ca²⁺ is bound to special Ca²⁺-binding proteins such as calreticulin thereby reaching Ca²⁺ concentrations of 3 mM within the ER.⁴⁷ Besides this, mitochondria represent another important store of intracellular Ca²⁺ and account for the remaining 25% of the Ca²⁺ pool.

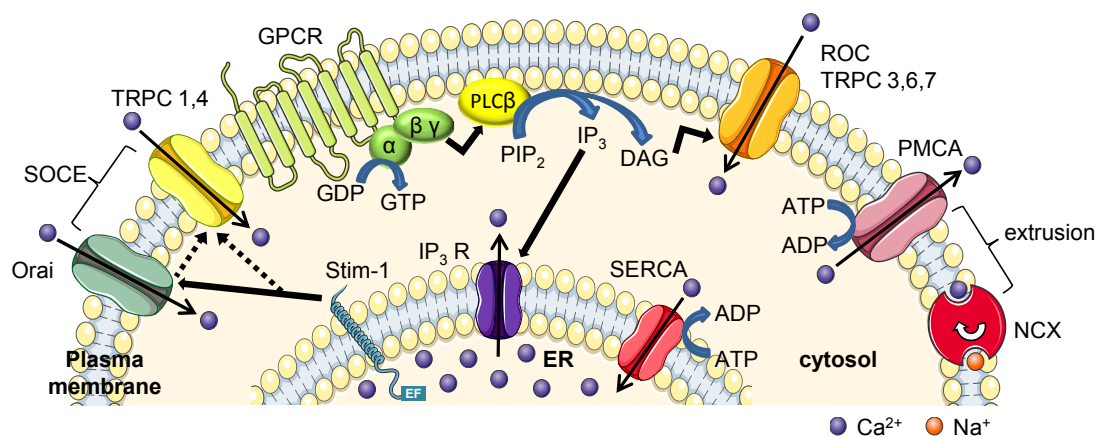


Figure 4 Calcium signaling in endothelial cells. Standard black arrows indicate Ca²⁺ flux across membranes. Black bold arrows demonstrate activation, dotted black arrows illustrate tentative interactions between Stim-1, Orai and TRPC channels.

An increase of [Ca²⁺]_i usually displays the initial response of endothelial cells to hormonal and chemical transmitters⁴⁵ or to mechanical stress.⁴⁸ Similar to other non-excitable cells, this Ca²⁺ rise appears in a biphasic manner: Ca²⁺ release from intracellular stores is followed by Ca²⁺ influx from the extracellular space. Figure 4 illustrates the fundamental properties and mechanisms of endothelial Ca²⁺-signaling.

The most important mechanisms that cause elevated Ca^{2+} levels in the endothelium are moderated by the activation of phospholipase C β (PLC β) through G-protein coupled receptors (GPCR) such as histamine receptor 1 (H_1R) or proteinase-activated receptor 1 (PAR1).^{47,49} PLC β provokes the formation of inositol-1,4,5-trisphosphate (IP_3) and diacylglycerol (DAG). IP_3 generates Ca^{2+} depletion from the ER through IP_3 receptors (IP_3R), whereas DAG activates Ca^{2+} influx from the extracellular space *via* canonical transient receptor potential (TRPC) channels TRPC 3, 6, and 7.^{50,51}

Subsequent to the ER depletion, a Ca^{2+} influx from the extracellular space typically amplifies the elevated cytosolic Ca^{2+} levels.⁵² This phenomenon is called store-operated Ca^{2+} entry (SOCE). But how is the ER depletion linked to SOCE? Hereby, stromal interaction molecule-1 (Stim-1) plays the pivotal role. With an EF-hand domain, Stim-1 senses the luminal Ca^{2+} concentration in the ER.⁵³ Decreasing Ca^{2+} concentrations evoke Stim-1 oligomerization into punctae. Afterwards, Stim-1 translocates to junctions adjacent to the plasma membrane within the ER. Thereby, it can activate proteins of the Orai family which function as pore-forming subunits of SOCE channels.⁵⁴ Additionally, TRPC channels TRPC 1 and 4 seem to be involved in SOCE as well. In contrast to the highly selective Orai channels, TRPC channels represent non-selective cation channels.⁵² However, it is not yet entirely clarified, whether TRPC channels are associated to Stim-1 and Orai or not.

To recover Ca^{2+} baseline levels, endothelial cells can either refill the ER by sarcoplasmic/endoplasmic reticulum Ca^{2+} ATPase (SERCA) or export excessive Ca^{2+} to the extracellular space by the plasma membrane Ca^{2+} ATPase (PMCA) and the $\text{Na}^+/\text{Ca}^{2+}$ -exchanger (NCX).⁵⁵⁻⁵⁷ Interestingly, SERCA is also responsible to compensate spontaneous Ca^{2+} leakage out of the ER.

2 MATERIALS AND METHODS

2.1 Materials

2.1.1 *Crataegus* extract WS[®] 1442

The *Crataegus* extract WS[®] 1442 was kindly provided by Dr. Willmar Schwabe GmbH & Co. KG (Karlsruhe, Germany). It is a well-defined special dry extract of leaves and flowers of mainly *Crataegus monogyna* and *laevigata* (4-6.6:1), standardized to a content of 17.3-20.1% oligomeric proanthocyanidins. For extraction, ethanol 45% (w/w) was utilized.

The extract was freshly dissolved to a concentration of 100 µg/ml, thereby using 0.1% DMSO for complete solubilization.

2.1.2 Fractions of *Crataegus* extract WS[®] 1442

WS[®] 1442 was stepwise fractionated using different chromatographic methods as indicated in the fractionation scheme (Figure 5). Most of the fractionation was performed by Evelyn Hartung within her Master Thesis⁵⁸ at the Ludwig-Maximilians-University Munich in collaboration with Dr. Willmar Schwabe GmbH & Co. KG.

The first fractionation step of WS[®] 1442 was designated 30 to 36 containing 4 different fractions. Subfractions of fraction 32 were numbered 32.1 to 32.10 for example.

The new fractions were investigated by immunocytochemistry (subfractions 34.x) or Ca²⁺ measurement (subfractions 32.x and the derived subfractions), respectively. Only those subfractions showing biological activity in these assays were taken into consideration and underwent additional subfractionation steps.

In a first case, WS[®] 1442 subfractions were utilized in fixed concentrations of 5 µg/ml or 10 µg/ml. Alternatively, subfractions were applied in concentrations related to their weight proportion (yield) of the original extract (100% $\hat{=}$ 100 µg/ml).

Similar to WS[®] 1442, subfractions were also dissolved using 0.1% DMSO just before starting the experiment.

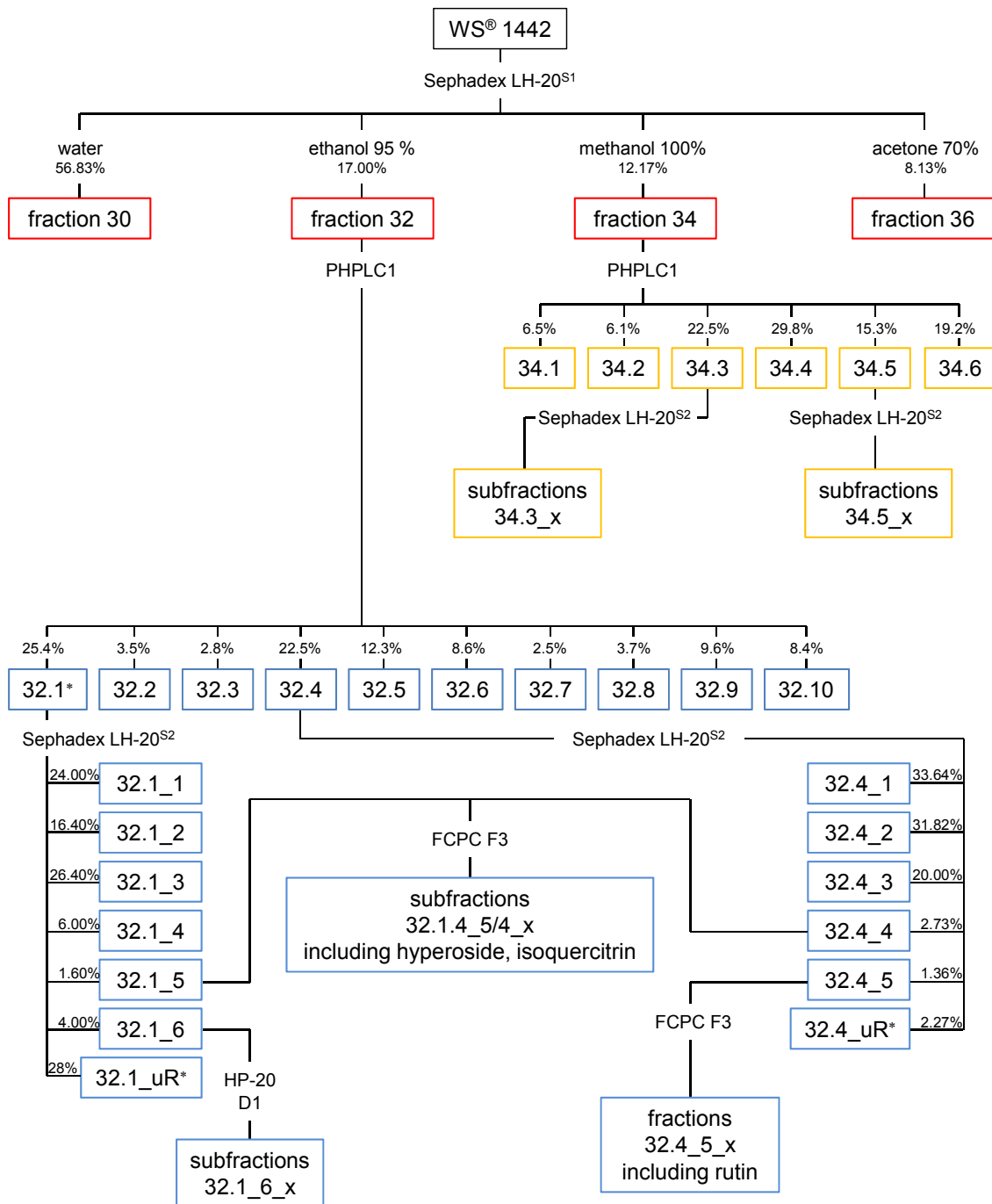


Figure 5 Fractionation scheme of WS® 1442. WS® 1442 was stepwise fractionated using different kinds of chromatography as indicated. *, insoluble residue. Fractions/subfractions were provided by Dr. Willmar Schwabe GmbH & Co. KG.

2.1.3 Biochemicals, inhibitors and cell culture reagents

Table 1 Biochemicals

Reagent	Producer
Non-fat dry milk powder (Blotto)	Carl Roth, Karlsruhe, Germany
Bovine serum albumin (BSA)	Sigma-Aldrich, Taufkirchen, Germany
DMSO	AppliChem, Darmstadt, Germany
Histamine	Sigma-Aldrich, Taufkirchen, Germany
Thrombin	Sigma-Aldrich, Taufkirchen, Germany
Triton X-100	Merck, Darmstadt, Germany
Tween [®] 20	BDH/Prolabo [®] , Ismaning, Germany

All other used biochemicals were purchased from Sigma-Aldrich, AppliChem, Carl Roth or Merck.

Table 2 Inhibitors

Inhibitor	Producer
2-Aminoethylidiphenyl borate (2-APB)	Sigma-Aldrich, Taufkirchen, Germany
Complete [®] mini EDTA free	Roche diagnostics, Penzberg, Germany
2,5-Di-tert-butylhydroquinone (BHQ)	Sigma-Aldrich, Taufkirchen, Germany
NaF	Merck, Darmstadt, Germany
Na ₃ VO ₄	ICN Biomedicals, Aurora, OH, USA
Ouabain	Sigma-Aldrich, Taufkirchen, Germany
Phenylmethylsulfonyl fluoride (PMSF)	Sigma-Aldrich, Taufkirchen, Germany
Thapsigargin	Santa Cruz, Heidelberg, Germany
U73122	Sigma-Aldrich, Taufkirchen, Germany

Table 3 Cell culture reagents

Reagent	Producer
Amphotericin B 250 µg/ml	AppliChem, Darmstadt, Germany
Collagen A/G	Biochrom AG, Berlin, Germany
Collagenase A	Roche, Mannheim, Germany
Dulbecco's modified Eagle's medium (DMEM)	Sigma-Aldrich, Taufkirchen, Germany
Endothelial Cell Growth Medium (ECGM) with Supplement Mix #C-39215	PromoCell, Heidelberg, Germany
FCS gold	PAA Laboratories, Pasching, Austria
HAT supplement 50x liquid	Invitrogen, Karlsruhe, Germany
M199 medium	PAA Laboratories, Pasching, Austria
MEM amino acids 50x	PAA Laboratories, Pasching, Austria
MEM vitamins 100x	PAA Laboratories, Pasching, Austria
Penicillin/Streptomycin 100x	PAA Laboratories, Pasching, Austria

2.2 Cell culture

2.2.1 Buffers, solutions and reagents

The following buffers, solutions and reagents were used for the isolation as well as for the cultivation of endothelial cells:

Table 4 Cell culture buffers

PBS (pH 7.4)		PBS ⁺ Ca ²⁺ /Mg ²⁺ (pH 7.4)	
NaCl	123.3 mM	NaCl	137 mM
Na ₂ HPO ₄	10.4 mM	KCl	2.68 mM
KH ₂ PO ₄	3.2 mM	Na ₂ HPO ₄	8.10 mM
H ₂ O		KH ₂ PO ₄	1.47 mM
		MgCl ₂	0.50 mM
		CaCl ₂	0.68 mM
		H ₂ O	

Table 5 Cell culture solutions

Growth medium HUVEC/HMEC		Stopping medium	
ECGM	500 ml	FCS gold	10%
Supplement Mix #C-39215	23.5 ml	M199	
FCS gold	50 ml		
Amphotericin B (250 µg/ml)	5 ml		
Penicillin (10,000 U/ml)/ Streptomycin (10 mg/ml)	5 ml		
DMEM		Growth medium EA.hy926 cells	
DMEM	10 g	FCS	9.9%
NaHCO ₃	0.85 g	HAT	0.99%
HEPES	6 g	DMEM	
Amphotericin B (250 µg/ml)	5 ml		
Penicillin (10,000 U/ml)/ Streptomycin (10 mg/ml)	10 ml		
H ₂ O	ad 1000 ml		
Freezing medium		Trypsin/EDTA (T/E)	
FCS gold	50%	Trypsin	0.05%
DMSO	8%	EDTA	0.02%
Growth medium		PBS	
Collagen G		Collagen A	
Collagen G	0.001%	Collagen A	0.01%
PBS		PBS	

FCS gold (fetal calf serum) was used after heat inactivation: FCS gold was partially thawed for 30 min at room temperature. Afterwards, it was totally thawed at 37°C and finally inactivated at 56°C for 30 min. FCS aliquots were stored at -20°C.

2.2.2 Endothelial cells

Endothelial cells (ECs) were cultured in an incubator (Heraeus, Hanau, Germany) ensuring constant humidity at 37°C with 5% CO₂. Utilizing the PCR detection kit Venor[®]GeM (Minerva Biolabs, Berlin, Germany), cells were routinely tested for mycoplasma contamination. 30 min before use, cell culture flasks, Petri dishes and multiwell plates were coated with Collagen G. Glass coverslips were pretreated with Collagen A. For EA.hy926 cells, coating was not necessary.

2.2.2.1 HMEC-1 – human dermal microvascular endothelial cells

The cell line CDC/EU.HMEC-1 was kindly provided by the Centers for Disease Control and Prevention (Atlanta, GA, USA). Transfecting human dermal microvascular endothelial cells with a plasmid coding for the transforming SV40 large T-antigen led to the formation of the immortalized HMEC-1 cell line. This cell line still maintains endothelial morphologic, phenotypic, and functional characteristics.^{59,60} HMECs were solely used for macromolecular permeability assays.

2.2.2.2 HUVECs – human umbilical vein endothelial cells

Human umbilical cords were kindly provided by Klinikum München Pasing, Frauenklinik München West/Krüsmannklinik, Rotkreuzklinikum München, and Wolfart Klinik Gräfelfing. After childbirth, umbilical cords were deposited in PBS⁺ Ca²⁺/Mg²⁺ containing penicillin (100 U/ml)/streptomycin (100 µg/ml), and stored at 4°C. Cells were freshly isolated every week. The umbilical vein was washed with PBS⁺ Ca²⁺/Mg²⁺, filled with 0.1 g/l collagenase A, and incubated for 45 min at 37°C. To attain endothelial cells, the vein was flushed with stopping medium and the cell suspension was centrifuged (1,000 rpm, 5 min). Subsequently, cells were resuspended in growth medium and plated in a 25 cm² flask (passage #0). After reaching confluency, cells were trypsinized and plated in a 75 cm² flask. Experiments were performed using cells at passage #3.

2.2.2.3 EA.hy926 cells

EA.hy926 cells were kindly provided by C.J.S. Edgell (NC, USA). These cells represent one of the most frequently used and best characterized permanent human umbilical vein endothelial cell line. They were generated by fusing human umbilical vein endothelial cells (HUVECs) with the human lung carcinoma cell line A549 by the aid of polyethylene glycol.⁶¹ This cell line was shown to still possess typical characteristics of the endothelial phenotype and function, like the presence of Weibel-Palade bodies containing von Willebrand factor or the upregulation of ICAM-, VCAM- and E-selectin-expression upon TNF α - treatment.^{60,62} EA.hy926 cells were employed in passages > 65 and cultivated using Dulbecco's modified Eagle's medium (DMEM) containing HAT (hypoxanthin, aminopterin, thymidine) for hybrid cell selection. EA.hy926 cells were exclusively used for calcium measurements.

2.2.3 Passaging

Having reached confluency, cells were either sub-cultured 1:3 in 75 cm² culture flasks or plated for experiments in multiwell-plates, dishes or on glass coverslips. For passaging, medium was removed and cells were washed twice with PBS. Afterwards, cells were incubated with T/E for 1-2 min at 37°C. Thereafter, cells were gradually detached and the digestion was terminated using stopping medium. After centrifugation (1,000 rpm, 5 min, 20°C), the pellet was resuspended in growth medium and cells were finally plated.

2.2.4 Freezing and thawing

HUVECs were only used until passage #3 without intermediate freezing/thawing steps. For freezing, confluent HMECs out of a 75 cm² flask were trypsinized, centrifuged (1,000 rpm, 5 min, 20°C) and resuspended in 3 ml ice-cold freezing medium. 1.5 ml aliquots were frozen in cryovials. After storage at -80°C for 24 h, aliquots were transferred into liquid nitrogen for long-term storage. To thaw cells, a cryovial was warmed to 37°C and the content was immediately mixed with prewarmed growth medium. In order to remove remaining DMSO, cells were centrifuged, resuspended in growth medium and cultured in a 75 cm² culture flask.

2.3 Cell viability assays

2.3.1 CellTiter-Blue[®] Cell Viability Assay

The CellTiter-Blue[®] Reagent contains the indicator dye resazurin. Viable cells retain the ability to reduce this non-fluorescent indicator resazurin into resorufin, which is highly fluorescent. The CellTiter-Blue[®] Cell Viability Assay was performed according to the manufacturer's protocol (Promega Corp., Madison, WI, USA): HUVECs were grown to confluency in 96-well plates and treated as indicated. Afterwards, cells were incubated for 3 h with the CellTiter-Blue[®] Reagent and fluorescence (ex: 560 nm, em: 590 nm) was measured using a SpectraFluorPlus plate reader (Tecan, Crailsheim, Germany).

2.3.2 Trypan Blue staining

HUVECs were cultured in 6-well plates and treated as indicated. Supernatant was collected and cells were washed twice with PBS. Cells were trypsinized and resuspended in M199 containing 10% FCS. Cell suspension and supernatant were mixed. Finally, cells were stained with trypan blue (Sigma Aldrich, Taufkirchen, Germany) and analyzed using a Vi-Cell[™] XR cell viability analyzer (Beckman Coulter, Fullerton, CA, USA).

2.3.3 ATP measurement

The luciferase-catalyzed, ATP dependent oxidation of luciferin causes light emission. This property was utilized to determine cellular ATP contents luminometrically. The ATP Bioluminescence Assay Kit HS II (Roche Diagnostics GmbH, Mannheim, Germany) was performed according to the manufacturer's protocol: Briefly, HUVECs were cultured in 24-well plates and treated as indicated. Cells were incubated for 5 min with pre-warmed lysis buffer to detach the adherent cells. Subsequently, cells were harvested on ice to prevent ongoing cellular events. Afterwards, HUVECs were boiled for cell lysis (2 min, 95°C), centrifuged and supernatants were diluted 1:1 with dilution buffer. Samples were analyzed by integrating the luciferase-generated luminescence signal over 10 s using an Orion II Microplate Luminometer (Berthold Detection Systems, Pforzheim, Germany).

2.4 Western Blot analysis

2.4.1 Sample preparation

Endothelial cells were treated as indicated, washed once with ice-cold PBS and then lysed in modified RIPA lysis buffer for phosphoproteins. Cells were frozen at -80°C . Afterwards, cells were scraped off on ice, transferred to Eppendorf tubes (Peske, Aindling-Arnhofen, Germany) and centrifuged (14,000 rpm, 10 min, 4°C). An aliquot of the supernatant was utilized to determine protein concentration *via* Bradford assay. Remaining supernatant was mixed with Laemmli sample buffer (3x) and samples were finally heated at 95°C for 5 min. Samples were kept at -20°C until Western blot analysis.

Table 6 Buffers for protein sample preparation

Lysis buffer for phosphoproteins		3x Laemmli buffer	
Tris/HCl (pH 7.4)	50 mM	Tris/HCl (pH 6.8)	187.5 mM
NaCl	150 mM	SDS (sodium dodecyl sulfate)	6%
Nonidet NP 40	1%	Glycerol	30%
Deoxycholic acid	0.25%	Bromphenol blue	0.025%
SDS	0.1%	H ₂ O	
Na ₃ VO ₄	0.3 mM	β -Mercaptoethanol	12.5%
NaF	1.0 mM		
β -Glycerophosphate	3.0 mM		
Pyrophosphate	10 mM		
H ₂ O			
Freshly added:			
Complete [®] mini EDTAfree	4.0 mM		
PMSF	1.0 mM		
H ₂ O ₂	600 μM		

2.4.2 Protein quantification – Bradford assay

In order to employ equal amounts of proteins in all samples for Western blot analysis, protein concentrations were determined using the Bradford Assay. After measurement, protein concentration was adjusted by adding Laemmli sample buffer (1x).

Bradford Assay was performed as previously described, thereby using Coomassie Brilliant Blue G250 (Carl Roth, Karlsruhe, Germany) to stain proteins.⁶³ 10 µl protein samples were incubated with 190 µl Bradford solution (Roti[®]-Quant Bradford Reagent, Carl Roth, Karlsruhe, Germany, 1:5 dilution in water) for 5 min upon shaking. Thereafter, absorbance was measured photometrically at 592 nm (Tecan Sunrise Absorbance reader, TECAN, Crailsheim, Germany). Protein standards were obtained by stepwise diluting a 2 mg/ml stock solution of bovine serum albumin (BSA). Linear regression was used to determine the actual protein concentration of each sample.

2.4.3 SDS-Page electrophoresis

According to Laemmli *et al.*,⁶⁴ proteins were separated by discontinuous SDS-polyacrylamide gel electrophoresis (SDS-PAGE). Equal amounts of protein were loaded on discontinuous polyacrylamide gels, which are composed of a separating and a stacking gel. Samples were separated using the Mini-PROTEAN 3 electrophoresis module (Bio-Rad, Munich, Germany). To ensure optimal separation of the proteins, the concentration of acrylamide (Rotiphorese[™] Gel 30, Carl Roth GmbH & Co. KG, Karlsruhe, Germany) in the separating gel was adapted to their molecular weights. Electrophoresis was run at 100 V for 21 min for protein stacking and at 200 V for 45 min for protein separation. By the aid of a prestained protein ladder (PageRuler[™], Fermentas, St. Leon-Rot, Germany), the molecular weight of the proteins was determined.

Table 7 Acrylamide gels and electrophoresis buffer

Separating gel 10%		Stacking gel	
Rotiphorese [™] Gel 30	33.3%	Rotiphorese [™] Gel 30	17%
Tris (pH 8.8)	375 mM	Tris (pH 6.8)	125 mM
SDS	0.1%	SDS	0.1%
TEMED	0.1%	TEMED	0.2%
APS	0.05%	APS	0.1%
H ₂ O		H ₂ O	

Electrophoresis buffer

Tris	0.3%
Glycine	1.44%
SDS	0.1%
H ₂ O	

2.4.4 Tank electroblotting

Subsequent to protein separation, proteins were transferred to a nitrocellulose membrane (Hybond-ECL™, Amersham Bioscience, Freiburg, Germany) by electroblotting.⁶⁵ A blotting sandwich was prepared in a box filled with 1x tank buffer as follows: cathode–pad–blotting paper–separating gel (from SDS-PAGE)–nitrocellulose membrane–blotting paper–pad–anode. The membrane was equilibrated with 1x tank buffer 15 minutes before starting the tank blot. Sandwiches were mounted on the Mini Trans-Blot® system (Bio-Rad, Munich, Germany) and the chamber was filled with ice-cold 1x tank buffer. Additionally, a cooling pack was inserted to avoid excessive heat. Transfers were performed at 4°C, 100 V for 90 min.

Table 8 Tank blotting buffer

5x Tank buffer		1x Tank buffer	
Tris base	240 mM	5x Tank buffer	20%
Glycine	195 mM	Methanol	20%
H ₂ O		H ₂ O	

2.4.5 Protein detection

Prior to the immunological detection of the relevant proteins, unspecific protein binding sites were blocked. For this purpose, the membrane was incubated for 2 h at room temperature in either non-fat dry milk powder 5% (Blotto) or BSA 5%. Afterwards, the membrane was incubated with the respective primary antibody at 4°C overnight. Subsequent to four washing steps with PBS containing 0.1% Tween® 20 (PBS-T), the membrane was incubated with the secondary antibody, followed by four additional washing steps. All incubation steps were performed under gentle agitation. For protein visualization, two different methods have been used depending on the labels of the secondary antibodies: enhanced chemiluminescence or infrared imaging.

2.4.5.1 Enhanced chemiluminescence

Membranes were incubated for 2 h with the HRP-conjugated secondary antibody. In order to detect protein bands, luminol (5-amino-2,3-dihydro-1,4-phthalazinedione) was used as a substrate. The membrane was incubated with ECL (enhanced chemiluminescence) solution for 1 minute (ECL Plus Western Blotting Detection Reagent RPN 2132, GE Healthcare, Munich, Germany). Protected from light, the membrane was exposed to an X-ray film (Super RX, Fuji, Düsseldorf, Germany), which detected the arising luminescence. Subsequently, the film was developed using the Curix 60 Developing system (Agfa-Gevaert AG, Cologne, Germany).

2.4.5.2 Infrared imaging

A secondary antibody coupled to Alexa Fluor[®] 680 with emission at 700 nm was used. Membranes were incubated for 1 h. The incubation as well as the washing procedure were performed protected from light. Protein bands of interest were detected utilizing the Odyssey imaging system (Li-COR Biosciences, Lincoln, NE).

Table 9 Primary antibodies

Antigen	Source	Dilution	In	Provider
β-actin	mouse monoclon.	1:1,000	Blotto 5%	Millipore
phos.-MLC2 ^{T18/S19}	rabbit polyclon.	1:1,000	BSA 5%	Cell Signaling

Table 10 Secondary antibodies

Antibody	Dilution	In	Provider
Alexa Fluor [®] 680 goat anti-mouse IgG	1:20,000	Blotto 1%	Molecular Probes
Goat anti-rabbit HRP	1:10,000	Blotto 1%	Dianova

2.4.5.3 Quantification

The intensity of Western blot bands detected with enhanced chemiluminescence was quantified using the ImageJ Gel analyzer (Version 1.43q; NIH, Bethesda, MD, USA).

Analysis of bands obtained from infrared imaging was performed with the Quant Data function of the Odyssey software (Odyssey 2.1, Infrared Imaging system, Li-COR Biosciences, Lincoln, NE).

2.5 Macromolecular permeability assay

HMECs were grown to confluency on collagen G-coated 12-well Transwell® inserts (pore size 0.4 µm; Corning, New York, NY, USA). At $t = 0$ min, fluorescein isothiocyanate (FITC)-dextran (40 kDa; 1 mg/ml; Sigma-Aldrich, Taufkirchen, Germany) was added to the upper compartment of the Transwell® plates and cells were treated as indicated. Out of the lower compartment, samples were taken at $t = 0/5/10/15/30/60$ min. To analyze the fluorescence increase of the samples (ex: 485 nm, em: 535 nm), a SpectraFluorPlus plate reader (Tecan, Crailsheim, Germany) was used. Mean fluorescence of samples from untreated cells at $t = 60$ min was defined as 1.0. Data are expressed as percent increase of fluorescence versus control.

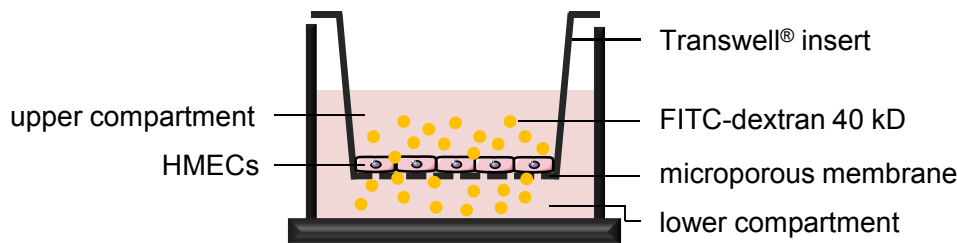


Figure 6 Scheme of a Transwell® insert with a HMEC monolayer

2.6 Immunocytochemistry and confocal laser scanning microscopy

A Zeiss LSM 510 META confocal microscope (40x oil objective, Zeiss, Oberkochen, Germany) was used to obtain immunofluorescence images of fixed cells.

HUVECs were grown to confluency in 8-well µ-slides (ibiTreat, ibidi GmbH, Martinsried, Germany). Cells were treated as indicated, washed with warm PBS⁺ Ca²⁺/Mg²⁺ and fixed with 10% Accustain® paraformaldehyde (Sigma-Aldrich, Taufkirchen, Germany) at room temperature for 10 min. After three washing steps with PBS, HUVECs were permeabilized for 2 min with 0.2% Triton X-100. Again, cells were washed three times and subsequently incubated for 20 min with 0.2% BSA to block unspecific binding. Thereafter, cells were incubated over night with the primary antibodies in 0.2% BSA at 4°C. Following three washing steps with PBS, cells were incubated for 1 h at room temperature with the respective AlexaFluor®-labeled secondary antibodies or rhodamine-phalloidin for F-actin staining in 0.2% BSA. Finally, preparations were again washed three times with PBS, embedded in FluorSave™

Reagent mounting medium (Merck, Darmstadt, Germany) and covered with 8 mm x 8 mm glass coverslips (custom made by Helmut Saur Laborbedarf, Reutlingen, Germany). Slides were stored at 4°C protected from light.

Table 11 Primary antibodies

Antigen	Source	Dilution	In	Provider
phos.-cortactin ^{Y421}	rabbit polyclon.	1:400	BSA 0.2%	Cell Signaling
VE-cadherin	mouse monoclon.	1:400	BSA 0.2%	Santa Cruz

Table 12 Secondary antibodies

Antibody/dye	Dilution	In	Provider
Alexa Fluor® 488 goat anti-rabbit IgG (H+L)	1:400	BSA 0.2%	Molecular Probes
Alexa Fluor® 633 goat anti-mouse IgG (H+L)	1:400	BSA 0.2%	Molecular Probes
rhodamine-phalloidin	1:400	BSA 0.2%	Molecular Probes

2.7 Patch clamp recordings

The patch clamp recordings were kindly performed by Dr. Oleksandr Bondarenko in the lab of Prof. Graier (Institute for Molecular Biology and Biochemistry, Medical University Graz, Austria).

HUVECs were grown on glass coverslips. Membrane potential was recorded by patch-clamp technique in a current-clamp mode using a List EPC7 amplifier (List, Germany). Borosilicate glass pipettes were pulled with a Narishige puller (Narishige Co. Ltd, Tokyo, Japan), fire-polished and had a resistance of 4–5 MΩ. The signals obtained were digitized with a sample rate of 10 Hz utilizing a Digidata 1200A A/D converter (Axon Instruments, Foster City, CA, USA). Data collection and analysis were performed with the Clampex and Clampfit software of pClamp (version 8.2, Axon Instruments). Figures show representative traces of a single cell measurement obtained from one adjacent cell out of a cell cluster. For K⁺-free measurements, the standard external solution was adapted to 150 mM NaCl to compensate the absence of KCl whereas all the other constituents remained unchanged.

Table 13 Buffers for patch-clamp measurements

Standard external solution (pH 7.4/NaOH)		Solution filled in patch pipette (pH 7.2/KOH)	
NaCl	145 mM	Potassium aspartate	100 mM
KCl	5 mM	KCl	40 mM
MgCl ₂	1.2 mM	HEPES	10 mM
HEPES	10 mM	MgCl ₂	1 mM
Glucose	10 mM	EGTA	0.2 mM
CaCl ₂	2.4 mM	H ₂ O	
H ₂ O			

2.8 Calcium imaging

To analyze cellular calcium responses, two different methods were used: Fura-2 calcium imaging and FRET-based calcium measurements.

Table 14 Frequently used agonists/antagonists of endothelial Ca²⁺-signaling

Agonist/antagonist	
2-APB ⁶⁶	IP ₃ R antagonist
BHQ ⁶⁷	Reversible SERCA antagonist
Histamine ⁶⁸	H ₁ R agonist
Thapsigargin ⁶⁷	Irreversible SERCA antagonist
Thrombin ⁶⁹	PAR1 agonist
U73122 ⁷⁰	PLC antagonist

Table 15 Buffers for Ca²⁺ measurements

Ca²⁺-containing HEPES buffer (pH 7.4/NaOH)		Ca²⁺-free HEPES buffer (pH 7.4/NaOH)	
CaCl ₂	2 mM	NaCl	138 mM
NaCl	138 mM	MgCl ₂	1 mM
MgCl ₂	1 mM	KCl	5 mM
KCl	5 mM	HEPES	10 mM
HEPES	10 mM	EGTA	1 mM
Glucose	10 mM	Glucose	10 mM
H ₂ O		H ₂ O	

**Ca²⁺-containing 0 Na⁺ HEPES buffer
(pH 7.4/KOH)**

CaCl ₂	2 mM
Choline chloride	138 mM
MgCl ₂	1 mM
KCl	5 mM
HEPES	10 mM
Glucose	10 mM
H ₂ O	

**Ca²⁺-free 0 Na⁺ HEPES buffer
(pH 7.4/KOH)**

Choline chloride	138 mM
MgCl ₂	1 mM
KCl	5 mM
HEPES	10 mM
EGTA	1 mM
Glucose	10 mM
H ₂ O	

**EA.hy926-loading buffer
(pH 7.35/NaOH)**

CaCl ₂	2 mM
Choline chloride	135 mM
MgCl ₂	1 mM
KCl	5 mM
HEPES	10 mM
NaHCO ₃	2.6 mM
KH ₂ PO ₄	0.44 mM
Na ₂ HPO ₄	0.34 mM
MEM amino acids 50x	2%
MEM vitamins 100x	1%
Glucose	10 mM
L-Glutamine	2 mM
Penicillin/Streptomycin	1%
Amphotericin B	1%
H ₂ O	

2.8.1 Fura-2 measurements

Changes of cytosolic calcium concentrations were detected ratiometrically using the fluorescent dye Fura-2.⁷¹ Upon calcium binding, the excitation maximum of Fura-2 is shifted from 380 nm to 340 nm, whereas the emission wavelength remains unchanged (510 nm). The emission ratio of 340/380 is directly correlated to the amount of cytosolic calcium. For measurements, a membrane-permeable derivative called Fura-2-acetoxymethyl ester (Fura-2-AM) was applied. Having crossed the cell membrane,

Fura-2-AM is cleaved through cellular esterases resulting in the generation of Fura-2, which is consequently trapped in the cell.

A static tempered and a perfusion system were used for Fura-2 measurements.

2.8.1.1 Perfusion system

The author performed all EA.hy926 cell calcium measurements at Prof. Graier's lab (Institute for Molecular Biology and Biochemistry at Medical University Graz, Austria). Graier's experimental setup of the perfusion system was adopted and successfully established at Prof. Vollmar's lab by the author. Thereafter, HUVEC measurements were carried out in Munich.

All experiments were performed at room temperature (20-23°C). HUVECs were cultured on glass coverslips (Ø 42 mm, Helmut Saur Laborbedarf, Reutlingen, Germany), loaded for 45 min in the dark with 4 µM Fura-2-AM (Biotrend, Cologne, Germany) in HEPES-buffered solution and washed twice. For further procedures the coverslips were mounted into an experimental chamber and perfused (1 ml/min, ismatec MS-reglo peristaltic pump/2 stop tubing Tygon R3607 ID 2.06 mm, IDEX Health & Science GmbH, Glattbrugg, Germany) with the appropriate HEPES-buffered solution. Fluorescence measurements (ex: 340/380 nm, em: 510 nm) were obtained by a Zeiss Axiovert 200 inverted microscope (40x objective) with a Polychrome V monochromator and an IMAGO-QE camera (TILL Photonics). Images were acquired every 3 s and analyzed with the TILLvisION Software 4.0.1.2 (TILL Photonics). Each data point of the graph was calculated from nine randomly chosen cells out of a uniform confluent cell monolayer. F_{340}/F_{380} values of these nine cells are expressed as mean ± S.E.M. One representative plot of each graph is shown for clarity. At least three independent experiments (with not less than three replicates per treatment) using different HUVEC preparations were performed.

In case of EA.hy926 cell measurements, 6 glass coverslips (Ø 30 mm, Paul Marienfeld GmbH & Co.KG, Lauda Königshofen, Germany) were loaded simultaneously for 45 min in the dark with 4 µM Fura-2-AM in EA.hy926-loading buffer. Cells were washed twice and kept in loading buffer at room temperature protected from light until measurement. The perfusion rate amounted to 2 ml/min. For data acquisition, a Zeiss Axiovert 200 M (40x oil objective, Zeiss) microscope, a polychromator illumination system (VisiChrome High Speed, Xenon lamp, Visitron Systems, Puchheim, Germany) and a thermoelectric-cooled CCD camera (Photometrics Coolsnap HQ, Visitron Systems)

were utilized. Data recordings and analysis were achieved by VisiView 2.0.6 (Universal Imaging, Visitron Systems, Puchheim, Germany). Experiments were performed once with at least three replicates per treatment.

2.8.1.2 Static tempered system

Experiments were performed at 37°C. HUVECs were grown to confluency on ibidi 8-well μ -slides (ibiTreat, ibidi GmbH) and incubated for 30 min with 2 μ M Fura-2-AM in HEPES buffer, washed twice, and treated as indicated. Fluorescence measurements were obtained using an incubator in addition to the identical technical equipment as described above. For each sample, a total period of 30 min with images being acquired every 5 s was analyzed with the TILLvisION Software 4.0.1.2 (TILL Photonics). Each data point of the different graphs was calculated from a randomly chosen rectangle containing at least 20 adjacent cells, of which mean values are expressed. One representative plot of each graph is shown for clarity. At least three independent experiments (with at least two replicates per treatment) using different HUVEC preparations were performed.

2.8.2 FRET analysis using D1ER

All FRET analyses were performed by the author in Prof. Graier's lab.

In this study, we took advantage of fluorescence resonance energy transfer (FRET) to detect alterations in the free Ca^{2+} concentration of the endoplasmic reticulum (ER) using the D1ER cameleon.⁷²⁻⁷⁴ The D1ER plasmid contains a mutant calmodulin (CaM)/skeletal muscle myosin light chain kinase (skMLCK) pair that is cloned between ECFP (donor) and citrine (acceptor). Moreover, a calreticulin signal sequence and a KDEL (lysine, aspartic acid, glutamic acid, leucine) ER-retention tag are inserted to facilitate an effective and specific localization of the construct inside the ER. Upon Ca^{2+} -binding, CaM wraps around M13 (CaM binding peptide of skMLCK) leading to a conformational change of the construct which in turn allows FRET.

For measuring FRET, cells were excited at 420 nm (ECFP) and the emitting fluorescence of ECFP (480 nm) as well as citrine (535 nm) were recorded to calculate the emission ratio of both wavelengths. This ratio is correlated to the free $[\text{Ca}^{2+}]_{\text{ER}}$.

2.8.2.1 Cell transfection

For transfection experiments, cDNA for D1ER was inserted into a pcDNA3 vector (Invitrogen, Karlsruhe, Germany). HUVECs and EA.hy926 cells were plated on glass coverslips (\varnothing 30 mm, cultured in 6-well plates) to approximately 80% confluency and transiently transfected with the plasmid DNA using the TransFast™ (Promega, Vienna, Austria) transfection reagent. For this purpose, 1.5 μ g DNA per each 6-well were diluted in 1 ml transfection medium (HUVEC: M199, EA.hy926: DMEM without Pen/Strep, AmB), mixed with 4 μ l TransFast™ reagent and incubated for 15 min at room temperature. Meanwhile, cells were washed once with transfection medium to exclude remaining FCS and antibiotics. Then, medium was removed and cells were incubated for 1 h with 1 ml of the transfection mixture at 37°C. Thereafter, 1 ml of pre-warmed culture medium was added per well. 4-5 h later, this medium mixture was aspirated and replaced by 2 ml of culture medium. Experiments were performed 48 h (EA.hy926 cells: 24 h) after transfection.

2.8.2.2 FRET measurements

Transfected cells were washed twice, transferred into the experimental chamber, perfused (2 ml/min) with HEPES-buffered solution and treated as indicated.

Images were obtained by using a Zeiss Axiovert 200 M (40x oil objective, Zeiss) microscope, a polychromator illumination system (VisiChrome High Speed, Xenon lamp, Visitron Systems, Puchheim, Germany) and a thermoelectric-cooled CCD camera (Photometrics Coolsnap HQ, Visitron Systems). D1ER-expressing cells were excited at 420 nm (high speed monochromator, Visitron Systems) and emission was recorded at 480 and 535 nm. Emission filters were adjusted through a filter-wheel (MAC 6000, Ludl Electronic Products, Hawthorne, NY, USA). Devices were controlled and data were recorded by VisiView 2.0.6 (Universal Imaging, Visitron Systems, Puchheim, Germany). To compensate the signal decay in the F535/F480 ratio during the experiments, which was probably due to photobleaching or photochromism of D1ER, the changes of the ER Ca²⁺ concentration were expressed as (F535/F480)/R₀. Cells were analyzed individually. The graph represents the result of one single cell measurement. Each run was repeated several times within the same experiment. Three independent experiments using different HUVEC preparations were performed. For EA.hy926 cells, experiments were performed once with at least three replicates per treatment.

2.9 Statistical analysis

Bar graph data are standardized to control measurements and expressed as mean \pm S.E.M. Each experiment was at least performed three times. In case of HUVECs, a different preparation (*i.e.* cells from a different donor) was utilized each time. The precise number of independently performed experiments is noted in the respective figure legend. Statistical analysis was performed using the GraphPad Prism software version 5.04 (GraphPad Software, San Diego, CA, USA). To compare only two different groups, a paired *t*-test was performed. For analyzing three or more groups, a one-way analysis of variance (ANOVA) followed by a Newman-Keuls post-test was carried out. Statistical significance was assumed if $p \leq 0.05$.

3 RESULTS

3.1 Mechanisms of WS[®] 1442-induced Ca²⁺-signaling in endothelial cells

Our group previously demonstrated that WS[®] 1442 preincubation prevents thrombin-induced Ca²⁺ response in HUVECs.² In the present study, we hypothesized that WS[®] 1442 preincubation *per se* elevates calcium baseline levels. Therefore, the first aim of this study was to explore the mechanisms of how WS[®] 1442 affects [Ca²⁺]_i in the human endothelium.

3.1.1 WS[®] 1442 elevates cytosolic Ca²⁺ levels in human endothelial cells

We investigated the basic impact of WS[®] 1442 on cytosolic Ca²⁺ levels in HUVECs (Figure 7). After a lag time of 5 min, WS[®] 1442 clearly augmented [Ca²⁺]_i, which finally reached a plateau value after 30 min of treatment. In contrast to untreated cells, which show the typical Ca²⁺ response caused by the hyperpermeability-inducing factor histamine, WS[®] 1442 treatment abrogated the histamine-evoked Ca²⁺ signal.

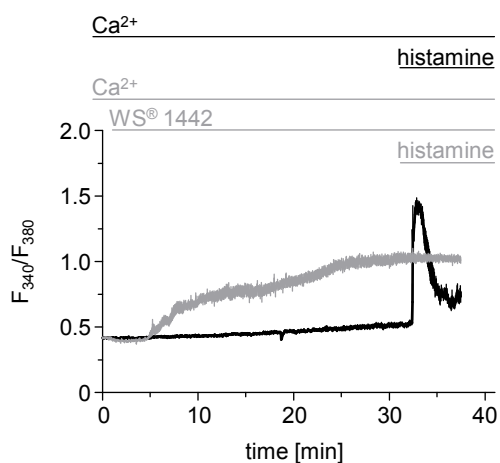


Figure 7 WS[®] 1442 increases [Ca²⁺]_i and prohibits a histamine-evoked Ca²⁺ response. The change of [Ca²⁺]_i was monitored using Fura-2-AM-loaded HUVECs in a perfusion system. Cells were treated for 30 min with WS[®] 1442 (100 µg/ml, grey line) in HEPES buffer or were left untreated (black line). At the end, histamine (100 µM) was added.

To clarify the reversibility of this observed phenomenon, cells were pretreated with WS[®] 1442 for 24 h (Figure 8, grey line). However, even after this pretreatment, freshly added WS[®] 1442 was still able to induce the same calcium response. Again, histamine could not change the elevated Ca²⁺ signal. Also base levels did not show any difference, pointing towards a reversible effect.

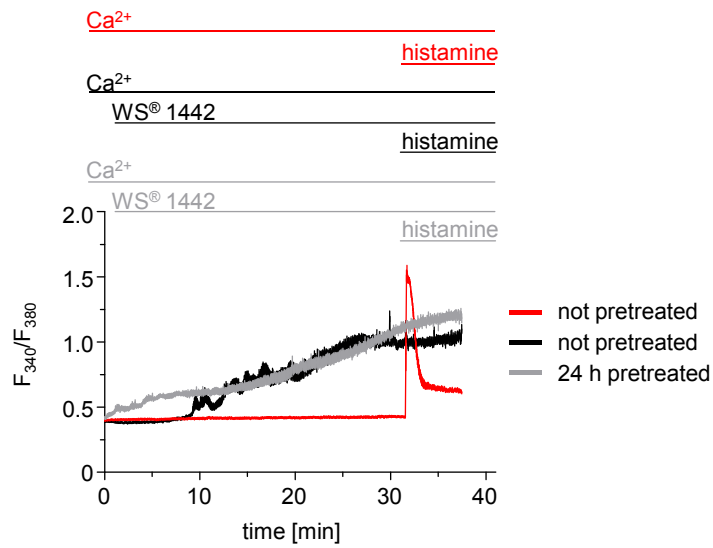


Figure 8 **WS® 1442 reversibly increases $[Ca^{2+}]_i$.** The change of $[Ca^{2+}]_i$ was monitored using Fura-2-AM-loaded HUVECs in a perfusion system. Cells were pretreated with WS® 1442 (100 $\mu\text{g/ml}$) for 24 h (24 h pretreated) or left untreated (not pretreated). Afterwards, cells were treated with WS® 1442 (30 min, 100 $\mu\text{g/ml}$) in HEPES buffer or left untreated. At the end, histamine (100 μM) was added.

Importantly, the rise of $[Ca^{2+}]_i$ was concentration-dependently starting at the lowest effective concentration of 20 $\mu\text{g/ml}$ and reaching saturation between 80-100 $\mu\text{g/ml}$ (Figure 9). Therefore, WS® 1442 was applied at 100 $\mu\text{g/ml}$ for all further experiments. Interestingly, also the onset of the Ca^{2+} signal was affected: higher concentrations led to an earlier onset.

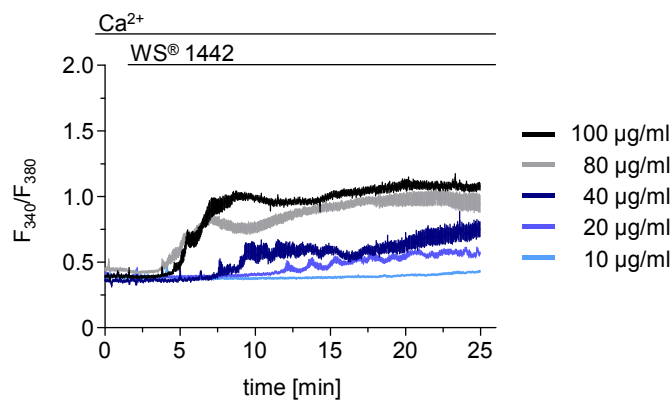


Figure 9 **WS® 1442 causes a concentration-dependent increase of $[Ca^{2+}]_i$.** The change of $[Ca^{2+}]_i$ was monitored using Fura-2-AM-loaded HUVECs in a perfusion system. Cells were perfused with different concentrations (10-100 $\mu\text{g/ml}$) of WS® 1442 in a Ca^{2+} -containing buffer ($n = 3$).

Hence, we conclude that WS® 1442 concentration-dependently increases $[Ca^{2+}]_i$ and inhibits an additional histamine-induced Ca^{2+} response.

3.1.2 WS[®] 1442 does neither influence endothelial barrier function nor endothelial cell contraction

A rise of $[Ca^{2+}]_i$ can trigger actomyosin mediated cell contraction leading to an increase of endothelial permeability.⁷⁵ To check whether WS[®] 1442 alters basal permeability, macromolecular permeability assays were performed. However, WS[®] 1442 did not affect endothelial barrier function (Figure 10) in contrast to the typical $[Ca^{2+}]_i$ -increasing agents thrombin and thapsigargin (irreversible SERCA inhibitor), which clearly induced hyperpermeability.^{76,77}

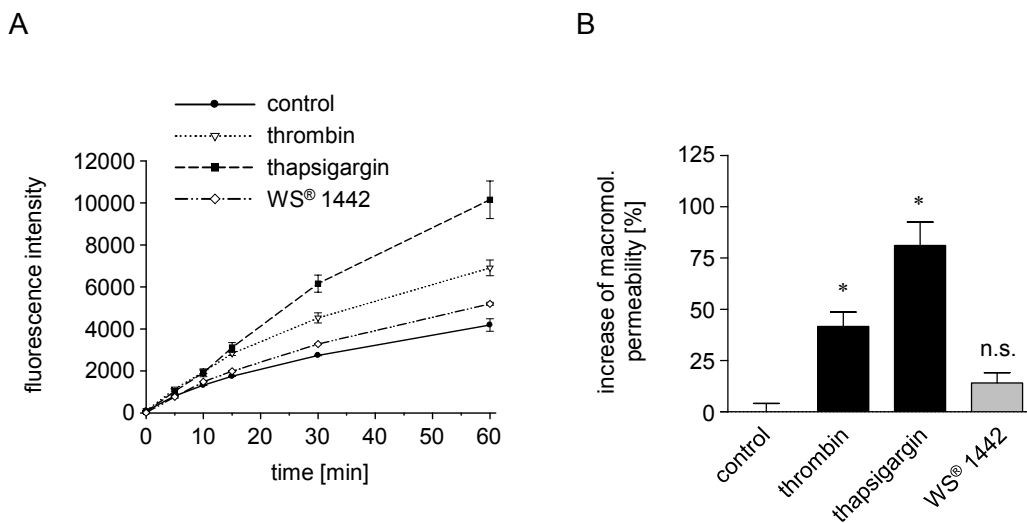


Figure 10 WS[®] 1442 does not induce endothelial hyperpermeability. A macromolecular permeability assay was performed. HMECs were treated with either WS[®] 1442 (100 μ g/ml), thrombin (3 U/ml), thapsigargin (1 μ M) or were left untreated. (A) One representative image illustrating the time course is shown. (B) Data are expressed as mean \pm S.E.M. at t = 60 min. *, $p \leq 0.05$ vs. control (n = 5).

WS[®] 1442 did also not influence endothelial cell contraction (*i.e.* contractile machinery), as indicated by Western blot analysis of the phosphorylation (Thr¹⁸/Ser¹⁹) status of myosin light chain 2 (MLC2). Thrombin and thapsigargin clearly increased MLC activation.

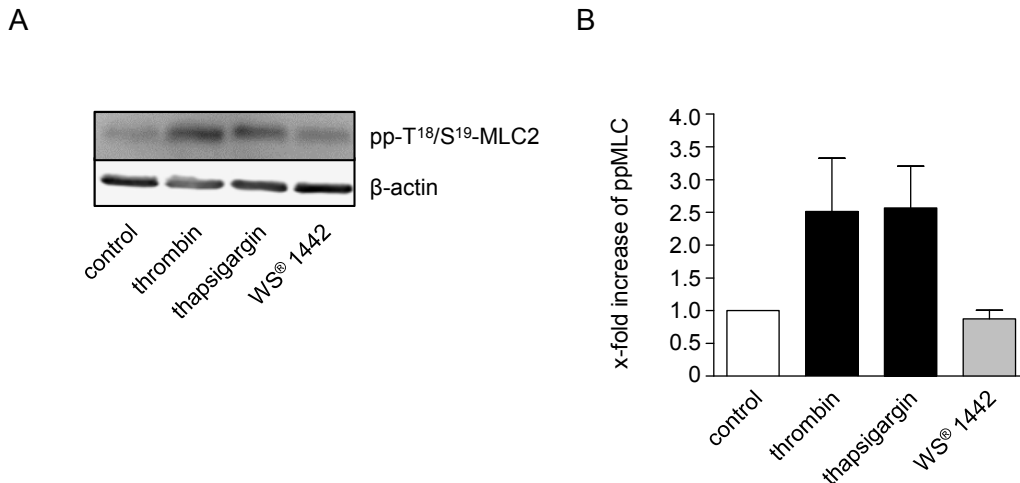


Figure 11 WS[®] 1442 does not increase the amount of phosphorylated myosin light chain (MLC). The phosphorylation status of MLC was investigated by Western blot analysis using a phospho-T¹⁸/S¹⁹-MLC2 antibody. HUVECs were treated for 30 min with thrombin (1 U/ml), thapsigargin (1 μM), WS[®] 1442 (100 μg/ml) or were left untreated. (A) One representative Western blot is shown. (B) Data are expressed as mean ± S.E.M (n = 3).

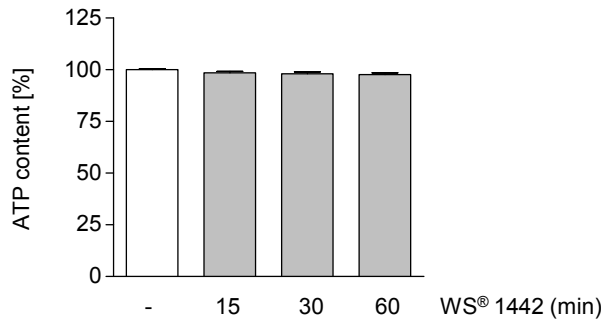
Thus, WS[®] 1442 does not influence basal endothelial barrier function or endothelial cell contraction, which is in striking contrast to typical $[Ca^{2+}]_i$ -elevating agents.

3.1.3 Cell viability is not affected by WS[®] 1442

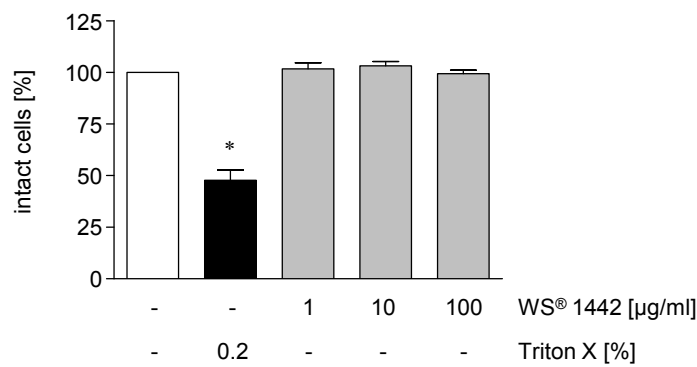
A rise of $[Ca^{2+}]_i$ could be a result of cellular stress induced by WS[®] 1442.^{78,79} To clarify if HUVECs were stressed upon WS[®] 1442 application, we studied various hallmarks of cell vitality, such as ATP content, cell membrane integrity and cellular metabolic activity. The endothelial ATP content did not change upon WS[®] 1442 (100 μg/ml) exposition within 15-60 min (Figure 12A). Moreover, even after long-term treatment (24 h) WS[®] 1442 (1-100 μg/ml) did not alter the percentage of cells with an intact plasma membrane (trypan blue dye exclusion, Figure 12B). At this, the detergent Triton X-100 served as a positive control. In addition, the metabolic activity of HUVECs was also not influenced by WS[®] 1442 (1-100 μg/ml) after 24 h (CellTiter-Blue[®] assay, Figure 12C).

These results demonstrate that WS[®] 1442 does not impair endothelial cell vitality.

A



B



C

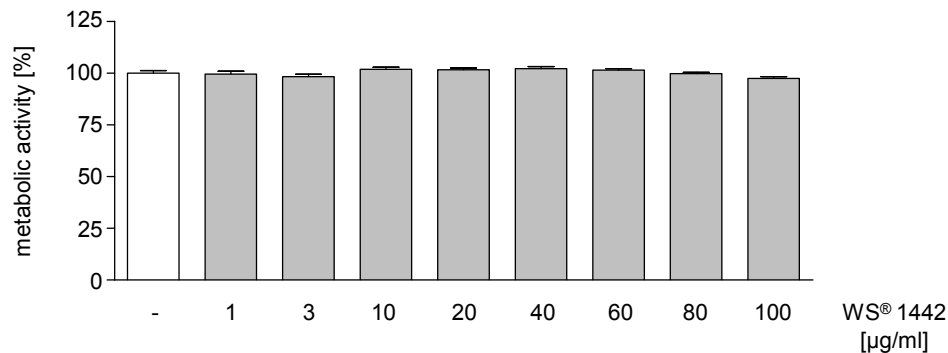


Figure 12 WS[®] 1442 does not impair cell viability. (A) WS[®] 1442 does not modify the cellular ATP content. Cells were treated with WS[®] 1442 (100 µg/ml) for 15, 30 or 60 min. Control cells were left untreated. ATP contents were determined. Data are expressed as mean ± S.E.M. *, $p \leq 0.05$ ($n = 3$). (B) WS[®] 1442 does not alter the proportion of intact cells. For 24 h, cells were either treated with different concentrations of WS[®] 1442 (1, 10, 100 µg/ml) or left untreated and a trypan blue staining was performed. The positive control was incubated with Triton X-100 (0.2%) just before staining. Data are expressed as mean ± S.E.M. *, $p \leq 0.05$ ($n = 3$). (C) The metabolic activity of HUVECs is not changed due to WS[®] 1442 treatment. Cells were treated with different concentrations of WS[®] 1442 (1-100 µg/ml) for 24 h and the CellTiter-Blue[®] assay was performed. Fluorescence intensity of the reduced dye, which correlates to the number of viable cells, was determined. Data are expressed as mean ± S.E.M. *, $p \leq 0.05$ ($n = 3$).

3.1.4 WS[®] 1442 does not interfere with the endothelial Na⁺/K⁺-ATPase

WS[®] 1442 was reported to interfere with the Ca²⁺ response in cardiomyocytes by blocking the Na⁺/K⁺-ATPase similar to the mode of action of cardiac glycosides.¹⁸ Information about an influence of WS[®] 1442 on endothelial Na⁺/K⁺-ATPase is not available. Using patch clamp technique, we investigated whether WS[®] 1442 affects the resting membrane potential of ECs, which is mainly controlled by this ATPase. As mentioned under 2.7, all patch clamp measurements were performed by *Dr. Oleksandr Bondarenko*. WS[®] 1442 transiently depolarized ECs by approx. 4 mV (Figure 13A). In comparison, the cardiac glycoside ouabain, used at a concentration sufficient to block both $\alpha 1$ and $\alpha 2$ ion-transporting subunits of the Na⁺/K⁺-ATPase,⁸⁰ depolarized the cells by approx. 10 mV (Figure 13A). Additional administration of WS[®] 1442 on an already ouabain-depolarized membrane potential had no further influence (Figure 13B).

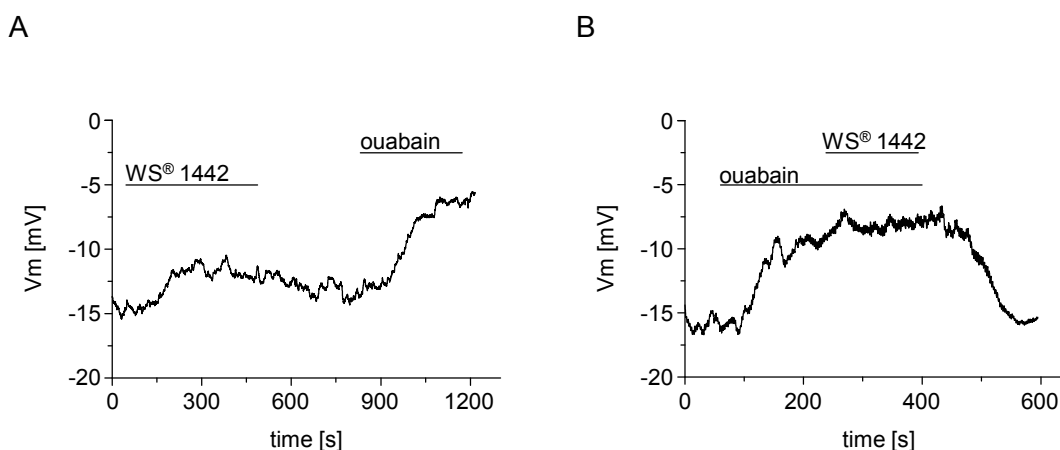


Figure 13 WS[®] 1442 differently affects endothelial membrane potential compared to ouabain. The membrane potential of HUVECs was recorded using patch clamp technique. (A) WS[®] 1442 only slightly depolarizes membrane potential in contrast to ouabain. HUVECs were treated with WS[®] 1442 (100 μ g/ml) for 430 s. After washing out, ouabain (100 μ M) was applied (n = 5). (B) WS[®] 1442 does not alter an already ouabain-depolarized membrane potential. 1 min after starting the run, HUVECs were treated with ouabain (100 μ M). 3 min later, WS[®] 1442 (100 μ g/ml) was added. At the end, both agents were washed out (n = 6).

Employing a K⁺ deprivation/readdition protocol (Figure 14), removal of extracellular K⁺, *i.e.* inhibition of the ATPase, caused a strong endothelial cell depolarization by approx. 11 mV. Accordingly, K⁺ readdition, which reestablished the functionality of the ATPase, repolarized the cell membrane. WS[®] 1442 did only marginally affect this repolarization process.

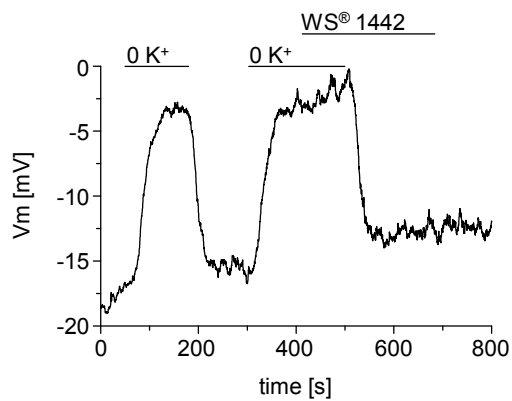


Figure 14 WS® 1442 does not inhibit Na⁺/K⁺-ATPase in HUVECs. The membrane potential of HUVECs was recorded using patch clamp technique. Cells were perfused with K⁺-free buffered solution for approximately 2 min. After K⁺ readdition (2 min), external K⁺ was removed again. 2 min later, cells were treated with WS® 1442 (100 µg/ml). After 1.5 min, external K⁺ was added whilst WS® 1442 treatment remained (n = 5).

Finally, we tested whether inhibition of the Na⁺/K⁺-ATPase by ouabain affects [Ca²⁺]_i in the endothelium. As shown in Figure 15, ouabain – irrespective of the used concentration – did not alter [Ca²⁺]_i.

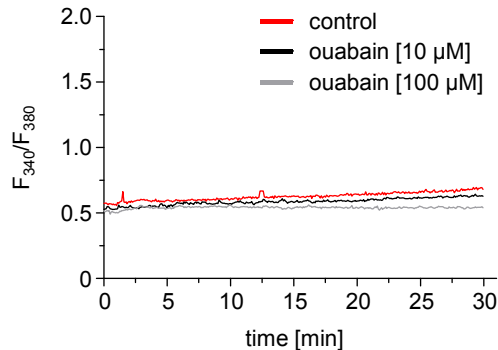


Figure 15 Ouabain does not affect [Ca²⁺]_i in HUVECs. The change of [Ca²⁺]_i was monitored using Fura-2-AM-loaded HUVECs in a tempered static system. 1 min after starting the measurement, ouabain (10 or 100 µM) was added. Control cells were left untreated (10 µM: n = 3, 100 µM: n = 2).

Therefore, our data suggest that WS® 1442 does not evoke the profound increase of [Ca²⁺]_i by targeting the endothelial Na⁺/K⁺-ATPase.

3.1.5 WS[®] 1442 increases $[Ca^{2+}]_i$ by emptying the ER with two different mechanisms involved

Under nominally Ca^{2+} -free conditions, WS[®] 1442 was still able to raise $[Ca^{2+}]_i$ (Figure 16, black line), suggesting that the increase of $[Ca^{2+}]_i$ is generated by intracellular calcium stores. The ER represents the main intracellular Ca^{2+} store. We depleted the ER by a combination of the IP₃-generating agonist histamine and the SERCA pump inhibitor BHQ. Then, histamine was removed and WS[®] 1442 was added, whilst BHQ was permanently present to prevent ER refilling. Upon store depletion, WS[®] 1442 was no longer able to affect cytosolic Ca^{2+} levels (Figure 16, grey line).

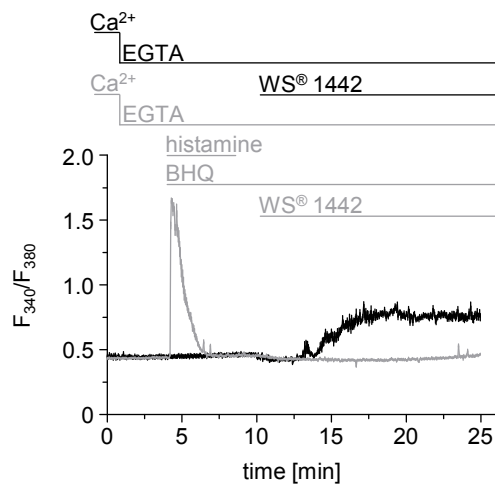


Figure 16 Having depleted the ER by the combination of histamine/BHQ, WS[®] 1442 is no longer able to increase $[Ca^{2+}]_i$. The change of $[Ca^{2+}]_i$ was monitored using Fura-2-AM-loaded HUVECs in a perfusion system. Cells were treated with a combination of histamine (100 μ g/ml)/BHQ (15 μ M) in EGTA-containing (thus Ca^{2+} -free) buffer. After removing only histamine, WS[®] 1442 (100 μ g/ml) was added. Control cells (black line) were only treated with WS[®] 1442 (100 μ g/ml) ($n = 4$).

Single cell Ca^{2+} -imaging FRET experiments were carried out in D1ER-expressing endothelial cells to verify the involvement of the ER. In a Ca^{2+} -containing environment, WS[®] 1442 clearly depleted the ER (Figure 17, grey line). Removal of calcium during a continuing WS[®] 1442 perfusion did not alter the signal. This behavior was similar to that of BHQ-treated cells, which served as control (Figure 17, black line). Interestingly, after removing WS[®] 1442 and switching to a Ca^{2+} -containing buffer, an ER refilling could not be observed, pointing towards an irreversible SERCA inhibition (at least during observation). In contrast, ER refilling immediately started when the reversible SERCA inhibitor BHQ was eliminated.

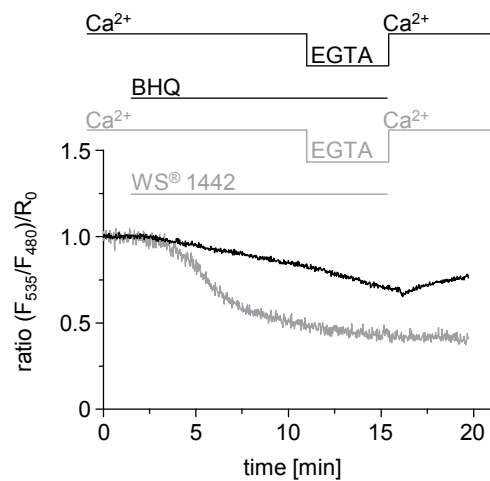
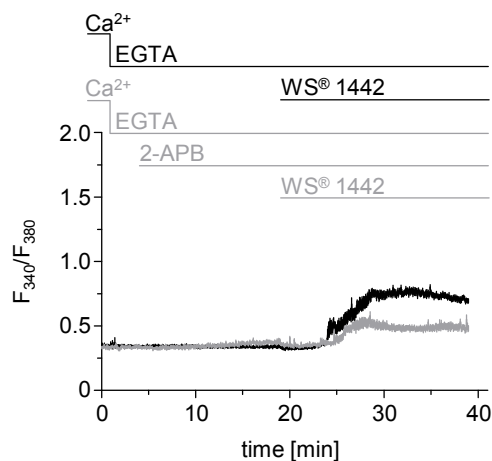


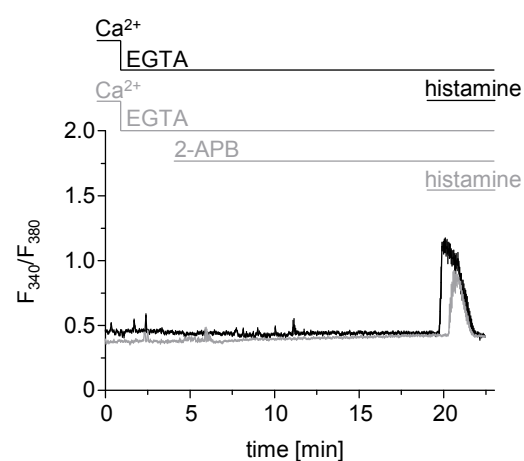
Figure 17 **WS[®] 1442 depletes the ER and prohibits its refilling.** $[Ca^{2+}]_{ER}$ was measured using FRET technique. D1ER transfected HUVECs were treated with either WS[®] 1442 (100 μ g/ml, grey line) or BHQ (15 μ M, black line) in Ca^{2+} -containing buffer. After 9.5 min, Ca^{2+} was removed by switching into EGTA-containing buffer. Approx. 4.5 min later, BHQ or WS[®] 1442 was removed and Ca^{2+} was added ($n = 3$).

Besides SERCA inhibition, the ER is well known to be depleted in endothelial cells by activating the IP₃ receptor, too.⁴⁷ Thus, we applied two different inhibitors of the IP₃ pathway: 2-APB (Figure 18A), an antagonist of the IP₃ receptor, and U73122 (Figure 18C), which blocks the formation of IP₃ by phospholipase C (PLC) inhibition. If endothelial cells were preincubated with these inhibitors in a Ca^{2+} -free buffer, the WS[®] 1442-triggered increase of $[Ca^{2+}]_i$ was either reduced (Figure 18A, grey line) or decelerated (Figure 18C, grey line) compared to control measurements (black lines). Functionality of these inhibitors was proven by confirming their inhibitory action on a $[Ca^{2+}]_i$ increase evoked by histamine (Figure 18B/D).

A



B



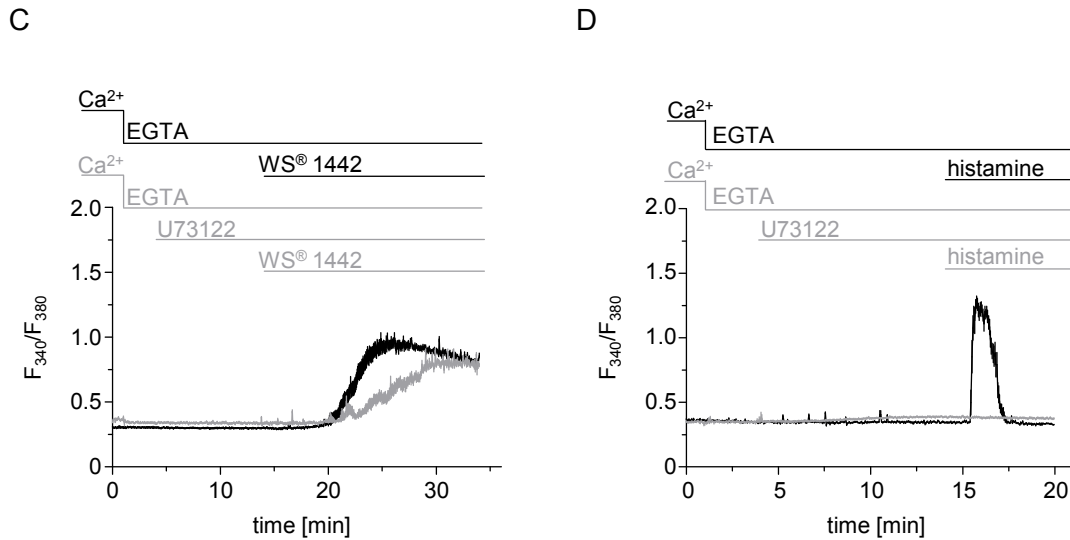


Figure 18 Pharmacological interaction with the IP₃ pathway alters the WS[®] 1442-evoked rise of $[Ca^{2+}]_i$. The change of $[Ca^{2+}]_i$ was monitored using Fura-2-AM-loaded HUVECs in a perfusion system. Cells were pretreated with either 2-APB (A, 100 μ M, 15 min, grey line) or U73122 (C, 1 μ M, 10 min, grey line) in EGTA-containing buffer or were left untreated (black line). Subsequently, WS[®] 1442 (100 μ g/ml) was added ($n = 3$). (B, D) Functionality of each inhibitor is demonstrated using histamine (100 μ M).

We conclude that WS[®] 1442 increases $[Ca^{2+}]_i$ by a dual mechanism: It blocks SERCA and activates the IP₃ pathway.

3.1.6 WS[®] 1442 inhibits store-operated Ca²⁺ entry and Ca²⁺ extrusion capacity

After a lag time of approx. 5 min, WS[®] 1442 clearly increased $[Ca^{2+}]_i$ in a Ca²⁺-containing as well as in a Ca²⁺-free (EGTA) buffer (Figure 19). The plateau values, the onset of the Ca²⁺ signal, and the areas under the curve were identical for the different buffers. This confirms that the WS[®] 1442-evoked rise of $[Ca^{2+}]_i$ does not depend on the extracellular $[Ca^{2+}]$.

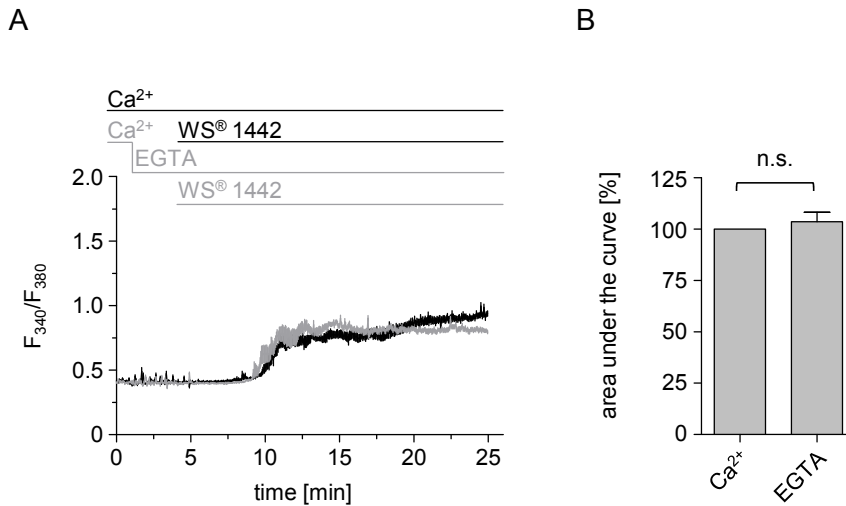


Figure 19 WS® 1442 induces a Ca^{2+} response that is independent of the extracellular $[Ca^{2+}]_i$. The change of $[Ca^{2+}]_i$ was monitored using Fura-2-AM-loaded HUVECs in a perfusion system. HUVECs were treated with WS® 1442 (100 μ g/ml) for 21 min in Ca^{2+} -containing (black line) or Ca^{2+} -free (grey line) buffer ($n = 3$). (A) One representative graph is shown. (B) Area under the curve was calculated taking into account all single graphs of Ca^{2+} -containing and Ca^{2+} -free measurements out of 3 independent experiments. The averaged area under the ratiometric signal was normalized to 100% for the Ca^{2+} -containing results. Data are expressed as mean \pm S.E.M. *, $p \leq 0.05$ ($n = 3$).

In contrast, histamine-treated cell recordings highlight the strong difference between Ca^{2+} -containing and Ca^{2+} -free measurements: In the Ca^{2+} -free buffer, the lack of SOCE prevented the development of an elevated plateau phase (Figure 20A). This effect could be mimicked by pretreating endothelial cells for 24 h with WS® 1442: Applying histamine to these pretreated cells in a Ca^{2+} -containing buffer did no longer cause the typical $[Ca^{2+}]_i$ plateau, suggesting an irreversible SOCE inhibition (Figure 20B).

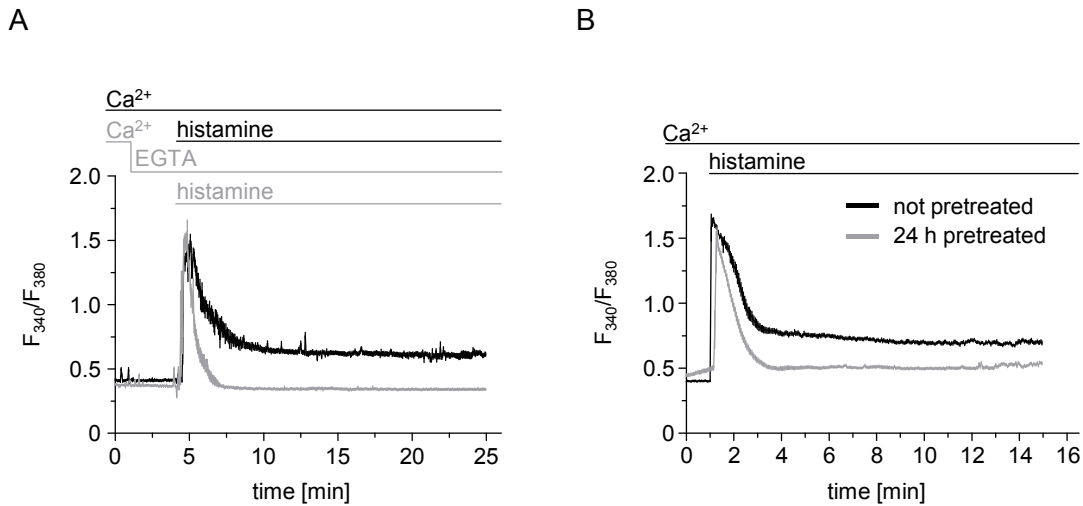


Figure 20 Histamine application on WS[®] 1442-pretreated cells in HEPES buffered solution imitates a Ca^{2+} -free measurement. The change of $[Ca^{2+}]_i$ was monitored using Fura-2-AM-loaded HUVECs in a perfusion system. (A) Histamine induces a Ca^{2+} response, which depends on the extracellular $[Ca^{2+}]_o$. HUVECs were treated with histamine (100 μ M) for 21 min in Ca^{2+} -containing (black line) or Ca^{2+} -free (grey line) buffer, respectively (n = 3). (B) WS[®] 1442 blocks store-operated calcium entry in an irreversible manner. Cells were pretreated for 24 h with WS[®] 1442 (100 μ g/ml) or only with vehicle (not pretreated). 1 min after starting the measurement, cells were perfused with histamine (100 μ M)-containing buffer (n = 4).

Furthermore, we found that the addition of extracellular Ca^{2+} does not alter the increased $[Ca^{2+}]_i$ levels upon application of WS[®] 1442 in a Ca^{2+} -free buffer (Figure 21, red line). This is in obvious contrast to BHQ-treated cells, which exhibited a clear SOCE due to the readdition of extracellular Ca^{2+} (Figure 21, black line). Combining both treatments by preincubating HUVECs with the SERCA inhibitor BHQ in a Ca^{2+} -free buffer before adding WS[®] 1442 also prevented SOCE after Ca^{2+} readdition (Figure 21, grey line).

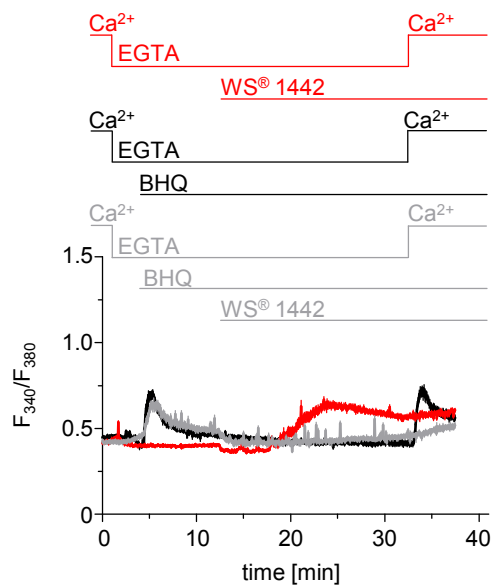


Figure 21 WS® 1442 prohibits BHQ-induced SOCE. The change of $[Ca^{2+}]_i$ was monitored using Fura-2-AM-loaded HUVECs in a perfusion system. In EGTA-containing buffer, HUVECs were treated with either BHQ (15 μ M, black line), WS® 1442 (100 μ g/ml, red line) or a combination of both (grey line), thereby preincubating the cells for 8.5 min with BHQ. At the end, external Ca^{2+} was added by switching to normal buffer ($n = 3$).

Besides the influence of WS® 1442 on Ca^{2+} influx, we investigated if the Ca^{2+} efflux is affected as well. We observed that WS® 1442-induced increase of $[Ca^{2+}]_i$ clearly remained at an elevated level even after extracellular Ca^{2+} had been removed (Figure 22, grey line). This is in striking contrast to histamine: Ca^{2+} removal clearly lowered $[Ca^{2+}]_i$ down to basal levels (Figure 22, black line).

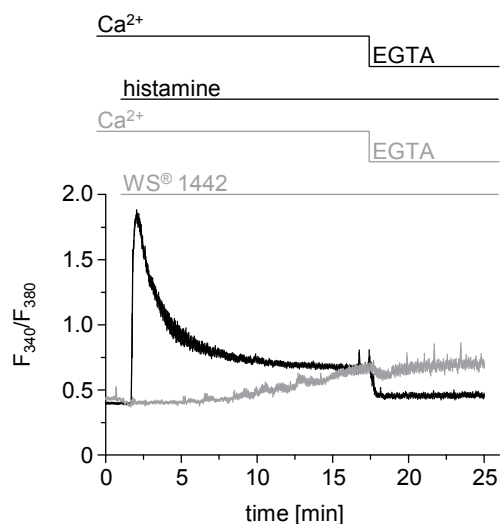


Figure 22 WS® 1442 prohibits the Ca^{2+} extrusion of HUVECs. The change of $[Ca^{2+}]_i$ was monitored using Fura-2-AM-loaded HUVECs in a perfusion system. Cells were treated with either histamine (100 μ M, black line) or WS® 1442 (100 μ g/ml, grey line) in HEPES buffer. 16.5 min later, extracellular Ca^{2+} was removed by changing the buffer solution to an EGTA-containing buffer ($n = 3$).

Thus, WS[®] 1442 prevents the wash out of augmented Ca²⁺ levels in ECs, which explains why the signal remains at an elevated range in the plateau phase even in Ca²⁺-free measurements. Obviously, Ca²⁺ is trapped within the cell at least in the time frame of our experiment, *i.e.* for more than 10 min. Nevertheless, after 24 h we routinely observed normal baseline [Ca²⁺]_i levels even in a Ca²⁺-containing buffer as shown in Figure 8 and Figure 20B.

These results suggest that WS[®] 1442 inhibits Ca²⁺ extrusion capacity and - despite its ER-depleting action - does not induce SOCE. Moreover, WS[®] 1442 even irreversibly prevents agonist-induced SOCE.

3.1.7 WS[®] 1442 induced Ca²⁺-signaling in EA.hy926 cells

Further research in this project will depend on the successful transfection of plasmids or siRNA into endothelial cells, which strongly limits the usage of primary HUVECs. EA.hy926 cells – easily to be transfected – represent a very well established cell line to investigate endothelial Ca²⁺-signaling. Several selected key experiments were performed in EA.hy926 cells to check their response to WS[®] 1442 treatment.

3.1.7.1 WS[®] 1442 increases cytosolic Ca²⁺ levels and inhibits Ca²⁺ extrusion capacity in EA.hy926 cells

WS[®] 1442 immediately increased [Ca²⁺]_i in a peak-plateau shaped manner (Figure 23A). Moreover, we detected that the WS[®] 1442-induced rise of [Ca²⁺]_i clearly remained on elevated levels when extracellular Ca²⁺ had been removed. Even if the extract had been excluded, Ca²⁺ levels still persisted in the elevated status. We further investigated this phenomenon. We applied WS[®] 1442 during the very strong histamine-induced plateau phase which prevented Ca²⁺ extrusion after removal of external Ca²⁺ (Figure 23B, grey line) in contrast to control measurements (Figure 23B, black line). In a Na⁺-free environment, the Na⁺/Ca²⁺-exchanger is deactivated and consequently, Ca²⁺ extrusion can only be generated by the plasma membrane Ca²⁺ ATPase (PMCA). Figure 23C clearly illustrates that Ca²⁺ extrusion was strongly inhibited in Na⁺-free buffer.

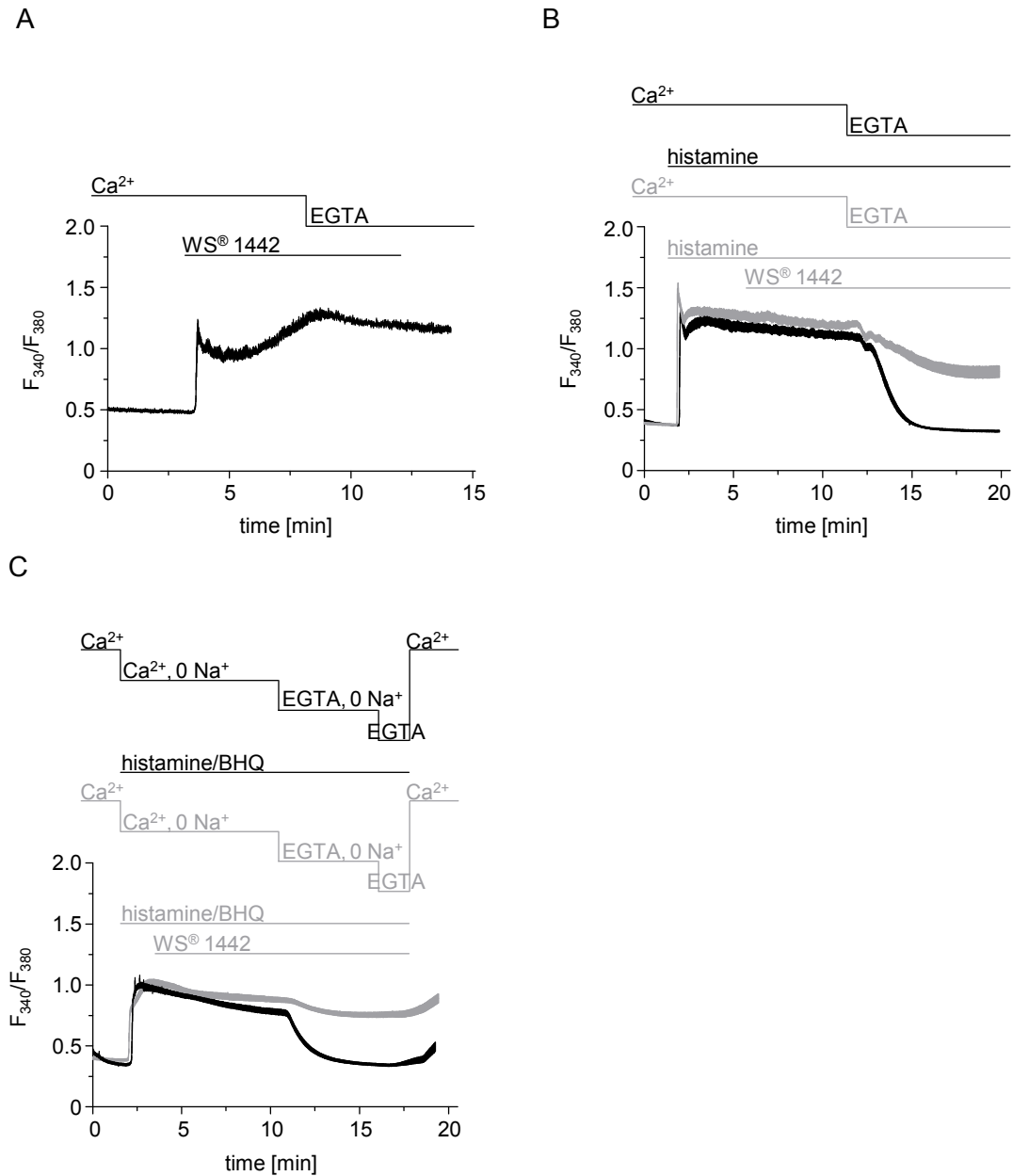


Figure 23 WS[®] 1442 influences [Ca²⁺]_i in EA.hy926 cells. The change of [Ca²⁺]_i was monitored using Fura-2-AM-loaded EA.hy926 cells in a perfusion system. (A) WS[®] 1442 immediately increases [Ca²⁺]_i in EA.hy926 cells. Cells were treated with WS[®] 1442 (100 µg/ml) in HEPES buffer. 5 min later, external buffer was changed into an EGTA-containing buffer. After 4 min, the extract was removed (n = 1). (B) WS[®] 1442 inhibits Ca²⁺ extrusion capacity. Cells were treated with histamine (100 µM) in HEPES buffer. After 5 min, WS[®] 1442 (100 µg/ml) was added and 6 min later, external Ca²⁺ was removed. Control cells (black line) were only treated with histamine (100 µM) (n = 1). (C) WS[®] 1442 alters Ca²⁺ extrusion mainly by blocking PMCA. Cells were treated with a combination of histamine (100 µM)/BHQ (15 µM) in Na⁺-free HEPES buffer. 2 min later, WS[®] 1442 (100 µg/ml) was added. After 7 min, external Ca²⁺ was removed and 5.5 min later, Na⁺ was added. At the end, only pure HEPES buffer was perfused. Control cells (black line) were only treated with histamine (100 µM)/BHQ (15 µM) (n = 1).

Thus, WS[®] 1442 increases $[Ca^{2+}]_i$ and in addition alters Ca^{2+} extrusion capacity mainly by blocking PMCA in EA.hy926 cells.

3.1.7.2 WS[®] 1442 raises $[Ca^{2+}]_i$ by depleting the ER

WS[®] 1442 was still able to raise $[Ca^{2+}]_i$ in EGTA-containing buffer, pointing towards an involvement of intracellular calcium stores (Figure 24A, black line). In Figure 24A (grey line) we used BHQ to deplete the ER. Subsequent to this ER depletion, WS[®] 1442 was no longer able to affect cytosolic Ca^{2+} levels. To verify these data FRET experiments of D1ER-expressing EA.hy926 cells were performed (Figure 24B). In EGTA-containing buffer, WS[®] 1442 clearly depleted the ER. Calcium readdition during a continuing WS[®] 1442 perfusion did not alter the signal. Even after removing WS[®] 1442, an ER refilling could not be observed, suggesting an irreversible SERCA inhibition (at least within our observation period).

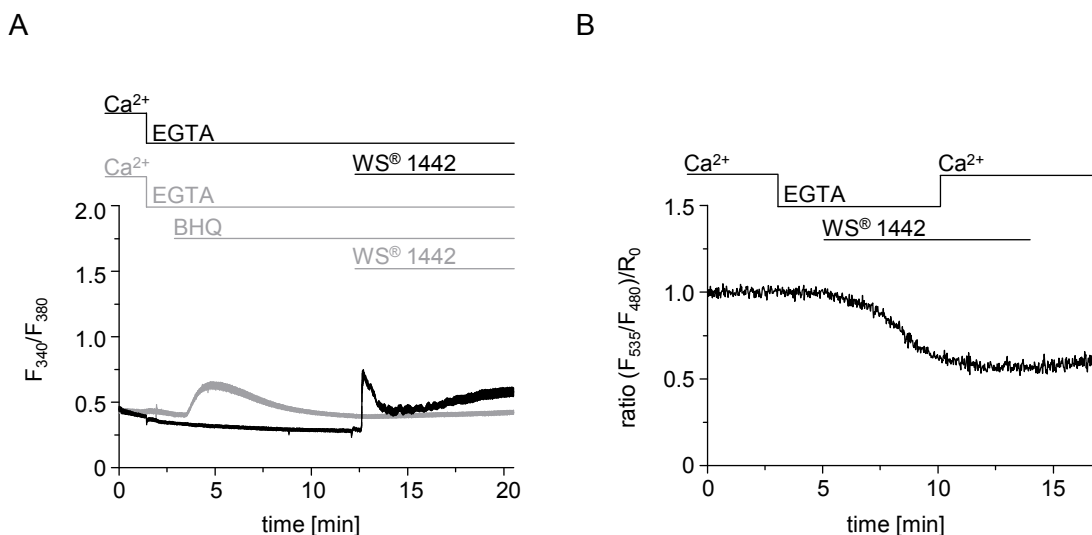


Figure 24 WS[®] 1442 depletes intracellular stores. (A) Having depleted the ER upon BHQ treatment, WS[®] 1442 is no longer able to increase $[Ca^{2+}]_i$. The change of $[Ca^{2+}]_i$ was monitored using Fura-2-AM-loaded EA.hy926 cells in a perfusion system. Cells were treated with BHQ (15 μ M) in EGTA-containing buffer. 9 min later, WS[®] 1442 (100 μ g/ml) was added. Control cells (black line) were only treated with WS[®] 1442 (100 μ g/ml) ($n = 1$). (B) WS[®] 1442 depletes the ER. $[Ca^{2+}]_{ER}$ was measured using FRET technique. D1ER transfected EA.hy926 cells were treated with WS[®] 1442 (100 μ g/ml) in EGTA-containing buffer. After 5 min, Ca^{2+} was added by switching into Ca^{2+} -containing buffer. 4 min later, WS[®] 1442 was removed ($n = 1$).

As a result, WS[®] 1442 increases $[Ca^{2+}]_i$ due to an ER depletion. Moreover, this depletion is at least partly caused by an irreversible SERCA inhibition.

3.2 In search of the bioactive compounds of WS[®] 1442

The original extract had been fractionated into four different fractions using column chromatography. By the aid of these fractions, we recently could show that the two different endothelial signaling mechanisms triggered by the extract can clearly be assigned to specific phytochemical groups of WS[®] 1442.⁴

Table 16 First fractionation of WS[®] 1442

Fraction	Eluate	% (m/m) of WS[®] 1442	Main compounds
30	H ₂ O	56.83	Non-phenolic, aliphatic compounds
32	Ethanol 95%	17.00	Flavonoids
34	Methanol 100%	12.17	Oligomeric proanthocyanidins
36	Acetone 70%	8.13	Proanthocyanidins n > 4

The most prominent activation of the barrier protecting cAMP/Rap1/Rac1 pathway could be detected using fraction 34 (oligomeric proanthocyanidins, OPCs). Concerning the inhibition of the barrier disrupting Ca²⁺/PKC/RhoA signaling, fraction 32 (small phenolic compounds, flavonoids) showed the strongest effect. However, both fractions still represent multi-component systems. For a better understanding of this complex polypharmacology, it would be important to identify the active principles of WS[®] 1442.

Consequently, the second part of this study aimed to elucidate the bioactive compounds of this multi-component phytopharmaceutical. Therefore, fractions 32 and 34, representing the active fractions of WS[®] 1442 in the endothelium, were stepwise subfractionated as indicated in the Materials and Methods part and examined for their endothelial activity.

3.2.1 Subfractions 32.x differently inhibit agonist-induced Ca²⁺-signaling

Fura-2-AM Ca²⁺ measurements were performed to determine which subfraction of fraction 32 still exhibits an inhibitory effect on agonist-induced Ca²⁺-signaling. For all experiments, thrombin was employed to activate the Ca²⁺-signaling cascade. In the following paragraph, only the active subfractions are visualized for clarity.

3.2.1.1 Subfractions 32.x

According to their weight proportion, subfractions were applied in concentrations related to 100 $\mu\text{g/ml}$ of the original extract. Only two out of ten subfractions, *i.e.* subfractions 32.1 and 32.4, could prevent the typical thrombin-induced biphasic Ca^{2+} response (Figure 25A, B). As described above for WS[®] 1442, both subfractions also had raised $[\text{Ca}^{2+}]_i$ during the preceding incubation period (Figure 25C, D).

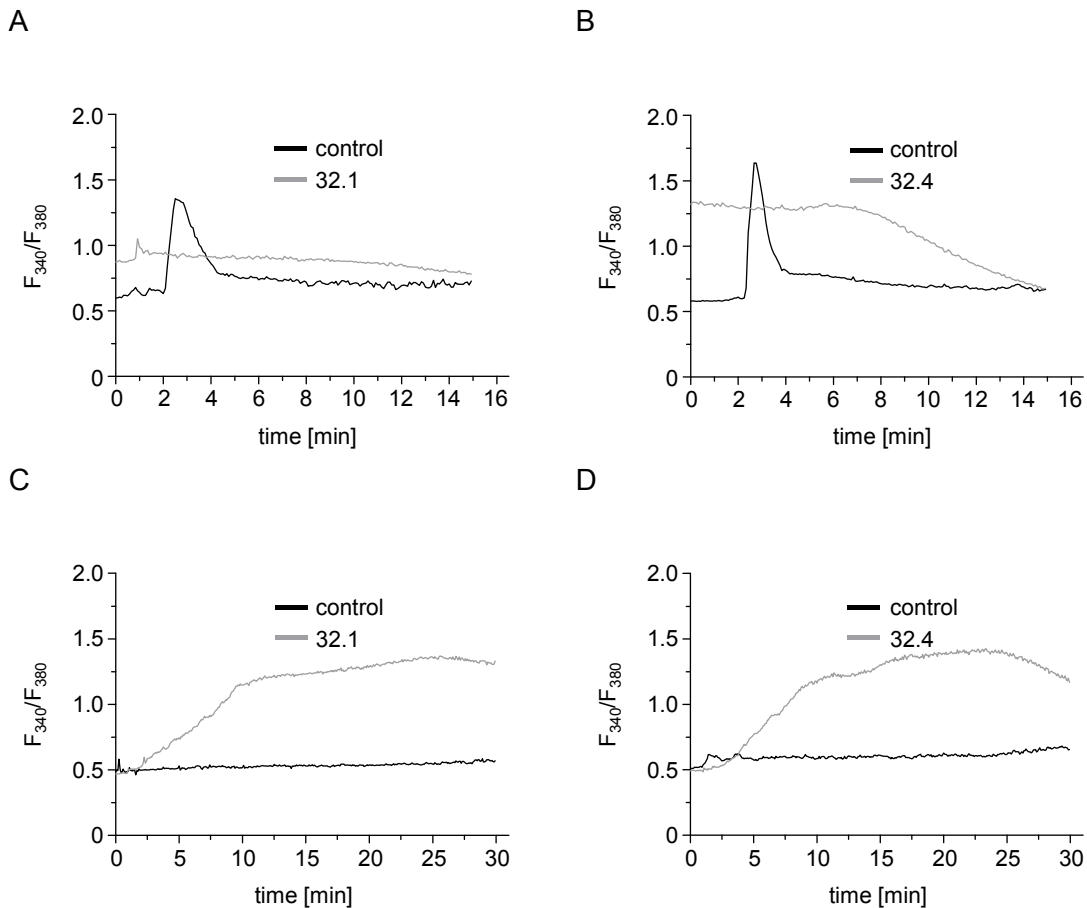


Figure 25 Only subfractions 32.1 and 32.4 affect endothelial Ca^{2+} -signaling. The change of $[\text{Ca}^{2+}]_i$ was monitored using Fura-2-AM loaded HUVECs in a tempered static system. (A, B) Subfractions 32.1 and 32.4 inhibit thrombin-induced Ca^{2+} response in HUVECs. Cells were either preincubated for 30 min with fraction 32.1 (A: 4.32 $\mu\text{g/ml}$), fraction 32.4 (B: 3.83 $\mu\text{g/ml}$) or left untreated. At $t = 1$ min, thrombin (1 U/ml) was added ($n = 3$). (C, D) Subfractions 32.1 and 32.4 raise $[\text{Ca}^{2+}]_i$ in HUVECs. HUVECs were either treated with subfraction 32.1 (C, 4.32 $\mu\text{g/ml}$), subfraction 32.4 (D, 3.83 $\mu\text{g/ml}$) or just vehicle at $t = 1$ min ($n = 3$).

Hence, subfractions 32.1 and 32.4, which represent the major part of fraction 32, were further fractionated (Figure 29) and analyzed.

3.2.1.2 Subfractions 32.1_x

Among subfractions 32.1_x, only subfractions 32.1_5 and 32.1_6 seemed to affect cytosolic calcium levels in concentrations related to their weight proportion. However, thrombin was still able to evoke its Ca^{2+} response (Figure 26A, C). As a result of repeated fractionation, the applied concentrations of the subfractions were already very low. Taking into account the loss of starting material during fractionation, we verified our results enhancing the concentrations to 5 $\mu\text{g}/\text{ml}$ of each subfraction. Once again, subfractions 32.1_5 and 32.1_6 altered cytosolic calcium levels (Figure 26B, D). This time, they even inhibited the Ca^{2+} signal caused by thrombin and exhibited clearly elevated baseline levels.

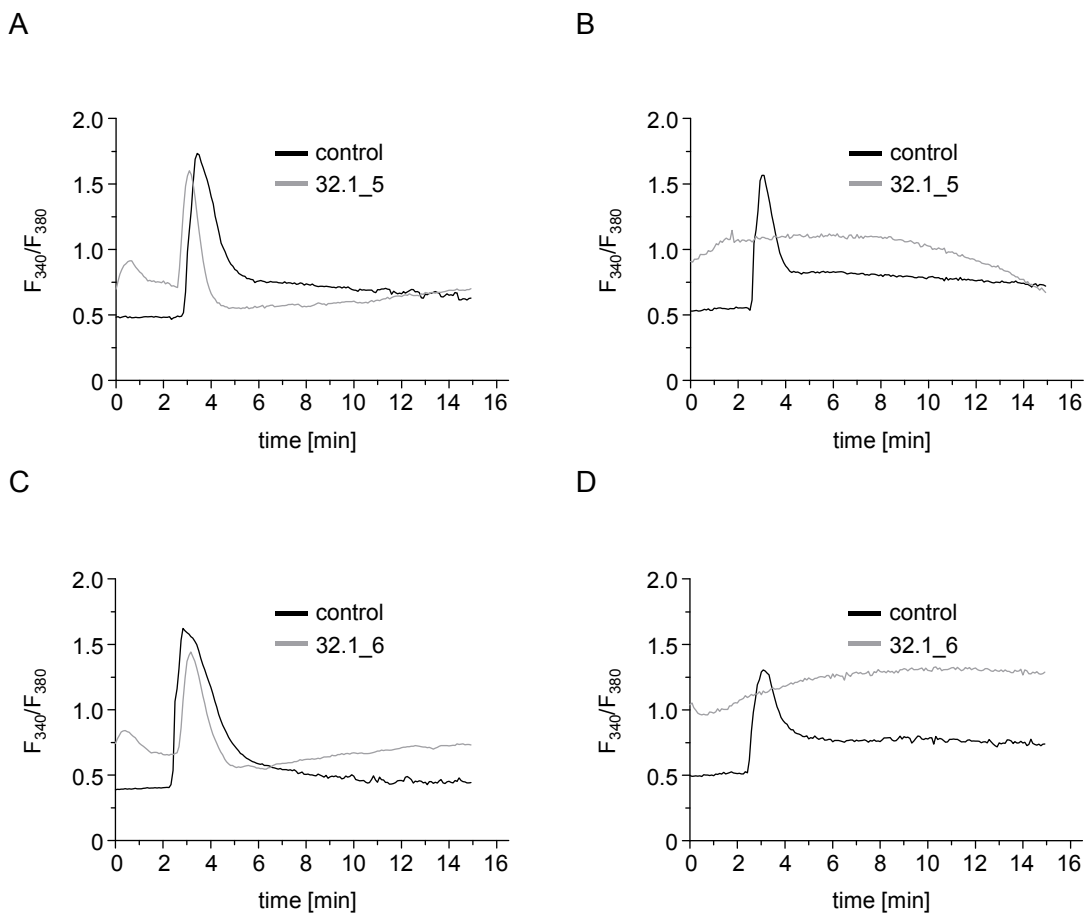


Figure 26 Only subfractions 32.1_5 and 32.1_6 affect endothelial Ca^{2+} -signaling. The change of $[\text{Ca}^{2+}]_i$ was monitored using Fura-2-AM loaded HUVECs in a tempered static system. (A, B) Cells were either preincubated for 30 min with subfraction 32.1_5 (A: 0.07 $\mu\text{g}/\text{ml}$, B: 5 $\mu\text{g}/\text{ml}$), subfraction 32.1_6 (C: 0.17 $\mu\text{g}/\text{ml}$, D: 5 $\mu\text{g}/\text{ml}$) or left untreated. At $t = 1$ min, thrombin (1 U/ml) was added ($n = 1$).

Interestingly, besides the two subfractions mentioned above, subfraction 32.1_uR turned out to influence endothelial Ca^{2+} -signaling as well (Figure 27). Thrombin was no longer able to induce SOCE – indicated through the lack of the elevated plateau phase – after preincubating HUVECs with subfraction 32.1_uR.

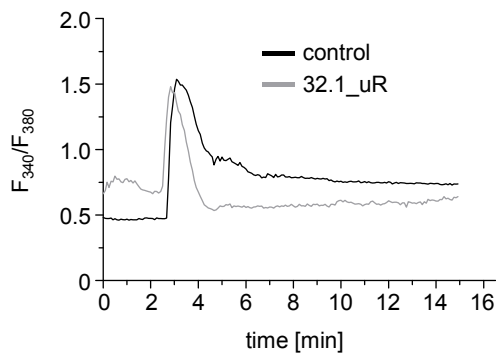


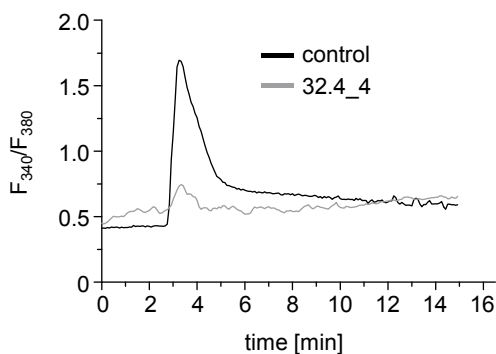
Figure 27 Subfraction 32.1_uR inhibits thrombin induced SOCE in HUVECs. The change of $[\text{Ca}^{2+}]_i$ was monitored using Fura-2-AM loaded HUVECs in a tempered static system. Cells were either preincubated for 30 min with subfraction 32.1_uR (5 $\mu\text{g}/\text{ml}$) or left untreated. At $t = 1$ min, thrombin (1 U/ml) was added ($n = 3$).

As a result, subfractions 32.1_5 and 32.1_6 were further fractionated (Figure 29).

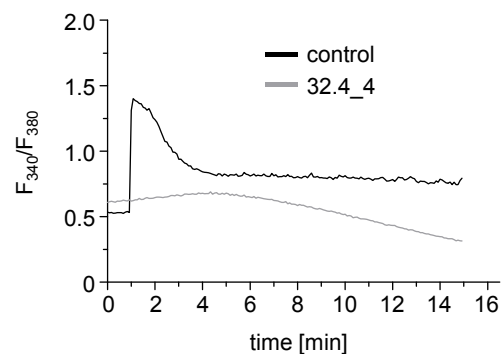
3.2.1.3 Subfractions 32.4_x

Regarding subfractions 32.4_x, we achieved similar results compared to subfractions 32.1_x. Again, the last two subfractions – subfraction 32.4_4 and 32.4_5 – influenced $[\text{Ca}^{2+}]_i$ and inhibited thrombin-evoked Ca^{2+} response (Figure 28A, C). Once more, we reassessed our results by applying both subfractions with 5 $\mu\text{g}/\text{ml}$ (Figure 28B, D): Both subfractions completely inhibited the Ca^{2+} signal caused by thrombin.

A



B



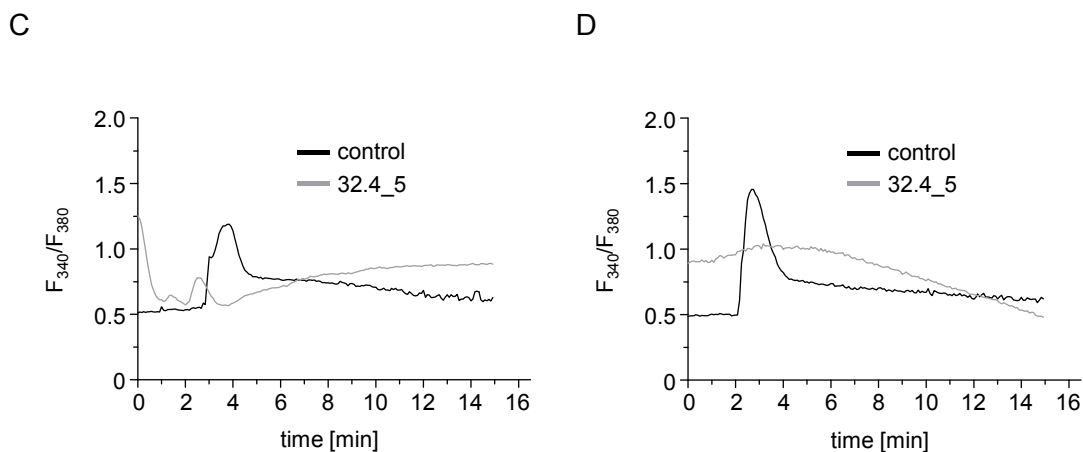


Figure 28 Only subfractions 32.4_4 and 32.4_5 affect endothelial Ca^{2+} -signaling. The change of $[\text{Ca}^{2+}]_i$ was monitored using Fura-2-AM loaded HUVECs in a tempered static system. (A, B) Cells were either preincubated for 30 min with subfraction 32.4_4 (A: 0.1 $\mu\text{g}/\text{ml}$, B: 5 $\mu\text{g}/\text{ml}$), subfraction 32.4_5 (C: 0.05 $\mu\text{g}/\text{ml}$, D: 5 $\mu\text{g}/\text{ml}$) or left untreated. At $t = 1$ min, thrombin (1 U/ml) was added ($n = 1$).

Hence, subfractions 32.4_4 and 32.4_5 were further fractionated.

Interestingly, additional data acquired by *Simone Fuchs* indicate that subfraction 32.4_uR applied with 5 $\mu\text{g}/\text{ml}$ affects SOCE similar to subfraction 32.1_uR.

At the end, the purification process led to the identification of three distinct flavonoids, namely rutin, hyperoside and isoquercitrin. However, these flavonoids did not exhibit any Ca^{2+} -signaling activity (*Simone Fuchs*). Consequently, other flavonoids/compounds that could not be identified so far, are expected to play the decisive role in Ca^{2+} -signaling.

Figure 29 summarizes the action profiles of subfractions 32.x as well as their fractionation scheme. According to this fractionation scheme, subfractions 32.1_x and 32.4_x were separated using the same chromatographic setup. Surprisingly, the sequence of the active subfractions is similar in both fractionation branches, suggesting that corresponding subfractions might contain comparable compounds.

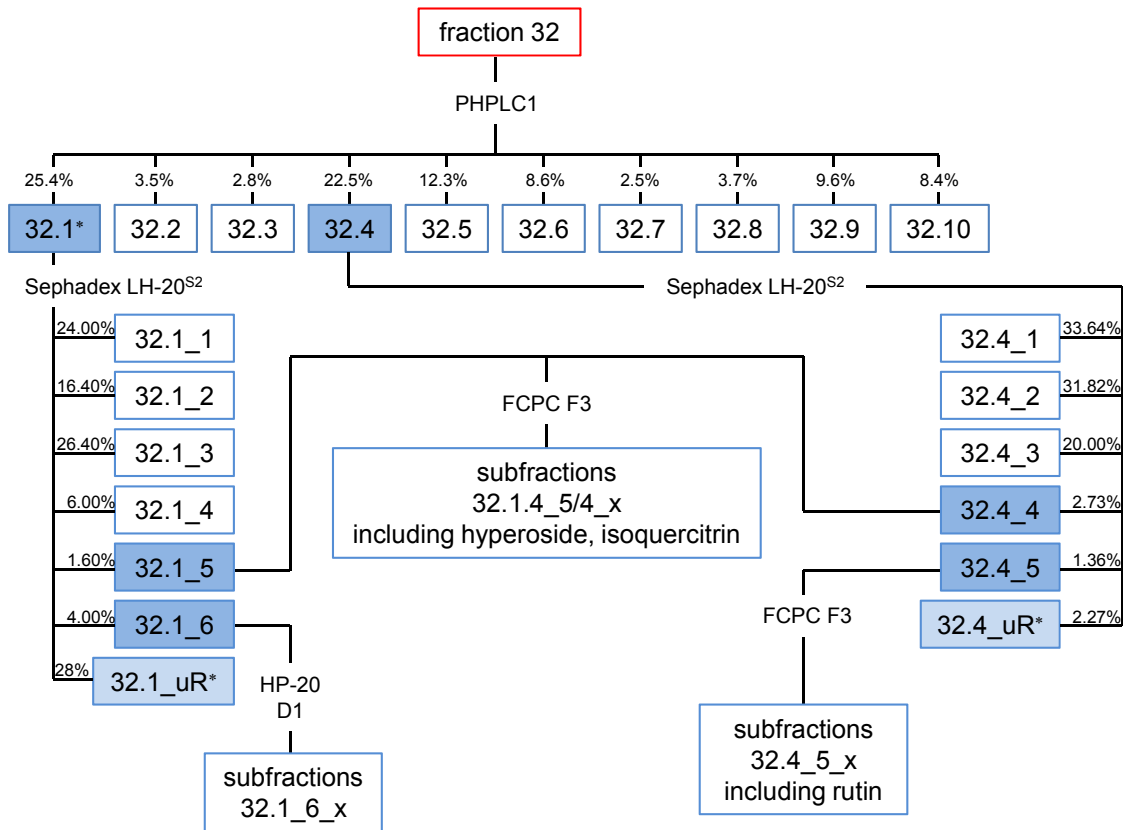
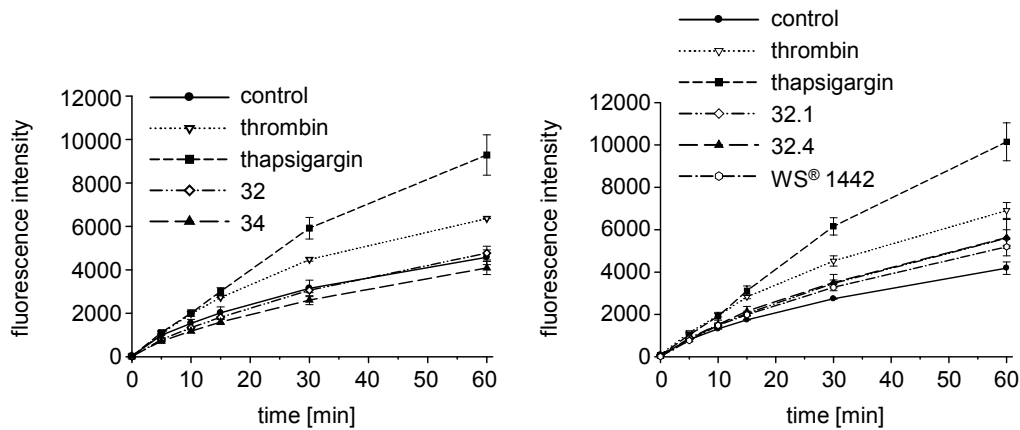


Figure 29 Fractionation scheme of fraction 32. Ca^{2+} -active fractions are marked by colored boxes (blue: highly active, light blue: slightly active). *, insoluble residue.

3.2.1.4 Ca^{2+} -active subfractions of WS[®] 1442 neither impair endothelial barrier integrity nor contractile machinery

As already mentioned above, an increase of $[\text{Ca}^{2+}]_i$ can activate the contractile machinery of endothelial cells which in turn induces hyperpermeability. Thus, we examined if the Ca^{2+} -active subfractions alter basal endothelial barrier integrity (Figure 30). In this setting, the cAMP pathway activating fraction 34 was utilized as negative control. Once again, only the typical $[\text{Ca}^{2+}]_i$ -increasing agents thrombin and thapsigargin clearly evoked hyperpermeability.

A



B

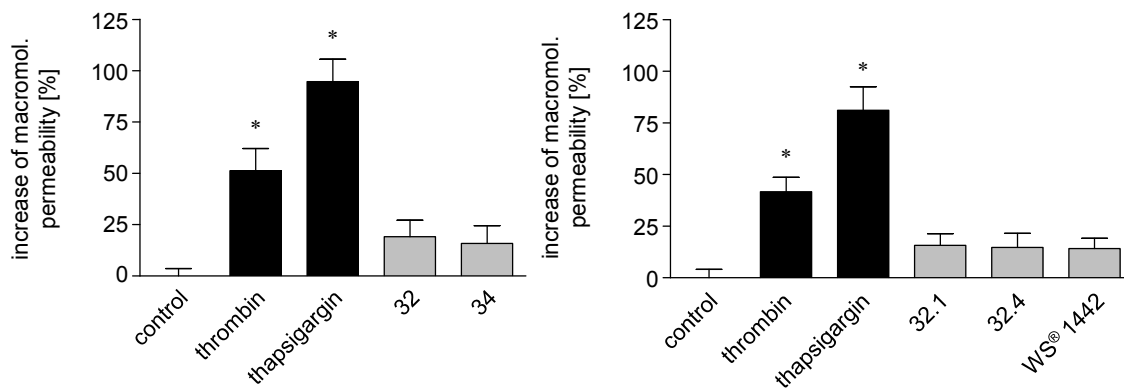
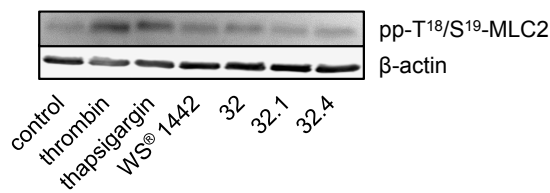


Figure 30 None of the selected fractions/subfractions of WS[®] 1442 induces endothelial hyperpermeability. A macromolecular permeability assay was performed. HMECs were treated with either WS[®] 1442 (100 µg/ml), thrombin (3 U/ml), thapsigargin (1 µM), fraction 32 (17 µg/ml), fraction 34 (12 µg/ml), subfraction 32.1 (4.32 µg/ml), subfraction 32.4 (3.82 µg/ml), or were left untreated. (A) One representative image illustrating the time course is shown. (B) Data are expressed as mean ± S.E.M. at t = 60 min. *, p ≤ 0.05 vs. control (left panel: n = 4, right panel: n = 5).

As indicated by Western blot analysis of the phosphorylation (Thr¹⁸/Ser¹⁹) status of myosin light chain 2 (MLC2), the contractile machinery was not influenced by the Ca²⁺-active subfractions which is in agreement with WS[®] 1442 treatment (Figure 31). By contrast, thrombin and thapsigargin clearly activated MLC.

A



B

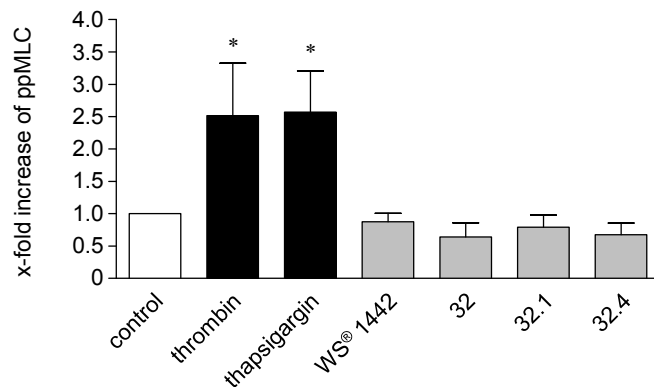


Figure 31 Ca²⁺-active fractions/subfractions of WS[®] 1442 do not increase the amount of phosphorylated myosin light chain (MLC). The phosphorylation status of MLC was investigated by Western blot analysis using a phospho-T¹⁸/S¹⁹-MLC2 antibody. HUVECs were treated for 30 min with thrombin (1 U/ml), thapsigargin (1 μM), WS[®] 1442 (100 μg/ml), fraction 32 (17 μg/ml), subfraction 32.1 (4.32 μg/ml), subfraction 32.4 (3.83 μg/ml) or were left untreated. (A) One representative Western blot is shown. (B) Data are expressed as mean ± S.E.M. *, p ≤ 0.05 (n = 3).

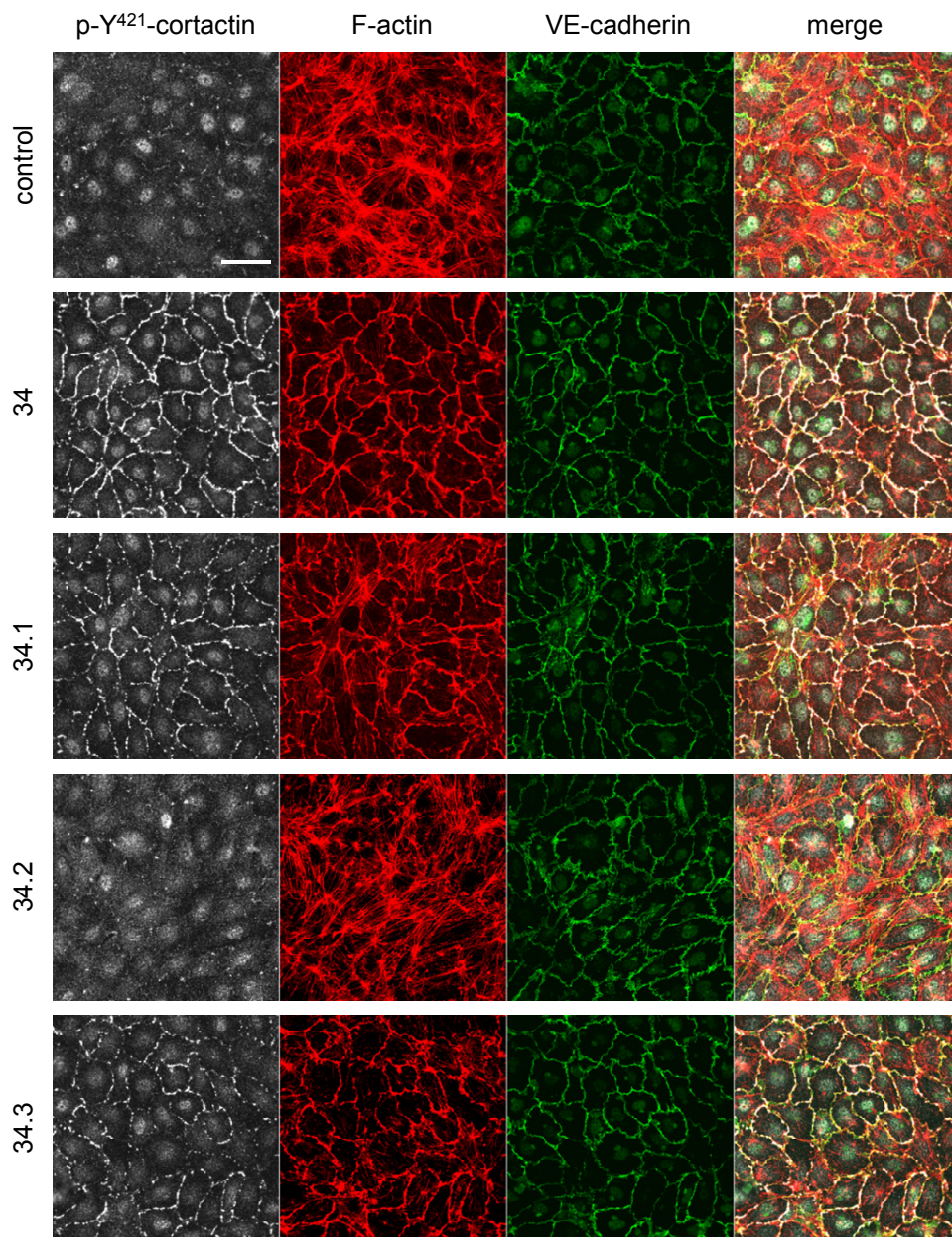
To conclude, Ca²⁺-active fractions/subfractions behave similar to the original extract. They do neither induce hyperpermeability nor activate endothelial cell contraction, which is in striking contrast to the well established Ca²⁺-increasing agents thrombin or thapsigargin.

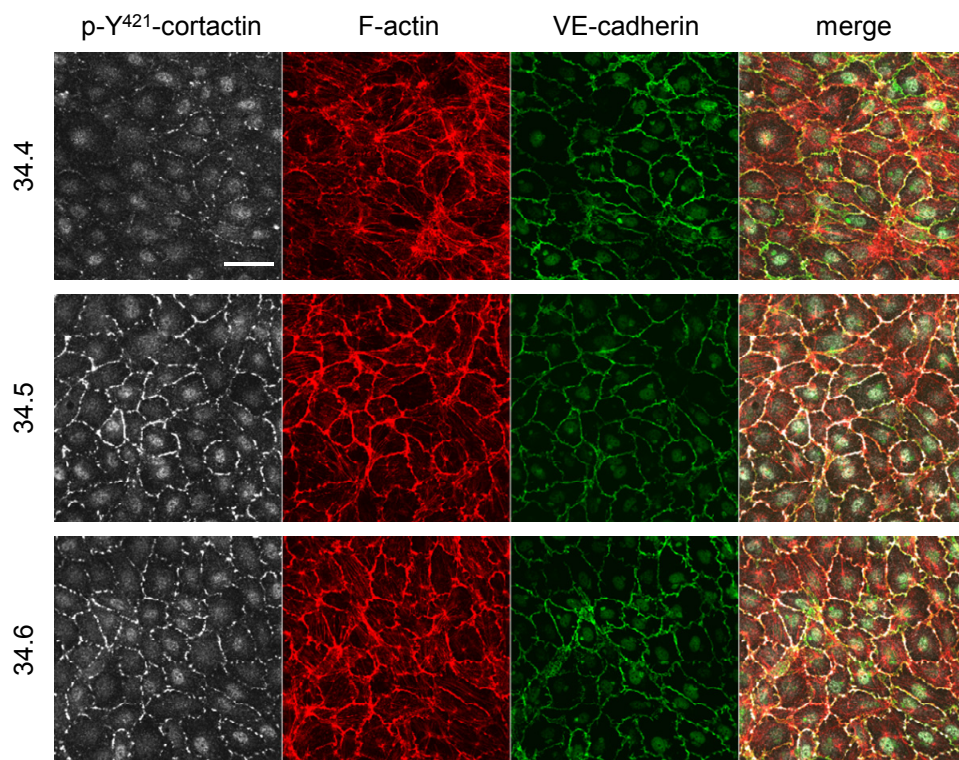
3.2.2 Subfractions 34.x differently affect cAMP pathway

In order to analyze cAMP pathway activation by the respective subfractions, we focused on cortactin, a downstream effector of cAMP/Rac1 signaling.^{81,82} Upon phosphorylation on Tyr⁴²¹, cortactin gets activated and mediates cortical actin rearrangement which tightens the endothelial barrier. Using confocal laser scanning microscopy, we investigated the phosphorylation status of cortactin triggered by the different subfractions of fraction 34. Original fraction 34 was used as positive control.

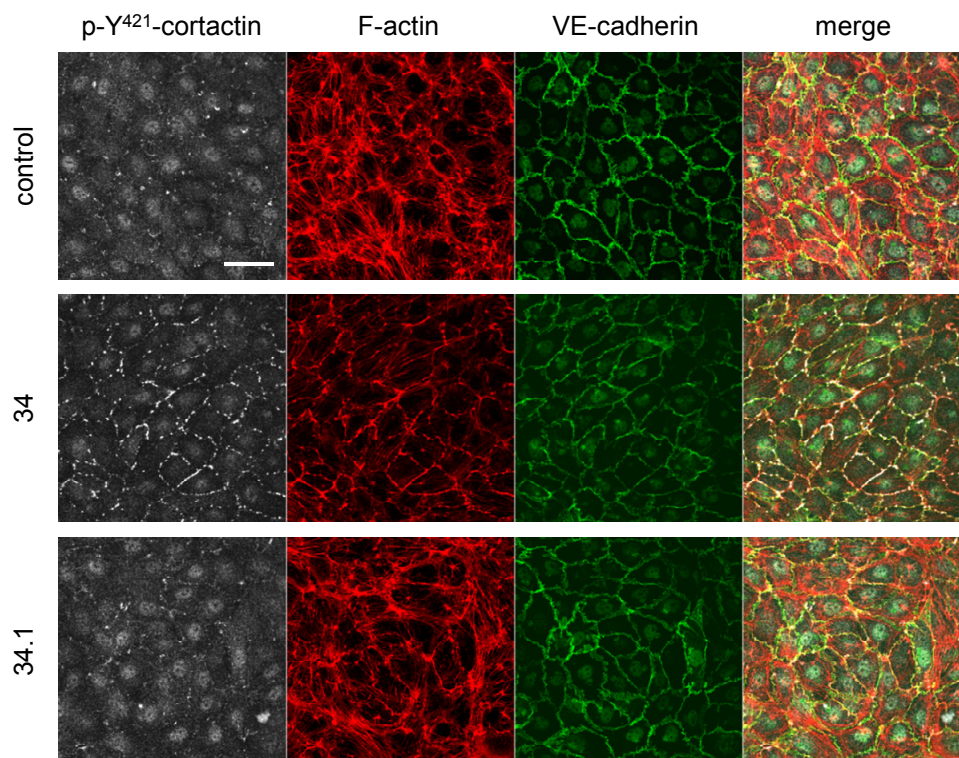
All subfractions apart from fraction 34.2 induced phosphorylation of cortactin and subsequent cortical actin formation in a concentration of 10 $\mu\text{g/ml}$ (Figure 32A). To distinguish between the biological activity of the different subfractions, experiments were repeated utilizing a lower concentration of 5 $\mu\text{g/ml}$ (Figure 32B). Only subfractions 34.3 and 34.5 were still able to evoke cortactin phosphorylation and actin rearrangement.

A





B



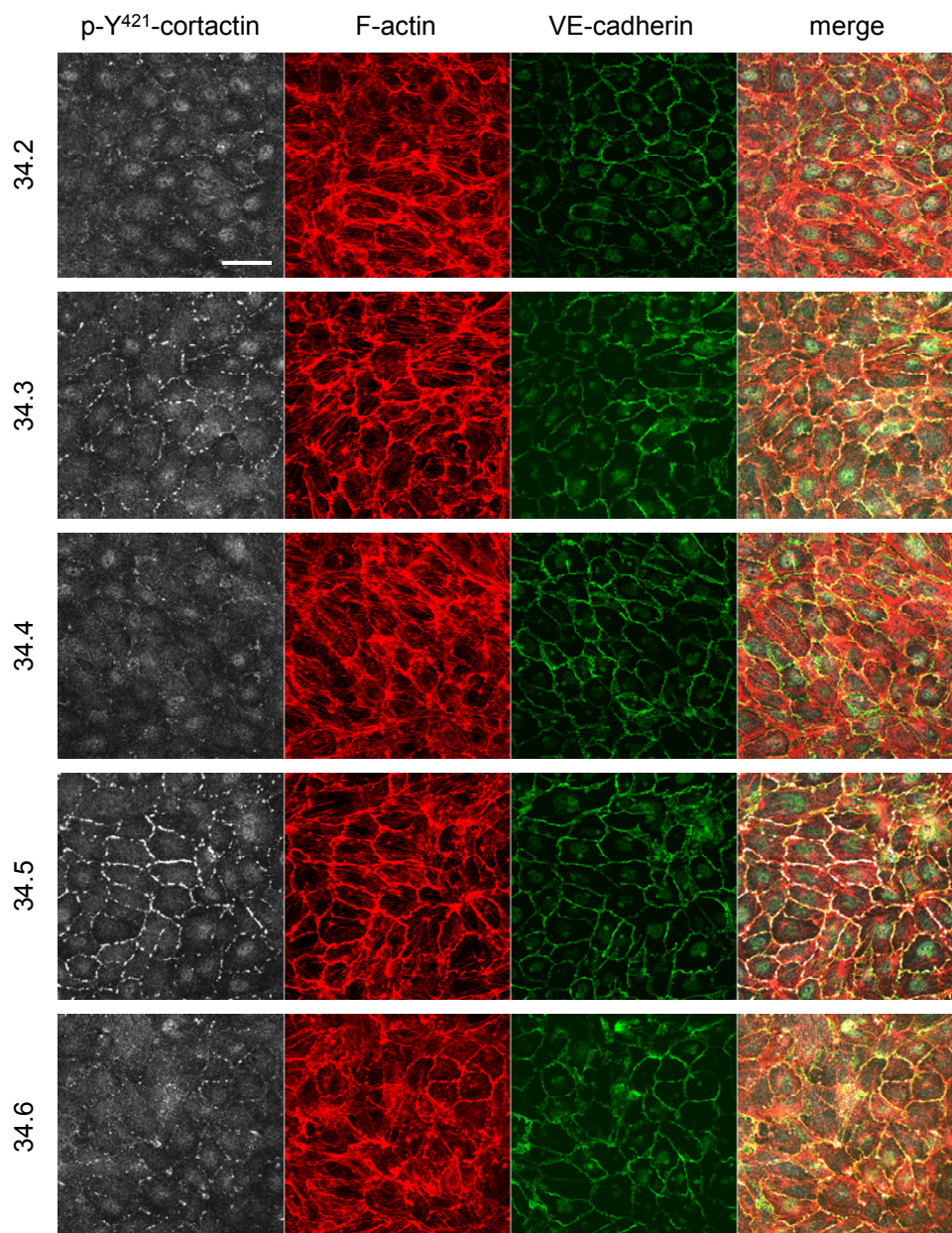


Figure 32 Subfractions 34.x differently affect cortactin and subsequently the actin cytoskeleton. Images were achieved by confocal microscopy after immunocytochemical staining. A confluent HUVEC monolayer was either left untreated, treated with fraction 34 (A: 30 $\mu\text{g/ml}$, B: 12 $\mu\text{g/ml}$) or with one of the different subfractions of fraction 34 (34.1-34.6, A: 10 $\mu\text{g/ml}$, B: 5 $\mu\text{g/ml}$) for 15 min. One representative image is shown for each type of treatment ($n = 3$). White bar: 50 μm .

To summarize, subfractions 34.3 and 34.5 exhibited the strongest activation of the cAMP pathway amongst all subfractions and thus were chosen to be further fractionated and analyzed (Figure 33).

This project has been pursued by *Simone Fuchs*. However, the available column chromatographical system Sephadex LH-20 was unable to properly separate these subfractions probably due to molecular rearrangements.⁸³ For this reason, two typical oligomeric proanthocyanidins – procyanidin B2 and C1 – that had been isolated from the original extract by Dr. Willmar Schwabe GmbH & Co. KG in a different attempt were applied. Indeed, it could be demonstrated that at least these two OPCs account for the WS[®] 1442-evoked activation of the cAMP pathway in human endothelial cells.

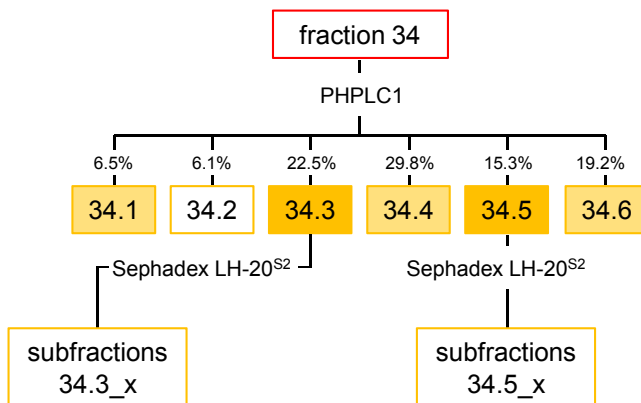


Figure 33 Fractionation scheme of fraction 34. cAMP-active subfractions are marked by colored boxes (orange: highly active, light orange: slightly active).

4 DISCUSSION AND CONCLUSIONS

4.1 WS[®] 1442 protects endothelial barrier integrity despite increasing $[Ca^{2+}]_i$

As yet, only two compounds have been described that reduce endothelial permeability despite increasing $[Ca^{2+}]_i$: ATP⁸⁴ and sphingosine 1-phosphate (S1-P),⁸⁵ the prototypical endogenous barrier-protecting agent. Our study for the first time shows that this action can also be evoked by a phytopharmaceutical, WS[®] 1442. S1-P was shown to induce Rac activation due to the rise of $[Ca^{2+}]_i$. Rac, in turn, ameliorated intercellular adhesion, thereby stabilizing endothelial barrier integrity. Our group had previously checked this potential connection between increased $[Ca^{2+}]_i$ and Rac activation in WS[®] 1442-treated ECs.⁴ However, a link does not exist in our model system.

4.1.1 Key role of SOCE in endothelial hyperpermeability

Instead of Ca^{2+} -triggered Rac activation, we propose another mode of action: Typically, an agonist-induced depletion of the ER – no matter if it is IP₃- or SERCA-mediated – causes the induction of a Stim-1-triggered SOCE from the extracellular space.^{52,86} Proteins of the Orai family function as pore-forming subunits of SOCE channels responsible for the so-called calcium release activated calcium current (I_{CRAC}). It is still a controversial matter if TRP channels connected to store-operated calcium currents (I_{SOC}) are also involved in Stim-1/Orai-gated regulation of SOCE or not.⁸⁷⁻⁸⁹ The presence of SOCE, accompanied by an interendothelial gap formation due to EC shape changes, is crucial for the induction of endothelial hyperpermeability.^{50,90} This phenomenon has been demonstrated in endothelial cells from various vascular beds.⁹¹⁻⁹³ Mechanistically, a further study impressively showed that in bovine artery ECs the activation of SOCE is coupled to the phosphorylation of MLC leading to the formation of intercellular gaps and increased permeability. Both thrombin and thapsigargin activated a Ca^{2+} entry and led to the phosphorylation of MLC, which could be prevented by blocking Ca^{2+} influx. Concerning thapsigargin, an inhibition of SOCE also prevented the induction of hyperpermeability.⁹⁴

In our study, we could confirm that these two agonists raise $[Ca^{2+}]_i$, cause MLC phosphorylation and increase permeability also in HUVECs. Surprisingly, although increasing $[Ca^{2+}]_i$, WS[®] 1442 did not cause these effects. We assume that this might be due to its inhibition of SOCE. Moreover, WS[®] 1442 did not trigger intercellular gap

formation. By contrast, WS[®] 1442 caused a substantial cortical F-actin distribution by activating the Epac1/Rap1/Rac1/cortactin pathway.²

4.1.2 Suggested modes of SOCE inhibition induced by WS[®] 1442

Interestingly, it has been described that the cytoskeleton plays a pivotal role in the modulation of SOCE.⁹⁵⁻⁹⁷ Galan *et al.*⁹⁷ demonstrated that stabilization of the cortical actin ring by the actin polymerizing agent jasplakinolide leads to the inhibition of thapsigargin-induced association of Stim-1 with SOC channels. This in turn prevents SOCE in HEK-293 cells. The authors assume that actin filaments as well as microtubules function as a cortical barrier which impedes the association between Stim-1 and the Ca²⁺ channels and consequently prohibits SOCE. Therefore, stabilizing these networks serves to prevent SOCE. As demonstrated in Figure 21, WS[®] 1442 is able to inhibit SOCE in a low Ca²⁺ environment after Stim-1 clustering has already been activated upon BHQ treatment. This indicates that WS[®] 1442 most likely impairs Stim-1/SOC channel communication. Thus, a possible mechanism for WS[®] 1442-evoked SOCE inhibition might be the strong rearrangement of cortical actin upon WS[®] 1442 treatment.²

Additionally, a negative feedback mechanism of Stim-1 regulation could supplement WS[®] 1442-induced SOCE inhibition. By the aid of an EF-hand domain, Stim-1 senses the Ca²⁺ concentration within the lumen of the ER.⁵³ Upon ER depletion, Stim-1 oligomerizes into punctae and translocates within the ER to junctions adjacent to the plasma membrane. Thereby, it can activate Orai.⁵⁴ Malli *et al.*⁹⁸ could demonstrate that an elevated cytosolic Ca²⁺ concentration is able to inhibit subplasmalemmal Stim-1 clustering, preventing SOCE and consequently cellular Ca²⁺ overload. Obviously, SOCE is under the control of cytosolic free Ca²⁺. This mechanism is crucial to maintain endothelial barrier integrity, since cytosolic Ca²⁺ overload is believed to evoke F-actin disintegration leading towards endothelial hyperpermeability.⁹⁹ Our preliminary results in EA.hy926 cells suggest that WS[®] 1442 treatment does not induce Stim-1 clustering in contrast to histamine addition. A possible explanation would be that the interplay between WS[®] 1442-induced increase of [Ca²⁺]_i and inhibition of Ca²⁺ extrusion might transiently generate a situation of high Ca²⁺ which prevents Stim-1 clustering.

According to the fact that WS[®] 1442 actually blocks agonist-induced SOCE in a low Ca²⁺ situation, we believe that actin rearrangement by activating cAMP/Epac1/Rap1 pathway² contributes in a superior way to WS[®] 1442-evoked SOCE inhibition compared to the negative regulation of Stim-1 clustering. Moreover, one might even speculate that this SOCE inhibition combined with the ER depletion enables WS[®] 1442 to overcome thrombin-induced deleterious effects on endothelial barrier. This will be an interesting topic of further research.

4.2 WS[®] 1442 and its influence on Ca²⁺ extrusion capacity

Concerning the endothelial Ca²⁺ extrusion capacity, the question arises of how WS[®] 1442 is able to hamper the decrease of elevated Ca²⁺ levels. WS[®] 1442 inhibits the SERCA pump, which prevents Ca²⁺ reuptake into the ER. As a result, increased Ca²⁺ levels can only be eliminated through a plasma membranous transport.¹⁰⁰ In principle, this can mainly be achieved by the plasma membrane Ca²⁺ ATPase (PMCA), by the Na⁺/Ca²⁺-exchanger (NCX) or by both,⁵⁵⁻⁵⁷ depending on the cell type or tissue. Originally, it has been believed that the predominant role of NCX is to counteract large and rapid raises of [Ca²⁺]_i in contrast to PMCA, which regulates the basal status. In calf pulmonary artery endothelial cells, it was shown that PMCA acts as a high-affinity Ca²⁺ removal system to correct baseline levels, whereas the low-affinity NCX erases fast and large increases of Ca²⁺.¹⁰¹ However, this hypothesis was refuted due to the strong functional versatility among the different isoforms of PMCA, of which some also allow a rapid Ca²⁺ clearance.¹⁰² PMCA belongs to the P-type ATPases, just as the SERCA pump, thereby sharing fundamental properties like membrane topology and reaction mechanism. The two pumps, however, display significant sequence differences leading to an altered regulation, action of some inhibitors, and role in cellular processes.¹⁰³ According to that, BHQ and thapsigargin specifically act on the SERCA pump.¹⁰⁴ Based on the inhibitory effect of WS[®] 1442 on SERCA function, we therefore cannot simply conclude that PMCA is blocked as well. However, in EA.hy926 cells we got first hints that Ca²⁺ extrusion is in fact considerably abolished by WS[®] 1442-induced PMCA inhibition. Further investigations are needed to clarify the role of PMCA and NCX in the WS[®] 1442-evoked repression of Ca²⁺ extrusion in our system.

4.3 Na⁺/K⁺-ATPase and WS[®] 1442

In cardiomyocytes, a different target of WS[®] 1442 was found that is responsible for a rise of [Ca²⁺]_i: WS[®] 1442 increases [Ca²⁺]_i by inhibiting Na⁺/K⁺-ATPase similar to the mode of action of cardiac glycosides. The extract concentration-dependently displaces the cardiac glycoside ouabain from its binding partner, the Na⁺/K⁺-ATPase, thereby enhancing the force of contraction in human failing and non-failing myocardium.¹⁸ In addition to its action on the heart, the Na⁺/K⁺-ATPase also plays an important role in pathological processes of the vasculature.¹⁰⁵ Although the regulation of Ca²⁺ levels differs between non-excitabile (e.g. endothelial) cells and excitable cardiomyocytes, it has nevertheless been reported that ouabain is able to alter [Ca²⁺]_i in the rat descending vasa recta¹⁰⁶ by targeting the Na⁺/K⁺-ATPase and subsequent inhibition of the Na⁺/Ca²⁺-exchanger. Interestingly, ECs were in fact found to express different isoforms of this ATPase¹⁰⁷ and ouabain, applied in the nanomolar range, was even shown to induce a breakdown of endothelial barrier integrity in ECs, which could be overcome by preventing Na⁺/K⁺-ATPase blockade using a special digoxin antibody.¹⁰⁸ Referring to Ca²⁺ measurements and patch clamp recordings, our work clearly shows that in the endothelium this ATPase is not the primary target of WS[®] 1442.

4.4 Comparison between HUVECs and EA.hy926 cells concerning WS[®] 1442-induced Ca²⁺-signaling

For *in vitro* experiments, immortalized cell lines like EA.hy926 are often chosen because of significant advantages such as stable cell viability, unaltered expression profile of endothelial cell markers during passaging and genetical homogeneity. In our case, EA.hy926 cells would offer the possibility to easier perform transfection experiments. It has been described that despite hybridization, EA.hy926 cells still maintain endothelial cell characteristics of native HUVECs.⁶² Nevertheless, we checked the comparability between HUVECs and EA.hy926 cells concerning WS[®] 1442-induced Ca²⁺-signaling.

This study shows that WS[®] 1442-induced Ca²⁺ response does not exclusively appear in HUVECs but also in EA.hy926 cells. However, there is a difference regarding the onset and the shape of the Ca²⁺ response: In EA.hy926 cells, WS[®] 1442 immediately elevates [Ca²⁺]_i in a peak-plateau shaped manner, whereas in HUVECs, a lag time of approximately 5 min is observed while the peak is completely missing. Because of the

immediate onset of the Ca^{2+} signal in EA.hy926 cells, an IP_3 involvement besides SERCA inhibition can be assumed. This would be in agreement with the dual mechanism demonstrated for HUVECs, but has yet to be examined. $\text{WS}^{\text{®}}$ 1442 treatment inhibits Ca^{2+} efflux in both cell types. However, focusing on the histamine-induced Ca^{2+} response, EA.hy926 cells exhibit a stronger Ca^{2+} influx, *i.e.* SOCE, which is indicated throughout the more pronounced plateau phase. Therefore, $\text{WS}^{\text{®}}$ 1442-induced SOCE inhibition should be revised in EA.hy926 cells as well.

To conclude, $\text{WS}^{\text{®}}$ 1442 treatment seems to influence similar Ca^{2+} -signaling pathways in both cell types. Apparent kinetic differences might originate from the epithelial portion of the hybrid cell line and, thus, from an altered expression pattern of Ca^{2+} channels.

4.5 Bioactive compounds of $\text{WS}^{\text{®}}$ 1442

The cardiovascular protective activity of hawthorn is ascribed to its flavonoid and oligomeric proanthocyanidin⁸ (OPC) content.⁹ Consequently, most of the studies dealing with the efficacy of hawthorn were accomplished utilizing one of the two standardized extracts LI 132 (MCM Klosterfrau Vertriebsgesellschaft mbH) or $\text{WS}^{\text{®}}$ 1442. LI 132 and $\text{WS}^{\text{®}}$ 1442 are adjusted to a definite content of flavonoids (2.2%, LI 132) or OPCs (18.75%, $\text{WS}^{\text{®}}$ 1442), respectively.

These polyphenols exert various bioactive properties^{109,110} such as antioxidant,¹¹¹⁻¹¹³ anti-inflammatory¹¹⁴⁻¹¹⁶ and vasodilatory^{28,117,118} actions. Interestingly, we could demonstrate that these two phytochemical groups also contribute to the observed endothelial activity in our study. In fact, we could even assign each group to one single pathway regulating endothelial barrier function.⁴

4.5.1 Flavonoids and their role in Ca^{2+} -signaling

Within all fractions, only the flavonoid containing fraction 32 as well as particular subfractions 32.x were able to prevent thrombin-induced increase of $[\text{Ca}^{2+}]_i$ and to concomitantly raise $[\text{Ca}^{2+}]_i$ by themselves. This observation suggests an involvement of flavonoids in the $\text{WS}^{\text{®}}$ 1442-evoked Ca^{2+} response, even if the three already identified flavonoids were not the active candidates.

Several groups have already established a clear alliance between flavonoids and cellular Ca^{2+} -signaling. For instance, flavonoids impair IgE-mediated proinflammatory mediator release¹¹⁹ or Ca^{2+} dependent cell oxidation¹²⁰ by inhibiting agonist-evoked increase of $[\text{Ca}^{2+}]_i$. Therefore, some flavonoids could provide health benefits in the treatment of allergic or inflammatory diseases. Additionally, flavonoids themselves are able to increase $[\text{Ca}^{2+}]_i$ by affecting SERCA,¹²¹ which could also be observed in WS[®] 1442 treated cells. Certain flavonoids alter ATP affinity to SERCA by binding to the cytosolic region of the Ca^{2+} ATPase between ATP-binding and phosphorylation domain. Moreover, they can stabilize the enzyme in one single conformational state (E1). As a result, both mechanisms suppress functionality of the pump.⁶⁷ Interestingly, polyhydroxylation of flavones with hydroxylation at position 3 and 6 were shown to be particularly relevant for the inhibitory activity.¹²² In the same study, one of our isolated flavonoids, *i.e.* rutin, was shown to not measurably inhibit SERCA, which is in agreement to our findings. In contrast to SERCA inhibition, the antioxidant flavonoids were also shown to even safeguard SERCA activity against oxidative damage,¹²³ whereby the ability to protect the functionality of the Ca^{2+} ATPase depends on the mode of oxidative injury.¹²⁴

Besides SERCA, flavonoids also interact with other Ca^{2+} ATPases, like the Ca^{2+} transport ATPase of synaptosomal vesicles¹²⁵ or the liver plasma membrane Ca^{2+} pump.¹²⁶ However, a repression of plasma membrane Ca^{2+} ATPase (PMCA) functionality, which is probably responsible for the altered Ca^{2+} extrusion capacity upon WS[®] 1442 treatment, has not been described for flavonoids so far.

Another aspect of flavonoid/ Ca^{2+} -signaling interaction concerns myosin light chain kinase (MLCK). An agonist-induced increase of $[\text{Ca}^{2+}]_i$ can activate Ca^{2+} /calmodulin regulated MLCK, which subsequently phosphorylates MLC leading towards cell contraction.¹²⁷ As already discussed above, WS[®] 1442 treatment does not cause MLC phosphorylation despite the clear rise of cytosolic Ca^{2+} levels. Additionally, WS[®] 1442 as well as the flavonoid-rich fraction 32 even block thrombin-evoked MLC phosphorylation.⁴ Interestingly, flavonoids were found to inhibit MLCK activity demonstrated *in vitro* on isolated, purified MLCK from chicken gizzard in a kinase assay.¹²⁷ This topic has not been studied in great detail until today, but could be an additional explanation for the influence of WS[®] 1442 on MLC-signaling.

We conclude that particular flavonoids of WS[®] 1442 probably inhibit SERCA function. Nevertheless, it is still an open question whether these flavonoids are also responsible

for the WS[®] 1442-evoked change of Ca²⁺ extrusion (NCX, PMCA) and IP₃-mediated ER depletion or not. It remains to be clarified if unidentified Ca²⁺-active compounds other than flavonoids exist which can complement the WS[®] 1442-induced Ca²⁺ response.

4.5.2 Oligomeric proanthocyanidins and endothelial barrier function

We could demonstrate that the OPC rich fraction 34 of WS[®] 1442,⁴ its subfractions 34.3 and 34.5 as well as the pure procyanidins B2 and C1 activate the barrier protecting and strengthening cAMP-signaling most significantly within all WS[®] 1442 fractions.

Several publications report a barrier protecting property of OPCs. With the aid of quantitative morphology, Robert *et al.* demonstrated that OPCs are able to prevent collagenase-induced permeability increase in rat cerebral capillaries, aorta and cardiac muscle capillaries.¹²⁸ In 2001, another publication described that OPCs counterbalance this deleterious effect of collagenase-evoked hyperpermeability in rat blood brain barrier by inhibiting proteolytic degradation of extracellular matrix macromolecules.¹²⁹ Furthermore, procyanidin¹³⁰ as well as an enriched fraction of OPCs from grape seeds¹³¹ were found to block agonist-induced edema formation in rat hind paw. It was also shown in rats that OPCs partially prevent the formation of a re-expansion pulmonary edema probably due to their antioxidant activity.¹³² Moreover, Endotélon[®] (Sanofi Aventis, Paris, France), a French pharmaceutical product of OPCs from grape seeds, reduces surgically-evoked lymphedema in rat hindlimb.¹³³ As a result, all these studies suggest a barrier protecting potential for oligomeric proanthocyanidins. The authors were not able to elucidate the distinct mechanisms of OPC-induced barrier protection. However, they speculate that binding of OPCs to areas with a high content of glycosaminoglycans¹³⁴ might prevent degradation of extracellular matrix. This anti-proteolytic property is believed to protect barrier function.

Beyond this, we discovered that OPCs in WS[®] 1442 activate cAMP-signaling thereby protecting endothelial barrier. To our best knowledge, neither a detailed mode of action, nor a link between OPCs and the cAMP-signaling has ever been described to date.

5 SUMMARY

We demonstrated for the first time that WS[®] 1442 increases $[Ca^{2+}]_i$ without impairing barrier integrity or cell viability. All important effects related to endothelial Ca^{2+} -signaling are illustrated schematically in Figure 34.

In brief, WS[®] 1442

- depletes the ER by activating IP₃ pathway and inhibiting SERCA.
- does not cause SOCE despite increasing $[Ca^{2+}]_i$.
- prevents agonist-induced SOCE generation.
- blocks endothelial Ca^{2+} extrusion capacity.
- does not target endothelial Na^+/K^+ -ATPase (in contrast to cardiomyocytes).

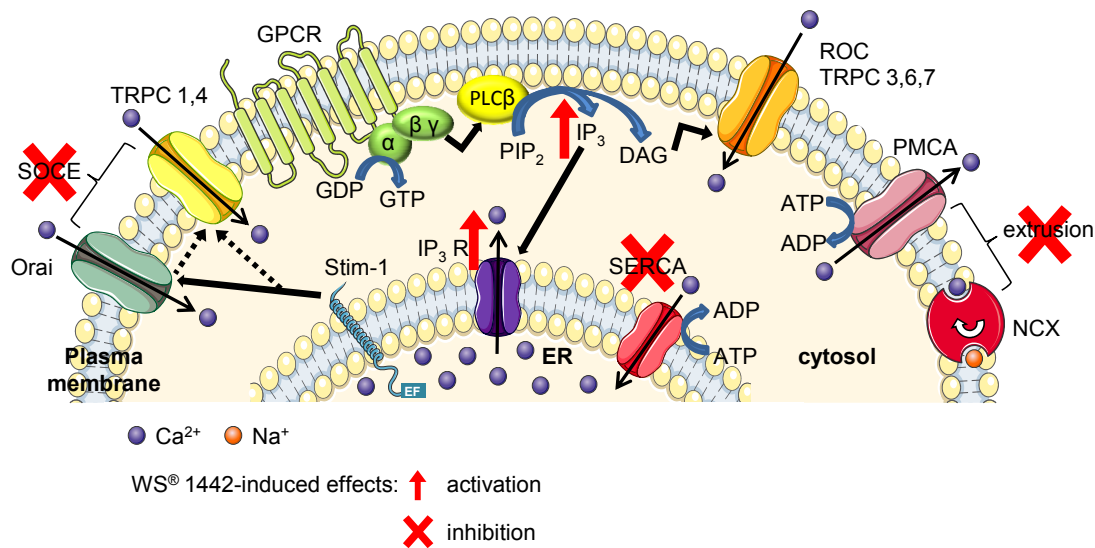


Figure 34 WS[®] 1442-induced Ca^{2+} -signaling

Focusing on the search for the bioactive compounds, only the flavonoid rich fraction 32 and particular subfractions are able to alter thrombin-induced Ca^{2+} -signaling. Similar to the original extract, the Ca^{2+} -active fractions do not cause cellular stress. Although three inactive flavonoids of the extract could be identified in our lab, we hypothesize that certain flavonoids provide the key players of WS[®] 1442-induced Ca^{2+} -signaling in agreement to the evidence found in literature. In the future, further fractionation procedures as well as structural analysis are needed to discover the Ca^{2+} -active single compound(s) of WS[®] 1442. Concerning cAMP-signaling, only the OPC rich fraction 34 as well as its subfractions 34.3 and 34.5 are found to activate this pathway most significantly. Additionally, the two isolated procyanidins B2 and C1 also induce

activation of the cAMP downstream effector cortactin. Therefore, we propose that OPCs in WS[®] 1442 are responsible for the activation of the cAMP pathway in the endothelium thereby protecting and strengthening endothelial barrier function.

These findings strengthen the rational basis for the use of this herbal medicinal product by providing a better understanding of the complex pharmacological action of WS[®] 1442.

6 REFERENCES

1. van Nieuw Amerongen, G.P. & van Hinsbergh, V.W. Targets for pharmacological intervention of endothelial hyperpermeability and barrier function. *Vascul Pharmacol* 39, 257-72 (2002).
2. Bubik, M.F. et al. A novel approach to prevent endothelial hyperpermeability: The Crataegus extract WS(R) 1442 targets the cAMP/Rap1 pathway. *J Mol Cell Cardiol* (2011).
3. Tiruppathi, C., Minshall, R.D., Paria, B.C., Vogel, S.M. & Malik, A.B. Role of Ca²⁺ signaling in the regulation of endothelial permeability. *Vascul Pharmacol* 39, 173-85 (2002).
4. Bubik, M.F. PhD thesis: Endothelial barrier protection by natural compounds - Crataegus extract WS 1442 and atrial natriuretic peptide inhibit endothelial hyperpermeability (2009).
5. Czygan, F.C. [A short cultural history in retrospect. Crataegus as a cardiac agent]. *Pharm Unserer Zeit* 34, 10-3 (2005).
6. Koch, E. & Malek, F.A. Standardized extracts from hawthorn leaves and flowers in the treatment of cardiovascular disorders--preclinical and clinical studies. *Planta Med* 77, 1123-8 (2011).
7. Petereit, F. & Nahrstedt, A. [Crataegus from the analytical viewpoint. Official contents of hawthorn drugs]. *Pharm Unserer Zeit* 34, 22-6 (2005).
8. Chatterjee, S.S., Koch, E., Jaggy, H. & Krzeminski, T. [In vitro and in vivo studies on the cardioprotective action of oligomeric procyanidins in a Crataegus extract of leaves and blooms]. *Arzneimittelforschung* 47, 821-5 (1997).
9. Crataegi folium cum flore. Hawthorn leaf and flower. *ESCOP monographs, Thieme: Exeter*, 98-106 (2003).
10. Hänsel, R. & Sticher, O. Pharmakognosie Phytopharmazie. *Springer Medizin Verlag Heidelberg* 8, 1188-1223 (2007).
11. Holubarsch, C.J., Colucci, W.S., Meinertz, T., Gaus, W. & Tendera, M. The efficacy and safety of Crataegus extract WS 1442 in patients with heart failure: the SPICE trial. *Eur J Heart Fail* 10, 1255-63 (2008).
12. Tauchert, M. Efficacy and safety of crataegus extract WS 1442 in comparison with placebo in patients with chronic stable New York Heart Association class-III heart failure. *Am Heart J* 143, 910-5 (2002).
13. Zapfe jun, G. Clinical efficacy of crataegus extract WS 1442 in congestive heart failure NYHA class II. *Phytomedicine* 8, 262-6 (2001).
14. Pittler, M.H., Guo, R. & Ernst, E. Hawthorn extract for treating chronic heart failure. *Cochrane Database Syst Rev*, CD005312 (2008).
15. Daniele, C., Mazzanti, G., Pittler, M.H. & Ernst, E. Adverse-event profile of Crataegus spp.: a systematic review. *Drug Saf* 29, 523-35 (2006).
16. Eggeling, T., Regitz-Zagrosek, V., Zimmermann, A. & Burkart, M. Baseline severity but not gender modulates quantified Crataegus extract effects in early heart failure - a pooled analysis of clinical trials. *Phytomedicine* 18, 1214-9 (2011).

17. Pöpping, S., Rose, H., Ionescu, I., Fischer, Y. & Kammermeier, H. Effect of a hawthorn extract on contraction and energy turnover of isolated rat cardiomyocytes. *Arzneimittelforschung* 45, 1157-61 (1995).
18. Schwinger, R.H., Pietsch, M., Frank, K. & Brixius, K. Crataegus special extract WS 1442 increases force of contraction in human myocardium cAMP-independently. *J Cardiovasc Pharmacol* 35, 700-7 (2000).
19. Müller, A., Linke, W. & Klaus, W. Crataegus extract blocks potassium currents in guinea pig ventricular cardiac myocytes. *Planta Med* 65, 335-9 (1999).
20. Swaminathan, J.K. et al. Cardioprotective properties of Crataegus oxycantha extract against ischemia-reperfusion injury. *Phytomedicine* 17, 744-52 (2010).
21. Veveris, M., Koch, E. & Chatterjee, S.S. Crataegus special extract WS 1442 improves cardiac function and reduces infarct size in a rat model of prolonged coronary ischemia and reperfusion. *Life Sci* 74, 1945-55 (2004).
22. Hwang, H.S. et al. Effects of hawthorn on cardiac remodeling and left ventricular dysfunction after 1 month of pressure overload-induced cardiac hypertrophy in rats. *Cardiovasc Drugs Ther* 22, 19-28 (2008).
23. Hwang, H.S., Boluyt, M.O., Converso, K., Russell, M.W. & Bleske, B.E. Effects of hawthorn on the progression of heart failure in a rat model of aortic constriction. *Pharmacotherapy* 29, 639-48 (2009).
24. Jayachandran, K.S., Khan, M., Selvendiran, K., Devaraj, S.N. & Kuppusamy, P. Crataegus oxycantha extract attenuates apoptotic incidence in myocardial ischemia-reperfusion injury by regulating Akt and HIF-1 signaling pathways. *J Cardiovasc Pharmacol* 56, 526-31 (2010).
25. Anselm, E. et al. Crataegus special extract WS 1442 causes endothelium-dependent relaxation via a redox-sensitive Src- and Akt-dependent activation of endothelial NO synthase but not via activation of estrogen receptors. *J Cardiovasc Pharmacol* 53, 253-60 (2009).
26. Brixius, K. et al. Crataegus special extract WS 1442 induces an endothelium-dependent, NO-mediated vasorelaxation via eNOS-phosphorylation at serine 1177. *Cardiovasc Drugs Ther* 20, 177-84 (2006).
27. Chen, Z.Y. et al. Endothelium-dependent relaxation induced by hawthorn extract in rat mesenteric artery. *Life Sci* 63, 1983-91 (1998).
28. Kim, S.H., Kang, K.W., Kim, K.W. & Kim, N.D. Procyanidins in crataegus extract evoke endothelium-dependent vasorelaxation in rat aorta. *Life Sci* 67, 121-31 (2000).
29. Shatoor, A.S. et al. Effect of Hawthorn (*Crataegus aronia* syn. *Azarolus* (L)) on Platelet Function in Albino Wistar Rats. *Thromb Res* (2012).
30. Dalli, E. et al. Crataegus laevigata decreases neutrophil elastase and has hypolipidemic effect: a randomized, double-blind, placebo-controlled trial. *Phytomedicine* 18, 769-75 (2011).
31. Dalli, E. et al. Hawthorn extract inhibits human isolated neutrophil functions. *Pharmacol Res* 57, 445-50 (2008).

32. Mehta, D. & Malik, A.B. Signaling mechanisms regulating endothelial permeability. *Physiol Rev* 86, 279-367 (2006).
33. Galley, H.F. & Webster, N.R. Physiology of the endothelium. *Br J Anaesth* 93, 105-13 (2004).
34. Komarova, Y. & Malik, A.B. Regulation of endothelial permeability via paracellular and transcellular transport pathways. *Annu Rev Physiol* 72, 463-93 (2010).
35. Vandenbroucke, E., Mehta, D., Minshall, R. & Malik, A.B. Regulation of endothelial junctional permeability. *Ann N Y Acad Sci* 1123, 134-45 (2008).
36. Dejana, E., Tournier-Lasserre, E. & Weinstein, B.M. The control of vascular integrity by endothelial cell junctions: molecular basis and pathological implications. *Dev Cell* 16, 209-21 (2009).
37. Spindler, V., Schlegel, N. & Waschke, J. Role of GTPases in control of microvascular permeability. *Cardiovasc Res* 87, 243-53 (2010).
38. Schlegel, N. & Waschke, J. Vasodilator-stimulated phosphoprotein: crucial for activation of Rac1 in endothelial barrier maintenance. *Cardiovasc Res* 87, 1-3 (2010).
39. Kooistra, M.R., Corada, M., Dejana, E. & Bos, J.L. Epac1 regulates integrity of endothelial cell junctions through VE-cadherin. *FEBS Lett* 579, 4966-72 (2005).
40. Metrich, M. et al. Role of the cAMP-binding protein Epac in cardiovascular physiology and pathophysiology. *Pflugers Arch* 459, 535-46 (2010).
41. Birukova, A.A. et al. Prostaglandins PGE(2) and PGI(2) promote endothelial barrier enhancement via PKA- and Epac1/Rap1-dependent Rac activation. *Exp Cell Res* 313, 2504-20 (2007).
42. Nishikawa, M., de Lanerolle, P., Lincoln, T.M. & Adelstein, R.S. Phosphorylation of mammalian myosin light chain kinases by the catalytic subunit of cyclic AMP-dependent protein kinase and by cyclic GMP-dependent protein kinase. *J Biol Chem* 259, 8429-36 (1984).
43. Qiao, J., Huang, F. & Lum, H. PKA inhibits RhoA activation: a protection mechanism against endothelial barrier dysfunction. *Am J Physiol Lung Cell Mol Physiol* 284, L972-80 (2003).
44. Michel, T. & Vanhoutte, P.M. Cellular signaling and NO production. *Pflugers Arch* 459, 807-16 (2010).
45. Tran, Q.K. & Watanabe, H. Calcium signalling in the endothelium. *Handb Exp Pharmacol*, 145-87 (2006).
46. Clapham, D.E., Runnels, L.W. & Strubing, C. The TRP ion channel family. *Nat Rev Neurosci* 2, 387-96 (2001).
47. Tran, Q.K., Ohashi, K. & Watanabe, H. Calcium signalling in endothelial cells. *Cardiovasc Res* 48, 13-22 (2000).
48. Prasad, A.R., Logan, S.A., Nerem, R.M., Schwartz, C.J. & Sprague, E.A. Flow-related responses of intracellular inositol phosphate levels in cultured aortic endothelial cells. *Circ Res* 72, 827-36 (1993).

49. Clapham, D.E. Calcium signaling. *Cell* 131, 1047-58 (2007).
50. Ahmmed, G.U. & Malik, A.B. Functional role of TRPC channels in the regulation of endothelial permeability. *Pflugers Arch* 451, 131-42 (2005).
51. Dietrich, A., Kalwa, H. & Gudermann, T. TRPC channels in vascular cell function. *Thromb Haemost* 103, 262-70 (2010).
52. Smyth, J.T. et al. Activation and regulation of store-operated calcium entry. *J Cell Mol Med* 14, 2337-49 (2010).
53. Liou, J. et al. STIM is a Ca²⁺ sensor essential for Ca²⁺-store-depletion-triggered Ca²⁺ influx. *Curr Biol* 15, 1235-41 (2005).
54. Penna, A. et al. The CRAC channel consists of a tetramer formed by Stim-induced dimerization of Orai dimers. *Nature* 456, 116-20 (2008).
55. Goto, Y., Miura, M. & Iijima, T. Extrusion mechanisms of intracellular Ca²⁺ in human aortic endothelial cells. *Eur J Pharmacol* 314, 185-92 (1996).
56. Shimizu, H., Borin, M.L. & Blaustein, M.P. Use of La³⁺ to distinguish activity of the plasmalemmal Ca²⁺ pump from Na⁺/Ca²⁺ exchange in arterial myocytes. *Cell Calcium* 21, 31-41 (1997).
57. Brini, M. & Carafoli, E. The plasma membrane Ca²⁺ ATPase and the plasma membrane sodium calcium exchanger cooperate in the regulation of cell calcium. *Cold Spring Harb Perspect Biol* 3 (2011).
58. Hartung, E. Master Thesis: Preparative isolation and phytochemical characterization of special subfractions of Crataegus extract WS[®] 1442 (2011).
59. Ades, E.W. et al. HMEC-1: establishment of an immortalized human microvascular endothelial cell line. *J Invest Dermatol* 99, 683-90 (1992).
60. Bouis, D., Hospers, G.A., Meijer, C., Molema, G. & Mulder, N.H. Endothelium in vitro: a review of human vascular endothelial cell lines for blood vessel-related research. *Angiogenesis* 4, 91-102 (2001).
61. Edgell, C.J., McDonald, C.C. & Graham, J.B. Permanent cell line expressing human factor VIII-related antigen established by hybridization. *Proc Natl Acad Sci U S A* 80, 3734-7 (1983).
62. Edgell, C.J. et al. Endothelium specific Weibel-Palade bodies in a continuous human cell line, EA.hy926. *In Vitro Cell Dev Biol* 26, 1167-72 (1990).
63. Bradford, M.M. A rapid and sensitive method for the quantitation of microgram quantities of protein utilizing the principle of protein-dye binding. *Anal Biochem* 72, 248-54 (1976).
64. Laemmli, U.K. Cleavage of structural proteins during the assembly of the head of bacteriophage T4. *Nature* 227, 680-5 (1970).
65. Kurien, B.T. & Scofield, R.H. Protein blotting: a review. *J Immunol Methods* 274, 1-15 (2003).
66. Maruyama, T., Kanaji, T., Nakade, S., Kanno, T. & Mikoshiba, K. 2APB, 2-aminoethoxydiphenyl borate, a membrane-penetrable modulator of Ins(1,4,5)P₃-induced Ca²⁺ release. *J Biochem* 122, 498-505 (1997).

67. Michelangeli, F. & East, J.M. A diversity of SERCA Ca²⁺ pump inhibitors. *Biochem Soc Trans* 39, 789-97 (2011).
68. Akdis, C.A. & Simons, F.E. Histamine receptors are hot in immunopharmacology. *Eur J Pharmacol* 533, 69-76 (2006).
69. Bogatcheva, N.V., Garcia, J.G. & Verin, A.D. Molecular mechanisms of thrombin-induced endothelial cell permeability. *Biochemistry (Mosc)* 67, 75-84 (2002).
70. Yule, D.I. & Williams, J.A. U73122 inhibits Ca²⁺ oscillations in response to cholecystinin and carbachol but not to JMV-180 in rat pancreatic acinar cells. *J Biol Chem* 267, 13830-5 (1992).
71. Grynkiewicz, G., Poenie, M. & Tsien, R.Y. A new generation of Ca²⁺ indicators with greatly improved fluorescence properties. *J Biol Chem* 260, 3440-50 (1985).
72. Palmer, A.E., Jin, C., Reed, J.C. & Tsien, R.Y. Bcl-2-mediated alterations in endoplasmic reticulum Ca²⁺ analyzed with an improved genetically encoded fluorescent sensor. *Proc Natl Acad Sci U S A* 101, 17404-9 (2004).
73. Demaurex, N. & Frieden, M. Measurements of the free luminal ER Ca(2+) concentration with targeted "cameleon" fluorescent proteins. *Cell Calcium* 34, 109-19 (2003).
74. Miyawaki, A. et al. Fluorescent indicators for Ca²⁺ based on green fluorescent proteins and calmodulin. *Nature* 388, 882-7 (1997).
75. Sandoval, R., Malik, A.B., Naqvi, T., Mehta, D. & Tiruppathi, C. Requirement for Ca²⁺ signaling in the mechanism of thrombin-induced increase in endothelial permeability. *Am J Physiol Lung Cell Mol Physiol* 280, L239-47 (2001).
76. Sandoval, R. et al. Ca(2+) signalling and PKCalpha activate increased endothelial permeability by disassembly of VE-cadherin junctions. *J Physiol* 533, 433-45 (2001).
77. Srinivas, S.P., Satpathy, M., Guo, Y. & Anandan, V. Histamine-induced phosphorylation of the regulatory light chain of myosin II disrupts the barrier integrity of corneal endothelial cells. *Invest Ophthalmol Vis Sci* 47, 4011-8 (2006).
78. Geeraerts, M.D., Ronveaux-Dupal, M.F., Lemasters, J.J. & Herman, B. Cytosolic free Ca²⁺ and proteolysis in lethal oxidative injury in endothelial cells. *Am J Physiol* 261, C889-96 (1991).
79. Ermak, G. & Davies, K.J. Calcium and oxidative stress: from cell signaling to cell death. *Mol Immunol* 38, 713-21 (2002).
80. Bondarenko, A. & Sagach, V. Na⁺-K⁺-ATPase is involved in the sustained ACh-induced hyperpolarization of endothelial cells from rat aorta. *Br J Pharmacol* 149, 958-65 (2006).
81. Head, J.A. et al. Cortactin tyrosine phosphorylation requires Rac1 activity and association with the cortical actin cytoskeleton. *Mol Biol Cell* 14, 3216-29 (2003).

82. Baumer, Y., Drenckhahn, D. & Waschke, J. cAMP induced Rac 1-mediated cytoskeletal reorganization in microvascular endothelium. *Histochem Cell Biol* 129, 765-78 (2008).
83. Rohr, G.E., Meier, B. & Sticher, O. Quantitative reversed-phase high-performance liquid chromatography of procyanidins in *Crataegus* leaves and flowers. *Journal of Chromatography A* 835, 59-65 (1999).
84. Noll, T. et al. ATP reduces macromolecule permeability of endothelial monolayers despite increasing $[Ca^{2+}]_i$. *Am J Physiol* 276, H1892-901 (1999).
85. Mehta, D., Konstantoulaki, M., Ahmmed, G.U. & Malik, A.B. Sphingosine 1-phosphate-induced mobilization of intracellular Ca^{2+} mediates rac activation and adherens junction assembly in endothelial cells. *J Biol Chem* 280, 17320-8 (2005).
86. Hirano, K., Hirano, M. & Hanada, A. Involvement of STIM1 in the proteinase-activated receptor 1-mediated Ca^{2+} influx in vascular endothelial cells. *J Cell Biochem* 108, 499-507 (2009).
87. Groschner, K. et al. Trp proteins form store-operated cation channels in human vascular endothelial cells. *FEBS Lett* 437, 101-6 (1998).
88. DeHaven, W.I. et al. TRPC channels function independently of STIM1 and Orai1. *J Physiol* 587, 2275-98 (2009).
89. Sundivakkam, P.C. et al. The Ca^{2+} Sensor STIM1 is Necessary and Sufficient for the Store-Operated Ca^{2+} Entry Function of TRPCs in Endothelial Cells. *Mol Pharmacol* (2011).
90. Moore, T.M. et al. Store-operated calcium entry promotes shape change in pulmonary endothelial cells expressing Trp1. *Am J Physiol* 275, L574-82 (1998).
91. Paria, B.C. et al. Tumor necrosis factor- α -induced TRPC1 expression amplifies store-operated Ca^{2+} influx and endothelial permeability. *Am J Physiol Lung Cell Mol Physiol* 287, L1303-13 (2004).
92. Wu, S. et al. Essential role of a Ca^{2+} -selective, store-operated current (ISOC) in endothelial cell permeability: determinants of the vascular leak site. *Circ Res* 96, 856-63 (2005).
93. Cioffi, D.L. & Stevens, T. Regulation of endothelial cell barrier function by store-operated calcium entry. *Microcirculation* 13, 709-23 (2006).
94. Moore, T.M. et al. Receptor-dependent activation of store-operated calcium entry increases endothelial cell permeability. *Am J Physiol Lung Cell Mol Physiol* 279, L691-8 (2000).
95. Holda, J.R. & Blatter, L.A. Capacitative calcium entry is inhibited in vascular endothelial cells by disruption of cytoskeletal microfilaments. *FEBS Lett* 403, 191-6 (1997).
96. Wu, S. et al. Microtubule motors regulate ISOC activation necessary to increase endothelial cell permeability. *J Biol Chem* 282, 34801-8 (2007).
97. Galan, C., Dionisio, N., Smani, T., Salido, G.M. & Rosado, J.A. The cytoskeleton plays a modulatory role in the association between STIM1 and the

- Ca²⁺ channel subunits Orai1 and TRPC1. *Biochem Pharmacol* 82, 400-10 (2011).
98. Malli, R., Naghdi, S., Romanin, C. & Graier, W.F. Cytosolic Ca²⁺ prevents the subplasmalemmal clustering of STIM1: an intrinsic mechanism to avoid Ca²⁺ overload. *J Cell Sci* 121, 3133-9 (2008).
 99. Piper, H.M. et al. Cytosolic Ca²⁺ overload and macromolecule permeability of endothelial monolayers. *Herz* 17, 277-83 (1992).
 100. Missiaen, L. et al. Ca²⁺ extrusion across plasma membrane and Ca²⁺ uptake by intracellular stores. *Pharmacol Ther* 50, 191-232 (1991).
 101. Sedova, M. & Blatter, L.A. Dynamic regulation of [Ca²⁺]_i by plasma membrane Ca(2+)-ATPase and Na⁺/Ca²⁺ exchange during capacitative Ca²⁺ entry in bovine vascular endothelial cells. *Cell Calcium* 25, 333-43 (1999).
 102. Strehler, E.E., Filoteo, A.G., Penniston, J.T. & Caride, A.J. Plasma-membrane Ca(2+) pumps: structural diversity as the basis for functional versatility. *Biochem Soc Trans* 35, 919-22 (2007).
 103. Brini, M. & Carafoli, E. Calcium pumps in health and disease. *Physiol Rev* 89, 1341-78 (2009).
 104. Missiaen, L. et al. Ca²⁺ uptake and release properties of a thapsigargin-insensitive nonmitochondrial Ca²⁺ store in A7r5 and 16HBE14o- cells. *J Biol Chem* 277, 6898-902 (2002).
 105. Marin, J. & Redondo, J. Vascular sodium pump: endothelial modulation and alterations in some pathological processes and aging. *Pharmacol Ther* 84, 249-71 (1999).
 106. Pittner, J., Rhinehart, K. & Pallone, T.L. Ouabain modulation of endothelial calcium signaling in descending vasa recta. *Am J Physiol Renal Physiol* 291, F761-9 (2006).
 107. Mayol, V. et al. Evidence that human endothelial cells express different isoforms of Na,K-ATPase. *J Hypertens* 16, 145-50 (1998).
 108. Wang, Y., Fan, R., Gu, Y. & Adair, C.D. Digoxin immune fab protects endothelial cells from ouabain-induced barrier injury. *Am J Reprod Immunol* 67, 66-72 (2012).
 109. Fraga, C.G. & Oteiza, P.I. Dietary flavonoids: Role of (-)-epicatechin and related procyanidins in cell signaling. *Free Radic Biol Med* 51, 813-23 (2011).
 110. Han, X., Shen, T. & Lou, H. Dietary Polyphenols and Their Biological Significance. *International Journal of Molecular Sciences* 8, 950-988 (2007).
 111. da Silva Porto, P.A., Laranjinha, J.A. & de Freitas, V.A. Antioxidant protection of low density lipoprotein by procyanidins: structure/activity relationships. *Biochem Pharmacol* 66, 947-54 (2003).
 112. Steffen, Y., Gruber, C., Schewe, T. & Sies, H. Mono-O-methylated flavanols and other flavonoids as inhibitors of endothelial NADPH oxidase. *Arch Biochem Biophys* 469, 209-19 (2008).

113. Gong, G. et al. Rutin inhibits hydrogen peroxide-induced apoptosis through regulating reactive oxygen species mediated mitochondrial dysfunction pathway in human umbilical vein endothelial cells. *Eur J Pharmacol* 628, 27-35 (2010).
114. Park, H.H. et al. Flavonoids inhibit histamine release and expression of proinflammatory cytokines in mast cells. *Arch Pharm Res* 31, 1303-11 (2008).
115. Lotito, S.B. & Frei, B. Dietary flavonoids attenuate tumor necrosis factor alpha-induced adhesion molecule expression in human aortic endothelial cells. Structure-function relationships and activity after first pass metabolism. *J Biol Chem* 281, 37102-10 (2006).
116. Min, Y.D. et al. Quercetin inhibits expression of inflammatory cytokines through attenuation of NF-kappaB and p38 MAPK in HMC-1 human mast cell line. *Inflamm Res* 56, 210-5 (2007).
117. Xia, M.L. et al. Rutin-induced endothelium-dependent vasorelaxation in rat aortic Rings and the underlying mechanism. *Conf Proc IEEE Eng Med Biol Soc* 6, 5595-7 (2005).
118. Schini-Kerth, V.B., Auger, C., Kim, J.H., Etienne-Selloum, N. & Chataigneau, T. Nutritional improvement of the endothelial control of vascular tone by polyphenols: role of NO and EDHF. *Pflugers Arch* 459, 853-62 (2010).
119. Kempuraj, D. et al. Flavonols inhibit proinflammatory mediator release, intracellular calcium ion levels and protein kinase C theta phosphorylation in human mast cells. *Br J Pharmacol* 145, 934-44 (2005).
120. Verstraeten, S.V., Mackenzie, G.G., Oteiza, P.I. & Fraga, C.G. (-)-Epicatechin and related procyanidins modulate intracellular calcium and prevent oxidation in Jurkat T cells. *Free Radic Res* 42, 864-72 (2008).
121. Shoshan, V., Campbell, K.P., MacLennan, D.H., Frodis, W. & Britt, B.A. Quercetin inhibits Ca²⁺ uptake but not Ca²⁺ release by sarcoplasmic reticulum in skinned muscle fibers. *Proc Natl Acad Sci U S A* 77, 4435-8 (1980).
122. Ogunbayo, O.A., Harris, R.M., Waring, R.H., Kirk, C.J. & Michelangeli, F. Inhibition of the sarcoplasmic/endoplasmic reticulum Ca²⁺-ATPase by flavonoids: a quantitative structure-activity relationship study. *IUBMB Life* 60, 853-8 (2008).
123. Viskupicova, J., Strosova, M., Sturdik, E. & Horakova, L. Modulating effect of flavonoids and their derivatives on sarcoplasmic reticulum Ca²⁺-ATPase oxidized by hypochloric acid and peroxynitrite. *Neuro Endocrinol Lett* 30 Suppl 1, 148-51 (2009).
124. Horakova, L. Flavonoids in prevention of diseases with respect to modulation of Ca-pump function. *Interdiscip Toxicol* 4, 114-24 (2011).
125. Barzilai, A. & Rahamimoff, H. Inhibition of Ca²⁺-transport ATPase from synaptosomal vesicles by flavonoids. *Biochim Biophys Acta* 730, 245-54 (1983).
126. Thiyagarajah, P., Kuttan, S.C., Lim, S.C., Teo, T.S. & Das, N.P. Effect of myricetin and other flavonoids on the liver plasma membrane Ca²⁺ pump. Kinetics and structure-function relationships. *Biochem Pharmacol* 41, 669-75 (1991).

127. Hagiwara, M. et al. Differential effects of flavonoids as inhibitors of tyrosine protein kinases and serine/threonine protein kinases. *Biochem Pharmacol* 37, 2987-92 (1988).
128. Robert, L. et al. [The effect of procyanidolic oligomers on vascular permeability. A study using quantitative morphology]. *Pathol Biol (Paris)* 38, 608-16 (1990).
129. Robert, A.M., Tixier, J.M., Robert, L., Legeais, J.M. & Renard, G. Effect of procyanidolic oligomers on the permeability of the blood-brain barrier. *Pathol Biol (Paris)* 49, 298-304 (2001).
130. Blazso, G. & Gabor, M. Oedema-inhibiting effect of procyanidin. *Acta Physiol Acad Sci Hung* 56, 235-40 (1980).
131. Zafirov, D., Bredy-Dobrev, G., Litchev, V. & Papisova, M. Antiexudative and capillaritonic effects of procyanidines isolated from grape seeds (*V. Vinifera*). *Acta Physiol Pharmacol Bulg* 16, 50-4 (1990).
132. Yucel, O. et al. Proanthocyanidin to prevent formation of the reexpansion pulmonary edema. *J Cardiothorac Surg* 4, 40 (2009).
133. Doutremepuich, J.D., Barbier, A. & Lacheretz, F. Effect of Endotelon (procyanidolic oligomers) on experimental acute lymphedema of the rat hindlimb. *Lymphology* 24, 135-9 (1991).
134. Fine, A.M. Oligomeric proanthocyanidin complexes: history, structure, and phytopharmaceutical applications. *Altern Med Rev* 5, 144-51 (2000).

7 APPENDIX

7.1 Abbreviations

Table 17 Abbreviations

Acronym	Term
AJ(s)	Adherens junction(s)
2-APB	2-Aminoethylidiphenyl borate
BHQ	2,5-Di-tert-butylhydroquinone
Blotto	Non-fat dry milk powder
BSA	Bovine serum albumin
cAMP	Cyclic adenosine monophosphate
$[Ca^{2+}]_{ER}$	Calcium concentration of the endoplasmic reticulum
$[Ca^{2+}]_i$	Intracellular calcium concentration
CaM	Calmodulin
DAG	Diacylglycerol
DMEM	Dulbecco's modified Eagle's medium
EC(s)	Endothelial cell(s)
ECGM	Endothelial cell growth medium
EPAC1	Exchange protein directly activated by cAMP 1
ER	Endoplasmic reticulum
FCPC	Fast centrifugal partition chromatography
FCS	Fetal calf serum
FITC	Fluorescein isothiocyanate
FRET	Fluorescence resonance energy transfer
GEF(s)	Guanine nucleotide exchange factor(s)
GPCR	G-protein coupled receptor
HAT	Hypoxanthin, aminopterin, thymidine
HMEC	Human dermal microvascular endothelial cells
HUVECs	Human umbilical vein endothelial cells
H ₁ R	Histamine receptor 1
IEJ(s)	Interendothelial junction(s)
IP ₃	Inositol-1,4,5-trisphosphate
MLC(K, P)	Myosin light chain (kinase, phosphatase)
NCX	Na ⁺ /Ca ²⁺ -exchanger
NYHA	New York Heart Association
OPCs	Oligomeric proanthocyanidins

Acronym	Term
PAR1	Proteinase activated receptor 1
PHPLC	Preparative high performance liquid chromatography
PKA	Protein kinase A
PKC α	Protein kinase C α
PLC β	Phospholipase C β
PMCA	Plasma membrane calcium ATPase
PMSF	Phenylmethylsulfonyl fluoride
SDS	Sodium dodecyl sulfate
SERCA	Sarcoplasmic/endoplasmic reticulum calcium ATPase
skMLCK	Skeletal muscle myosin light chain kinase
SOC(E)	Store-operated calcium (entry)
Stim-1	Stromal interaction molecule-1
S1-P	Sphingosine 1-phosphate
T/E	Trypsin/EDTA
TRPC channel	Canonical transient receptor potential channel
VASP	Vasodilator-stimulated phosphoprotein
VE-cadherin	Vascular endothelial cadherin

7.2 Publications

7.2.1 Original publications

Bubik MF, Willer EA, Bihari P, Jürgenliemk G, Ammer H, Krombach F, Zahler S, Vollmar AM, Fürst R. A novel approach to prevent endothelial hyperpermeability: The *Crataegus* extract WS[®] 1442 targets the cAMP/Rap1 pathway. *J Mol Cell Cardiol.* 2012 Jan;52:196-205.

Willer EA, Malli R, Bondarenko AI, Zahler S, Vollmar AM, Graier WF, Fürst R. The vascular barrier-protecting hawthorn extract WS[®] 1442 raises endothelial calcium levels by inhibition of SERCA and activation of the IP₃ pathway.

Submitted

Barbič M, Willer EA, Heilmann J, Fürst R, Jürgenliemk G. Compounds from *Ruscus rhizoma* reduce the thrombin-induced hyperpermeability of endothelial cells.

Submitted

Mayer BA, Hornburger MC, Leonhardt S, Willer EA, Vollmar AM, Fürst R. IAP antagonists protect from thrombin-induced endothelial hyperpermeability.

In preparation

7.2.2 Poster presentations

Willer EA, Bubik MF, Ammer H, Zahler S, Vollmar AM, Fürst R. First insights into the bioactive principles of hawthorn extract WS[®] 1442 responsible for endothelial barrier protection. 51st Annual Meeting of the Deutsche Gesellschaft für Experimentelle und Klinische Pharmakologie und Toxikologie, March 23-25, 2010, Mainz, Germany. *Naunyn-Schmiedeberg's Arch Pharmacol.* 2010; 381 Suppl. 1, Abs. 244.

Willer EA, Bubik MF, Ammer H, Zahler S, Vollmar AM, Fürst R. Investigations into the bioactive entities of hawthorn extract WS[®] 1442 responsible for its endothelial barrier protecting activity. 58th International Congress and Annual Meeting of the Society for Medicinal Plant and Natural Product Research, August 29–September 2, 2010, Berlin, Germany. *Planta Medica* 2010; 76, Abs. P580.

Barbic M, Willer EA, Fürst R, Jürgenliemk G. Aesculin from Butcher's broom reduces the permeability of endothelial cells in vitro. 58th International Congress and Annual Meeting of the Society for Medicinal Plant and Natural Product Research, August 29–September 2, 2010, Berlin, Germany. *Planta Medica* 2010; 76, Abs. P585.

Willer EA, Malli R, Zahler S, Vollmar AM, Graier WF, Fürst R. Insights into the Ca²⁺-regulating molecular mechanisms of the hawthorn extract WS[®] 1442 in endothelial cells. 77th Annual Meeting of the Deutsche Gesellschaft für experimentelle und klinische Pharmakologie und Toxikologie, March 30–April 1, 2011, Frankfurt a.M., Germany. *Naunyn Schmiedebergs Arch Pharmacol.* 2011; 383 Suppl.1, Abs. P148.

Willer EA, Malli R, Zahler S, Vollmar AM, Graier WF, Fürst R. Mechanistic insights into the rise of cytosolic Ca²⁺ levels during endothelial barrier protection induced by the hawthorn extract WS[®] 1442. Joint Meeting European Society of Microcirculation (ESM) and Society of Microcirculation and Vascular Biology (GfMVB), October 13–16, Munich, Germany. *Journal of Vascular Research*, 2011; 48 Suppl. 1, Abs. P130

7.3 Curriculum vitae

Personal data

Name	Elisabeth Armella Willer
Place of birth	Munich

Academic Education

January 2009-April 2012	PhD thesis at the Department of Pharmacy, Pharmaceutical Biology, University of Munich, Prof. Dr. A. M. Vollmar
December 2008	Licensure as a pharmacist (Approbation)
November 2007-October 2008	Compulsory Internship (Pharmaziepraktikum) Hof-Apotheke, Schriesheim (November 2007-April 2008) F. Hoffmann-La Roche AG, Basel (May 2008-October 2008)
October 2003-October 2007	Study of Pharmacy, University of Munich

7.4 Acknowledgements

This study was supported by the German Research Foundation (DFG, Deutsche Forschungsgemeinschaft) [FU691/7-1]. The extract WS[®] 1442 was kindly provided by the company Dr. Willmar Schwabe GmbH & Co. KG, Karlsruhe, Germany.

There is no duty more obligatory than the repayment of kindness

(Marcus Tullius Cicero)

First and foremost, I would like to thank Prof. Dr. Angelika M. Vollmar for giving me the opportunity to perform my PhD thesis in her laboratories, for her great mentoring and for always listening. I also highly appreciate that she trusted in me and my work and therefore gave me the chance to collaborate with Prof. Graier's group in Graz. Moreover, I would like to express my deepest gratitude to PD Dr. Robert Fürst for his outstanding and competent supervision, his scientific input, for always paying attention to my ideas and doubts and finally for being the second examiner on my thesis. I really enjoyed our discussions and the joint participation in conferences.

In addition, I am very thankful to Prof. Dr. Stefan Zahler who helped me to establish Fura-2 measurements in our lab and always had a wise advice for technical problems of every description. I also honor his suggestions and critical thoughts in our meetings.

Sincere thanks are given to Prof. Dr. Christian Wahl-Schott, PD Dr. Manfred Ogris, Prof. Dr. Franz Bracher and Prof. Dr. Gerhard Winter for their time and attendance in my thesis committee.

Very special thanks go to Prof. Dr. Wolfgang Graier (Medical University of Graz) and his lab for their interest, their support, their effort and the very warm welcome. Particularly, I want to express my gratitude to Assoc. Prof. Dr. Roland Malli for his excellent supervision, his ideas and his technical advice. Additionally, I thank Dr. Oleksandr Bondarenko for performing patch clamp recordings.

Furthermore, I want to thank Jana Peliskova for her great support in every day's lab work and Rita Socher for providing basic buffers and preparing the equipment for the students' practical course. I am grateful to all my former and current lab mates for the delightful working ambience. Moreover, I am indebted to the "Crataegus-Team"

consisting of Dr. Martin Bubik, Evelyn Hartung and Simone Fuchs. I express my gratitude to Dr. Johanna Liebl and Michael Hornburger for their advice and the enjoyable conversations we had. Special thanks go to Dr. Romina Wiedmann for the nice time in the new PhD room. I really enjoyed our talks as well as scientific discussions and really appreciated your calmative words. Finally, I am deeply thankful to Dr. Bettina Mayer, Dr. Sabine Weitensteiner and Bianca Hager. I really honored your company in the lab, your support, our leisure time activities and your friendship.

Furthermore, I am indebted to my brother and his wife as well as to my boyfriend and his family for assisting me ever and anon.

Last but not least, I am deeply grateful to my beloved parents. Without your unlimited and never ending encouragement, your understanding and your love, I would have never been able to go my way! Thank you so much for being there whenever I need you!